2009

Slab-on-girder prestressed concrete bridges: linear and nonlinear finite element analysis and experimental load tests

Marcio Costa Araujo
Louisiana State University and Agricultural and Mechanical College, marauj1@lsu.edu

SLAB-ON-GIRDER PRESTRESSED CONCRETE BRIDGES: LINEAR AND NONLINEAR FINITE ELEMENT ANALYSIS AND EXPERIMENTAL LOAD TESTS

A Dissertation
Submitted to the Graduate Faculty of the
Louisiana State University and
Agricultural and Mechanical College
in partial fulfillment of the
requirements for the degree of
Doctor of Philosophy

in

The Department of Civil and Environmental Engineering

by
Marcio Costa Araujo
B.S., Universidade Federal do Piauí, Brazil, 1998
M.S., Louisiana State University, Baton Rouge, 2002
May, 2009

DEDICATION

To my parents. For their love, example and vision.

ACKNOWLEDGEMENTS

Words can reverberate empty if not followed by suitable actions. Actions of respect for our profession as civil engineers and for the society we serve shall follow the achievement of a doctorate degree. In order to show true appreciation to those who were instrumental in this feat, I shall exercise my profession with zeal and delight, humbly realizing that the surface of knowledge has just been scratched.

First and foremost, I would like to thank Professor Steve Cai for his guidance and encouragement as my graduate advisor. Thanks for directing me with his knowledge and experience in many long discussions on various topics related to my research. Also, for the discipline he instilled in me regarding hard work and professionalism. For his patience sometimes as a big brother, and for his forthrightness as a mentor who envisions the best for his apprentice.

I would like to express my thankfulness to my graduate committee members as well: Professor Ayman Okeil, Professor Jing Wang, Professor Guoping Zhang and Boyd Professor George Voyiadjis. Thank you for your constructive comments and contribution to this work.

Thanks to Professor Richard Avent for his guidance and to Walid Alaywan for his support during the course of this work. Thanks also to LTRC for its financial support through project number No. 03-3ST.

I would like to thank my fellow graduate students for their assistance throughout this journey. Special thanks to Xiaomin Shi, Anchana Nair, Wenjie Wu, Xianzhi Liu, Anand Chandolu, Stanley Oghumu and Lu Deng. I will always cherish the memories of our time together as a group.

Finally, I would like to express my gratitude to my family, for their unconditional support and prayers at all times. When my knees got feeble they were right next to me to help me stand up. To my parents, siblings, in-laws, and to my precious wife Susana and my beloved sons Andrew and Lucas, thank you.

TABLE OF CONTENTS

LIST OF TABLES

LIST OF FIGURES

ABSTRACT

"A diaphragm is a transverse stiffener, which is placed between girders in order to maintain section geometry", (AASHTO, 2002). Intermediate diaphragms, usually placed at the midspan or third points of a bridge, are thought to contribute to the overall distribution of live loads in bridges. Cast-in-place concrete intermediate diaphragms were investigated in this study in order to assess their load distribution effectiveness in prestressed concrete I-girder bridges. Finite element packages (Ansys and GT STRUDL) were used to perform the analyses for multiple bridge configurations, including a parametric study of span length, girder spacing, and concrete strength. It was found that intermediate diaphragms do not contribute significantly to live load distribution and that they are not needed if there is no possibility of impact by an over-height truck. If the risk of a lateral collision to the girders is present, intermediate diaphragms should be placed over the respective traffic lane so that the potential impact takes place at the diaphragms location. Temporary steel diaphragms can be used to stabilize girders during construction.

Static and Dynamic live load tests were performed and experimental results were compared to the finite element analysis. Various pavement roughnesses were simulated with the use of wood boards up to 1.5" in depth. A dump truck, driven at 30 MPH, 38.5 MPH and 40 MPH, produced strains and deflections which were processed for load distribution and dynamic allowance (IM) factors. According to the results obtained, there is a more uniform live load distribution as the speed and roughness increase. However, driving at 40 MPH over the 1.5" wood board produced an impact factor almost twice as large as the one specified by AASHTO LRFD (2004).

Finally, nonlinear analyses of the tested bridge were performed in order to predict its ultimate capacity. Two bridge configurations were analyzed. The first one was modeled without any diaphragms or edge stiffeners, while the second one with end diaphragms and edge stiffeners. Ultimate loading results show that AASHTO LRFD presents conservative values.

CHAPTER 1. INTRODUCTION

1.1 Background

About 27 percent of the 590,750 bridges in the country are classified as structurally deficient or functionally obsolete. In Louisiana, this number is 32 percent (ASCE, 2005). Live loads play a key role in the structural degradation of bridges as crack initiators and propagators and have been a focal concern in bridge design for a long time, with their regulation appearing in the form of empirical distribution factors in the first edition of the AASHTO code in 1931. In order to better forecast the behavior of bridge systems beyond service loads, a predictive method using nonlinear finite element analysis is proposed.

According to the Standard Specifications for Highway Bridges by the American Association of Highway and Transportation Officials (AASHTO, 2002), "A diaphragm is a transverse stiffener, which is placed between girders in order to maintain section geometry." Due to the high labor cost of cast-in-place concrete diaphragms in prestressed concrete bridges, use of intermediate diaphragms (IDs) is considered as an added and perhaps unnecessary cost to bridge construction. Since the benefits of using IDs are still questionable and each US state has its own policy, further investigation has become a nationwide issue in order to justify their use.

Diaphragms have been thought to contribute to the overall distribution of live loads in bridges. Cast-in-place concrete diaphragms are commonly used in prestressed concrete I-girder bridges. Steel diaphragms are another possibility. Diaphragms located along the span are called intermediate diaphragms. Whether intermediate diaphragms are necessary for prestressed concrete slab-on-girder bridges or not has been a debated issue for the last three decades.

Intermediate diaphragms and bridge decks are the two major transverse components that connect adjacent longitudinal girders together. Some of the issues below are at the center of the controversy involving IDs and their applications.

Some of the arguments in favor of using IDs rely on the fact that they can:

a. Transfer lateral loads to and from the deck;
b. Distribute vertical live loads between girders, thus reducing maximum deflection and moment for each individual girder;
c. Provide lateral supports to girders during construction; and
d. Distribute lateral impact loads from over-height trucks to all girders, thus reducing the total damage.

On the other hand, there are also a few arguments in favor of eliminating the IDs because:

a. Using IDs increases the cost and time of construction;
b. Instead of limiting damage from over-height truck, IDs may actually spread the damage, according to some studies; and
c. Some analytical results show that IDs do not necessarily reduce the controlling moment in girder design.

Based on a survey conducted by Garcia (Garcia, 1999), 8 out of 51 states and regions do not require IDs. Currently, Texas has eliminated the practice of using IDs. In Florida, diaphragms are not required for non-skewed bridges. In Iowa, reinforced concrete (RC) IDs are used where traffic flows under the bridge, and steel diaphragms are used in prestressed concrete (PC) bridges where there is no traffic flowing under the bridge (Andrawes, 2001). Similarly, inconsistency exists in the guidelines that are put forward by different local state departments of transportation in terms of the number of IDs provided, type, depth, and their connection to the girder. In Louisiana, the current practice is to provide RC IDs for PC bridges. Examining the current practice in Louisiana and Florida demonstrates the differences in ID use among states.

According to the current LADOTD Bridge Design Manual (LADOTD, 2002), the ID requirement is related to the span length L as:

a. For $L \leq 50$ ft, no diaphragm is required.

b. For 50 ft $< L \leq 100$ ft, one diaphragm is required.

c. For $L > 100$ ft, two diaphragms are required.

In Florida, the ID requirement is related to the skew angle as:

a. For skew angle $\leq 30^{o}$, if no diaphragm is provided, the live load of girders shall be increased by 5 percent.

b. For skew angle $> 30^{o}$, provide diaphragms per AASHTO (AASHTO, 2002) Article 8.12.

The AASHTO Standard Specifications (AASHTO, 2002) recommend that IDs be used at the point of the maximum positive moment for spans in excess of 40 ft. It is stated in AASHTO Load and Resistance Factor Design (LRFD, 2004) that IDs can improve live load distributions, but this effect is not included in the design specifications. In AASHTO Standard (2002), section 8.12.1 for reinforced concrete and 9.10.1 for prestressed concrete allow omitting IDs where tests or structural analyses show adequate strength. AASHTO LRFD (2004), Article 5.13.2.2 has a similar statement allowing the omission of the IDs if tests or structural analyses show them to be unnecessary.

This work concentrates on Louisiana's typical highway bridges and recommended diaphragm's applications.

1.2 Objectives

The objectives of the first part of this research were to assess the need for IDs in concrete highway bridges and to investigate if the use of steel diaphragms is justified. These objectives were achieved by focusing on Louisiana practices, synthesizing previous nationwide research results, and developing a comprehensive plan to provide supplemental information to reach conclusions and recommendations. The disputed need for intermediate diaphragms in prestressed concrete bridges was assessed through 3D finite element simulations and field testing of a simple span slab-on-girder bridge. Experimental results of strains and deflections of this bridge were compared to the

predictions made by the 3D full finite element model. The main motivation was to eventually achieve more economical bridge construction in Louisiana, while meeting construction, serviceability, and strength capacity requirements.

The objectives of the second part of this study were focused on the inelastic behavior of bridge systems. Bridge performance at the ultimate stage has not been extensively studied and may be significantly different from that in the service stage. With the purpose of narrowing the gap between service and ultimate analyses, the main objectives are to:

a. demonstrate how the load distribution affects the behavior of each girder as the live load is increased up to the bridge's ultimate capacity;
b. understand bridge systems' performance in inelastic stages;
c. predict bridges' ultimate capacity.

This information will help engineers evaluate bridge capacity more accurately, thus avoiding unnecessary and costly bridge postings as well as identifying unsafe bridges from the transportation network. Particularly for the present study, a nonlinear analysis would help researchers understand the actual capacity of prestressed bridges, especially if the IDs are eliminated. Two bridges measuring 55 and 105 feet in span length were analyzed up to failure under two different loading conditions using a three-dimensional (3D) finite element model. Two HS20 trucks, later described, were positioned side by side with their middle axle at the midspan in order to create maximum effects on one interior and one exterior girder in each loading condition. Comparisons of load distributions were performed using strains, deflections, and section moments obtained from the full 3D finite element model developed for this research. The finite element model predictions were compared to AASHTO LRFD (2004) and AASHTO Standard Specifications (2002).

1.3 Scope

This work investigates only common types of AASHTO girders sections with the

dimensions specified in the Louisiana Bridge Design Manual (LADOTD, 2002), which consist of the majority of Louisiana's bridge inventory as presented in chapter 6. Simply-supported and continuous straight slab-on-girder bridges, both with and without skew only are investigated. Box girder and curved girder bridges were excluded from this study, as they have special requirements regarding IDs.

The influence of IDs on load distribution was not included in the AASHTO LRFD (2004) because of the controversy regarding its effectiveness, as discussed earlier. A parametric study was conducted in an attempt to narrow the existing disagreement gap.

An alternative configuration of steel diaphragms was determined that could potentially replace the reinforced concrete (RC) IDs and provide a stiffness greater than the target stiffness value, which was taken as 40 percent of the absolute stiffness of RC diaphragms. The configurations of steel IDs where channel section placed horizontally connecting the girder webs and X-type bracing with a bottom strut based on girder geometry were considered. The stiffness contribution of these steel diaphragm configurations was calculated and their influence in load distribution was also determined.

The effect of different diaphragms on bridge performance under the impact of over-height trucks at the bottom of girders was assessed. Also, design forces developed in the steel bracing members during deck construction were determined. This was achieved by performing a finite element analysis using a 3D solid model to check the ability of the bracing members to carry the loads coming onto them during construction.

End diaphragms have almost always been used in practice; therefore, they were included in the model. The continuity diaphragms for continuous spans have been included in the finite element models.

High strength concrete bridges are becoming commonplace. High strength concrete materials were thus included in this study, but in a selected and limited number of analysis cases. Including high strength concrete in the finite element analysis will help make more systematic recommendations for IDs, as was rather easily done in the numerical analysis.

Since the objective of this study was to investigate the relative effect of IDs, the application of loads to the finite element model was limited to HS20 truck loadings. Lane loads were, therefore, ignored. The results should be valid for both AASHTO LRFD (2004) and Standard (2002) specifications. In order to obtain results that closely represent actual loading conditions in the field, the Chart for Span Range Limit for Precast Prestressed Girders in the LADOTD Bridge Design Manual (LADOTD, 2002) was used to set up the bridge parameter ranges.

Static and dynamic loading tests were performed at different speeds with different pavement unevenness. Results for live load distribution and dynamic allowance were discussed and presented in tables and figures.

The ultimate load distribution and load capacity of two bridges are determined using full 3D finite element models. Results obtained for live load distribution, rating factors and effective width were then compared to the respective predictions from AASHTO LRFD (2004) and AASHTO Standard (2002).

A brief summary of each chapter is presented herein. Chapter 1 presents an introduction to this work, including objectives and scope of this research.

In Chapter 2, a summary of a number of publications in topics related to this work is presented, including linear and nonlinear research.

Chapter 3 describes the methodology applied in this research for both the simplified and full 3D finite element models and their applications.

Chapter 4 describes in depth the finite element modeling technique and presents the equations utilized.

Chapter 5 shows the model validation starting with a simple support beam and expanding its application to predict the load distribution in a full 3D bridge model.

Chapter 6 discusses the analytical assessment of IDs along with the presentation of multiple bridges classified by ID type as observed in Louisiana.

Chapter 7 describes bridge loading tests which took place along the course of this work. Both loading and instrumentation are presented in detail.

Chapter 8 presents bridge loading tests and their comparison to finite element predictions for both static and dynamic loadings using the full 3D model developed by the author.

Chapter 9 presents nonlinear results obtained from different bridge configurations and loading scenarios relevant to this research.

Chapter 10 presents conclusions and recommendations for future research work.

This work was developed concurrently with "Assessing the Needs for Intermediate Diaphragms in Prestressed Concrete Bridges.", LTRC Project No. 03-3ST, LA State Project No. 736-99-1134, 2006. Some of the topics presented herein can also be found, sometimes in more depth, in this reference.

CHAPTER 2. LITERATURE REVIEW

2.1 Historic Overview

One of the important components of this study was to conduct a thorough review of existing literature on various aspects of intermediate diaphragms for prestressed concrete (PC) girder bridges. This was done with the purpose of gaining a better understanding of issues related to intermediate diaphragms in PC bridges. A literature review was also done on load distribution factor, diaphragm effects in steel bridges, and finite element modeling.

Debate on the need for IDs in slab-over-prestressed-concrete-girder bridges started in the late 1960s, with some studies stating that in some cases, IDs are counterproductive. The first of the reports which raised the question on the need for IDs in PC bridges was the report by Lin and Van Horn (1968). Results from their study were obtained from the field tests conducted on a bridge in Philadelphia and produced surprising conclusions. Diaphragms were found to transmit the loads laterally. However, when various lanes were loaded at the same time, the experimentally determined distribution factors were not appreciably affected. Moreover, the deflections in the girder reduced slightly with the provision of the IDs in the bridge structure, thereby putting the advantage of IDs in load distribution into question.

Sithichaikasem and Gamble (1972) carried out a parametric study for various bridge geometries for simply supported right bridges to understand the influence of IDs in PC bridges. The parameters considered in this study are as follows:

a. Aspect ratio, which is the ratio of girder spacing to span length;
b. Relative flexural stiffness parameter, which is the ratio of composite girder stiffness to deck stiffness;
c. Relative torsional stiffness, which is the ratio of the torsional stiffness to flexural stiffness of the girder;

d. Warping stiffness, which is the ratio of the warping rigidity of the girder to the product of the square of the span of the bridge and the torsional rigidity of the girder; and
e. Relative flexural stiffness of diaphragm, which is the ratio of the flexural stiffness of the diaphragm to that of the girder.

Charts of the moment coefficients versus girder spacing were plotted, which include the variation in the number and location of diaphragms as well as the different positions of live load. Some of the observations they made were as follows:

a. When the loading is close to exterior girders, the diaphragms increase the controlling moment and, therefore, prove to be detrimental, while for other cases it may either be helpful or harmful.
b. The influence of the number of diaphragms is insignificant, and
c. The diaphragm must be of correct flexural stiffness to be effective, otherwise any increase in diaphragm stiffness beyond a particular limit would increase the girder moments.

Wong and Gamble (1973) also considered the same parameters as Sithichaikasem and Gamble (1972) in determining the effect of diaphragms and continuity on load distribution in straight continuous bridges. The conclusions of this research were as follows:

a. Changes in maximum moments are not sensitive to diaphragm stiffness, and the effects of diaphragms are more pronounced in simply supported bridges than in continuous bridges.
b. The effects of continuity tend to cause a greater reduction in the maximum positive moment in the edge girder than in the interior girder.
c. In bridges with a spacing-to-span ratio of less than 0.05, the presence of a diaphragm may do more harm than good.

d. Except for temporary erection purposes, diaphragms are not required in straight bridges.

Sengupta and Breen (1973) have conducted experimental tests on four test bridges which were scaled down to 1/5.5 ratio with the variables being length, skew, and location of intermediate diaphragms for simply supported bridges under both static and dynamic loading in the vertical and lateral direction. The testing was done with and without diaphragms under cyclic and impact loads. They observed a pattern of results similar to that of earlier researchers. Concerning to the dynamic behavior, Sengupta and Breen (1973) stated that, when bridges are subjected to cyclic load, IDs did not influence the natural frequency of the bridges. Additionally, no effect was observed on the damping coefficient of bridge vibration. For bridges under lateral impact by over-height trucks, this study revealed that diaphragms reduce the energy absorption capacity of the girders. Consequently, the addition of diaphragms would make bridge girders more vulnerable to this type of damage.

Kostem (1977) investigated the effect of diaphragms on the lateral distribution of live load in simple-span, beam-slab bridges with prestressed concrete I-beams without skew. Data from two field tested bridges were used to validate the finite element model. The bridges had span lengths of 71.5 ft. and 68.5 ft. It was found that only 20 to 30% of the stiffness of midspan reinforced concrete diaphragms contributes to load distribution. This contribution becomes negligible when all lanes are loaded, in which case the bridge models behaved as if there were no diaphragms. The contribution of diaphragms to load distribution, contrary to intuitive beliefs, was not of relevant importance regardless of the loading pattern.

Contrary to their expectations, the increase in the number of diaphragms did not necessarily correspond to a more even distribution of loads at mid-span. Overall, the contribution of intermediate diaphragms was not found to be significant. According to the authors, these findings can be applied to bridges with moderate skew (0 to 30^{o}) as well as right continuous bridges. A

recommendation was made that vehicle overload and large skew effects be considered before eliminating the use of IDs.

In the late 1980s, the Florida Department of Transportation (FDOT) reconsidered its long-standing practice of using IDs. They concluded that the cost and time saved by eliminating the IDs far outweighed the benefits of using IDs. The Federal Highway Administration (FHWA) reviewed and approved the FDOT petition to eliminate the IDs on tangent bridges, with a caveat that, for bridges without diaphragms, the design live load of girders would be increased by 5%. This was promptly adopted by the FDOT. There are a number of major bridges in Florida designed and built without IDs. One example is the Structure A that leads to the Sunshine Skyway Bridge across Tampa Bay, St. Petersburg, FL. Another one is the Choctawhatchee Bay Bridge in Florida's northwestern panhandle. Since the early 1980s, the FDOT has maintained an extensive and comprehensive bridge testing program using specially designed test vehicles. Although most of the tests were conducted on existing older bridges, some were carried out on newer bridges without diaphragms.

Cheung et al. (1986) found that previous researchers disagree not only on the effectiveness of IDs in the lateral distribution of vertical live loads, but also on the optimal position of the IDs. Abendroth *et al*. (2003) focused their research on diaphragms. Their work incorporated a wide-ranging literature review, survey of design agencies, the testing of a full scale, simple span, P/C girder bridge model, and the finite element analysis of the bridge model considering pinned and fixed end conditions. They concluded that the vertical load distribution was independent of the type and location of the ID. The horizontal load distribution was found to be a function of the ID location and type. Constructional details at the girder supports formed substantial rotational end restraint for vertical and horizontal loading. Steel IDs essentially showed the same type of response

as the reinforced concrete (R/C) ones. It was also shown that the finite element method (FEM) generally enveloped the experimental results.

2.2 Contemporary Studies

Stallings *et al.* (1996) assessed the effects of removing all interior channel diaphragms from an existing and simple-span bridge with rolled-steel girders (this is a steel bridge, discussed here for information only). The effects were evaluated based on field measurements of the girder stresses and deflections made before and after the diaphragms were removed. The outcome of the tests with trucks of known weights indicated that the removal of diaphragms resulted in 6 to 15% increase in the maximum bottom flange stresses experienced by the most heavily loaded girder. The outcome of the tests with trucks of unknown weights in normal traffic indicated that the most heavily loaded girder can carry up to 17% more load due to diaphragm removal. These increased girder stresses were well within the limit of stresses calculated by the AASHTO specifications (Standard, 2002 and LRFD, 2004), implying that the effect diaphragm removal was inconsequential.

Griffin (1997) researched the influence of intermediate diaphragms on load distribution in prestressed concrete I-girder bridges. The studies included two bridges that were constructed with a 50^{o} skew angle along the coal haul route system of Southeastern Kentucky. One of the bridges has concrete intermediate diaphragms. Bridges of similar design along coal haul routes have experienced unusual concrete spalling at the interface of the diaphragms and the bottom flange of girders. The IDs appeared to be contributing to the increased rate of deterioration and damage instead of reducing the moment coefficient and distributing the traffic loads as expected. Experimental static and dynamic field testing were conducted on both bridges. All field tests were completed prior to the opening of the bridges. Once the calibration of the finite element models was completed using the test data, analysis was conducted with actual coal haul truck traffic to investigate load distribution and the cause of the spalling at the diaphragm-girder interface. Based

on the results obtained in the research study, IDs did not create a significant advantage in structural response. Although large differences were noted percentage-wise between the responses of the two bridges, analysis suggested that the bridge without IDs would experience displacements and stresses well within AASHTO and the American Concrete Institute (ACI) design requirements. The finite element analysis also revealed the cause of concrete spalling witnessed in the diaphragm girder interface region. The tendency of the girders to separate as the bridge was loaded played a large role in generating high stress concentrations in the interface region. Other mitigating factors included the presence of the diaphragm anchor bars and the fact that the bridge was subjected to overloads of coal trucks. It also stated that to resolve this problem would require the removal of the concrete ID. In summary, the total elimination of IDs was not recommended since they are required during construction and in the event that the deck has to be replaced. Hence, the use of steel diaphragms as substitution to concrete diaphragms was recommended.

Barr et al. (2001) studied the evolution of flexural live-load distribution factors in a three-span prestressed concrete girder bridge, where a bridge with three spans with lengths of 80 ft, 137 ft, and 80 ft. and a skew angle of 40^{o} was tested. A finite element model was developed to assess the live-load distribution procedures recommended by the AASHTO code. For both interior and exterior girders, the addition of IDs had the least effect on the live-load distribution factor among the variables investigated in this study, agreeing with Sithichaikasem and Gamble (1972). For the exterior girders, IDs slightly increased the live-load distribution factor for low skew angles. For skew angles larger than 30^{o}, the addition of IDs was slightly beneficial, again agreeing with earlier findings by Sithichaikasem and Gamble (1972). According to this study, for design consideration from a structural standpoint, the largest changes would be credited to the addition of end diaphragms, while almost no changes would occur due to the addition of intermediate diaphragms, since these showed almost no change in the distribution factors.

Eamon and Nowak (2002) studied the combined effects of secondary elements such as diaphragms, sidewalks, and barriers on load distribution in the elastic and inelastic domains, as well as their effects on the ultimate capacity of steel girder bridges. According to this study, diaphragms tend to be more effective at wider girder spacing and longer spans in terms of maximum girder moment reduction, and increasing the number of IDs does not significantly affect the results. Diaphragms showed to reduce the maximum girder moment up to 13% with an average reduction of about 4%. The ratio of girder stiffness to diaphragm stiffness was observed to be the most important factor effecting load distribution. It was observed that the improvement of the ultimate capacity due to IDs in the inelastic region was not very significant. They found that the girder spacing has very little effect on the moment capacity increase factor, and that the effect of diaphragms on the ultimate load carrying capacity in the inelastic region is insignificant. Eamon and Nowak (2004) furthered this work by assessing the effect of secondary elements on the reliability of bridges. According to them, the results suggested that a variation of reliability will exist on bridge structural systems if secondary elements are included, and this was found to be a function of span length and spacing. They also suggested that a structural system-based calibration of the LRFD code may be useful in providing a uniform level of reliability to bridge structures and their components.

Cai *et al.* (1998) investigated six prestressed concrete bridges in Florida, and the results were compared with field measurement of these bridges. It was found that the finite element prediction that did not consider IDs had better agreement with field test results, implying that the effectiveness of IDs of these bridges are insignificant in distributing the live loads. Further examination of the details of these bridges found that the diaphragm connections are weak. Numerically, the diaphragms would have more significant effects on vertical live load distribution if a full moment connection is ensured between the diaphragms and girders where the ID stiffness is

about 10% of that of the girder. It was also found that if no ID is in position, an increase in skew angle will decrease the load distribution factor. However, when the ID is in position, the increase in skew angle tends to increase the load distribution factor. These results imply that:

a. If a right bridge without IDs is safe in carrying the design loads, a skew bridge without IDs will be safer, given the other parameters are the same.
b. Furthermore, if a right bridge with IDs is safe, a skew bridge with IDs may not necessarily be safer, given the other parameters are the same.

Green *et al.* (2002) analyzed bridge performance, considering temperature change effects on bridges of different skew angles with and without IDs. When full ID stiffness was considered in the analysis where diaphragms were modeled using solid finite elements, the diaphragms were found to have contributed up to a 15% reduction in load distribution. Both the intermediate diaphragm and the positive temperature gradient decreased the maximum girder moment and the stresses at the mid-span. Green *et al.* (2004) have extended this research by making a study on the influence of skew and bearing stiffness on the maximum deflection of girder at mid-span. The results show that the influence of intermediate diaphragm decreases with an increase in skew angle. A decrease in deflection due to the presence of IDs for 0º, 15-30º, and 60º skew is about 18%, 11%, and 6%, respectively. By increasing the stiffness of bearing from 0.0 to 0.655 GPa, the maximum deflection reductions are of 11.5% and 5.9% for 30º and 60º, respectively. Increasing the bearing stiffness further to 6.895 MPa, the girder deflections decreased by 14.3% and 10.2% for 30 and 60º skewed bridges, respectively.

Khaloo and Mirzabozorg (2003) had taken skew angle, girder spacing, and span length for bridges as the parameters for carrying out a parametric study for skew bridges. They considered four kinds of configurations of bridges in their study, with the first type being without ID, the second type having an ID parallel to the supporting lines, and for the third and fourth

configurations, the diaphragms were perpendicular to the girders. For the third type, IDs were provided as per AASHTO requirement, while for the fourth type, the diaphragms were provided at the quarter and mid-span. The following conclusions were drawn from this study:

1. The configuration of IDs in the bridges has a significant effect on the load distribution pattern and their effect varied for different skew angles.
2. Bridges with IDs perpendicular to the longitudinal girders are the best arrangement for load distribution.
3. The effect of girder spacing on the influence of IDs on load distribution was found to be insignificant.

Abendroth and Fanous (2003) developed a finite element model for skewed and non-skewed PC girder bridges. They analyzed the bridge model for a lateral impact load both at and away from the location of the diaphragm configurations. Dynamic loading with 0.1s impact duration was used, and a single impact load was applied on either exterior girder. An investigation on whether analysis for single span can effectively be replaced for a four-span bridge was carried out. Only a 15% maximum difference in strains was observed, which is within tolerable limits. Therefore, single-span was used for further analysis. The following results were observed:

a. When the impact load was applied at the diaphragm location, the diaphragm reduced the strains effectively, and the performance was dependent on configuration of diaphragm. But when the impact was away from the diaphragm, the diaphragm did not distribute load effectively, and there was no significant difference in performance of different diaphragms.
b. When the impact load was applied at the diaphragm for both skewed and non-skewed bridges, reinforced concrete diaphragms provided the largest degree of impact protection.

Cai and Shahawy (2004) studied the effects of field factors, such as bearing restraints and non-structural members such as barriers and diaphragms, on prestressed concrete bridge performance. It was found that these field results collectively result in much less girder moment than that calculated according to AASHTO specifications (Standard, 2002 and LRFD, 2004). Therefore, the current AASHTO specifications are very conservative for prestressed concrete girders.

Other reviews included the work done by Zokaie *et al.* (1991) and Zokaie (2001) which gave the foundation of AASHTO LRFD. Chen (1995), Eamon and Nowak (2002) and Chen and Aswad (1996) discussed in detail finite element modeling and the load distribution factor calculation for bridges, which were reviewed as well.

A summary of conclusions from previous studies includes the following:

a. The addition of IDs may not reduce the maximum design moments and may, in some cases, actually cause a moderate increase. The deflection and moment of the interior girders are usually reduced, while the opposite is true for exterior girders. The test results show that the design loads are very conservative and provide sufficient capacity to carry the actual loads. In the cases that additional capacity is necessary, it may be more economical to solve this problem through a modest increase of girder capacity than by providing costly IDs.
b. Test results show that the hardened deck slab can provide enough lateral support and load distribution among girders, which may justify the temporary use of the IDs and their removal after the construction.
c. Only the ID near the section of maximum moment (usually near mid-span) can have a measurable effect on the controlling moment. This mid-span diaphragm, however, may

have no effect on lateral impact load since the traffic lanes are usually not underneath the mid-span of the girders.

d. IDs must have correct flexural stiffness to be effective. The torsional stiffness of girders is a critical component for load distributions, and it is one of the primary differences between steel and concrete bridges.

e. Some of the previous analyses, however, were based on simplified structural models due to the limitation of computational capacity at that time. New studies using modern finite element techniques and computation capacities are needed. Furthermore, a more systematic study is needed to establish guidelines for engineers to decide when to use IDs, and how to more efficiently use them.

Burdette and Goodpasture (1973) performed experimental tests on four highway bridges. The tested bridges were subjected to exploratory loads, truck loads up to twice the HS20 loads, and finally to static loads up to failure. All bridges were two-lane deck-on-girder with four longitudinal girders. One of the four tested bridges was a composite simple span with AASHTO type III precast, prestressed concrete girders spaced 8'-10" on center. This bridge was 66 feet long and skewed by 70 degrees.

In the tests performed, the ultimate loading was defined as the maximum load attained in a test to failure, and failure was said to occur when deflections continued to increase at sustained loads. It was observed that concrete diaphragms cracked at early loading steps. This early cracking, however, had no measurable effect on the load-deflection behavior on any of the tested bridges. The prestressed concrete bridge failure occurred when interior girders failed in shear at total load equal to 1140 kips. Results obtained from the other three bridges are not relevant to this work; therefore, are not discussed here.

CHAPTER 3. METHODOLOGY

3.1 Introduction

Two 3D finite element models were used to develop this study. A full ANSYS 3D finite element model was developed and used for loading cases that required more detailed analysis, such as the simulation of lateral loading due to over-height truck lateral impact to the bridge girders. A simplified GT-STRUDL 3D finite element model was also used to perform parametric studies and to determine the effectiveness of IDs in load distributions for various bridge configurations. This simplified model was used to predict lateral distribution of vertical loads. These models are discussed below along with and the methodology implemented to calculate load distribution factors.

3.2 Full 3D Finite Element Model Using ANSYS

This model was built using eight-node SOLID45 and SOLID65 elements to simulate the bridge concrete, both conventionally reinforced and prestressed. These solid elements have three-degrees of freedom per node. Prestressing tendons were modeled using LINK8 elements, which have two nodes and three degrees of freedom per node. Steel diaphragms were modeled using LINK8 or SHELL28 elements, which are 3D truss elements and two-dimensional shell elements, respectively.

In order to facilitate repeated modeling, Excel spreadsheets were used to generate the ANSYS 3D solid finite element models and the simplified 3D input files. Key point coordinates were defined to build the bridge geometry, which was then joined to generate the solid elements. After the 3D model was built, it was then meshed, loaded, and analyzed. This solid model was used for the cases in which the bridges undergone lateral impact loading as well as temporary bracing forces during construction. The vehicular traffic orientation on the bridge indicates the z-axis of the full 3D model, the y-axis indicates the vertical direction and x-axis is along the transverse direction.

The reference point (0,0,0) indicates the model's origin and is located at the mid-point of the bottom flange at one end of one of the exterior girder. All other points were within the model were located in relation to the origin.

In the full 3D finite element model, the loads were applied as uniform pressure simulating the contact area between truck wheels and pavement. Boundary conditions were carefully evaluated in order to avoid unwanted constraints to the nodes and, consequently, to the model. The number of constraints required to provide stability to the bridge models was kept to the minimum possible, keeping in sight that actual bridge behavior and performance had to be achieved. Unnecessary constraints would generate secondary stresses, thus altering the stresses distribution in the certain elements. Consequently, results based on strains, stresses and deflections could be inaccurate.

Girder supports were simulated by applying proper boundary conditions to nodes at both ends, as shown in Figure 3.1. Displacements in all directions were restricted at the support of one of the exterior girders. At the opposite end of this same girder, displacements along x- and y-axis were restricted. This was done to avoid unwanted rotation around the y-axis of the model. The Supports for the remaining girders were modeled by restricting displacements in the y-axis direction only. Finally, the opposite exterior girder had its z-direction restricted. A partial view of the full 3D model is shown in Figure 3.1 displaying girders, both end and intermediate diaphragms, and boundary conditions.

In the full 3D finite element model, stresses, strains and deflections were obtained directly from the elements at the locations of interest.

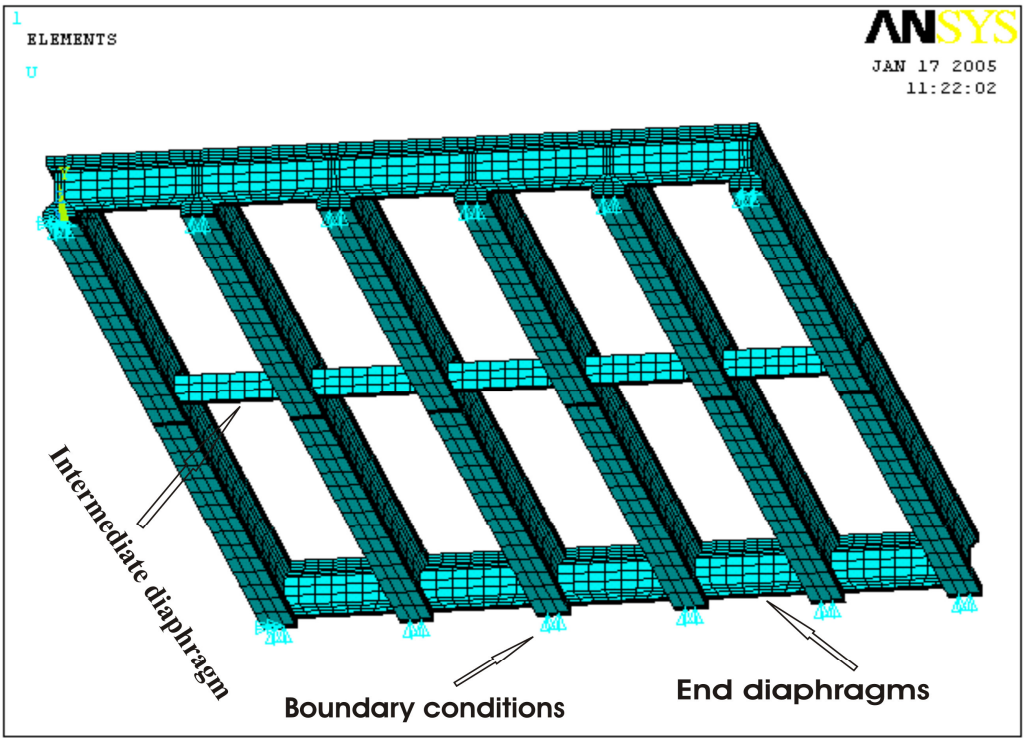

Figure 3.1
Full 3D finite element model
showing girders, diaphragms and boundary conditions

3.3 Simplified 3D Finite Element Model Using GT-STRUDL

A simplified 3D model was used to evaluate the effects of intermediate diaphragms on live load distribution through a parametric study. The simplified model did not need as much computer "horse-power" as the full 3D model, thus making repeated runs more time efficient while performing the parametric study.

The bridge was modeled using plate and line elements. The bridge deck was modeled using four-node quadrilateral plate elements physically located on the plane of its centroidal axis. Girders and diaphragms were modeled using line elements located along their centroidal axes. Line elements were built by connecting nodes offset from the ones used to model the deck. Girder and

diaphragm elements were then connected to the deck using rigid links. Figures 3.2 and 3.3 show the simplified 3D model and its respective elements.

In the simplified 3D model, the vehicular traffic direction of the bridge is along the x-axis, while the y-axis represents the transverse direction and the z-axis represents its vertical orientation. Nodal moments were released at the end nodes at the location of the supports, representing simply supported conditions. At one end of the simply supported bridge, all girder supports were modeled as roller supports by allowing the nodes to translate in the vehicular traffic direction. Girder section properties were readily available in published literature; however, the full 3D model was used in order to determine torsional moments of inertia.

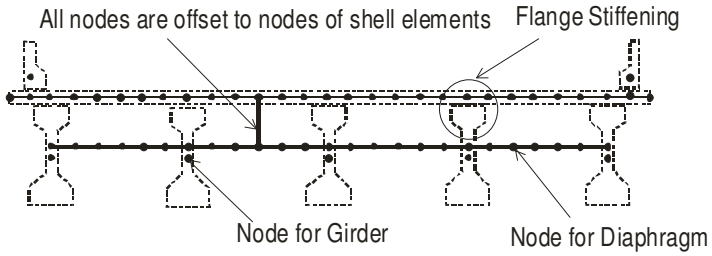

Figure 3.2
Elevation of Simplified 3D bridge model in GT STRUDL

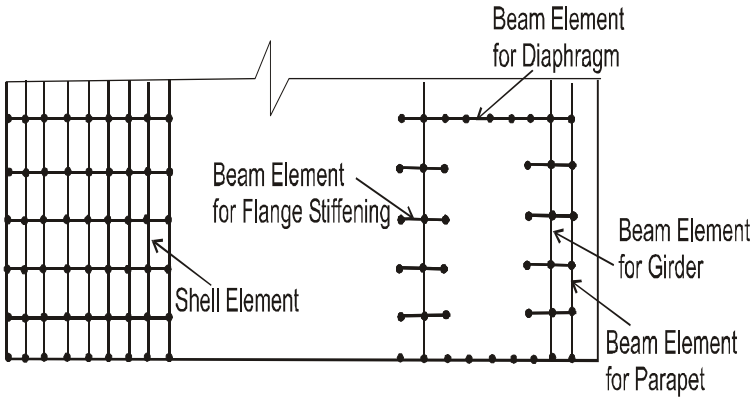

Figure 3.3
Partial plan view of GT STRUDL model

Excel spreadsheets were used to calculate parameters and generate various bridge configurations in the simplified model as well, thus generating input files. Characteristics such as

geometry, material properties and boundary conditions, were defined in the spreadsheets in order to create analytical models; in addition, the results needed from the analysis were specified. A few changes made to parameters in the spreadsheets resulted in the generation of an entirely different bridge configuration. This approach was more time efficient when compared to create an entire bridge model using GT-STRUDL directly. The simplified model is illustrated in Figure 3.4.

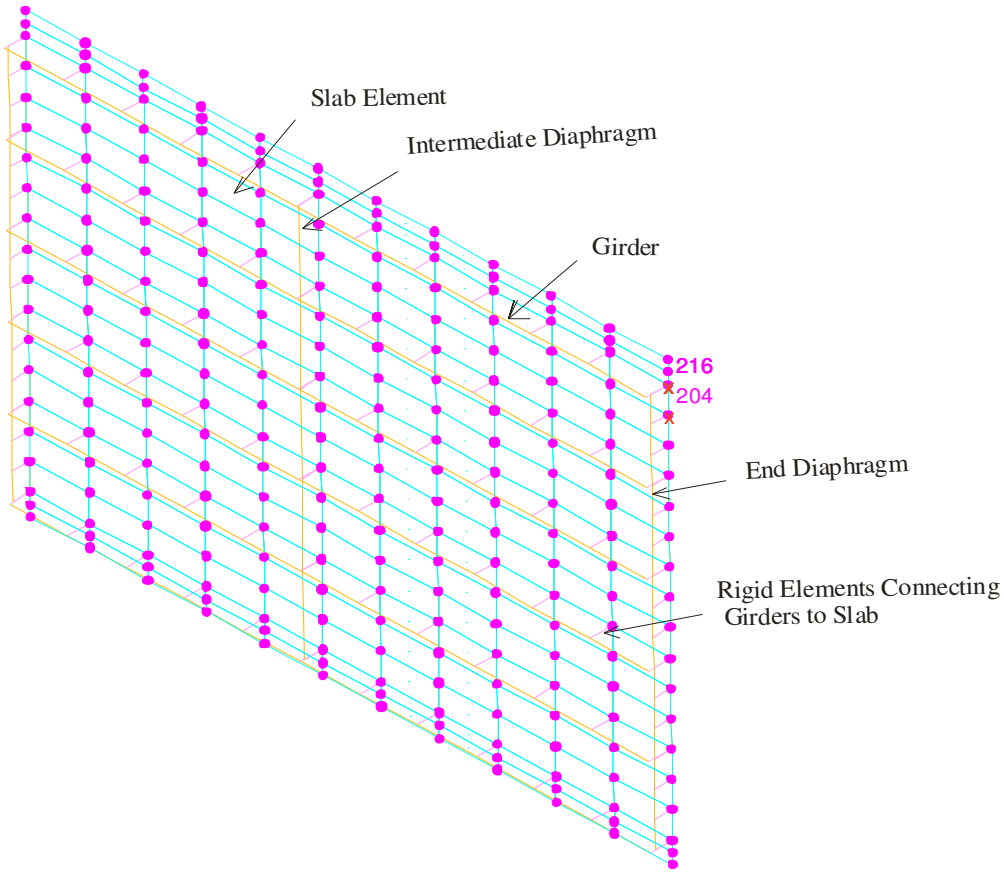

Figure 3.4
Simplified 3D bridge model in GT STRUDL.

Live loads were applied as point loads in the simplified model. When the point of application did not correspond to with nodal locations, equivalent static load were applied to the four nodes surround the load application point. The bridge system was meshed keeping the distance between nodes in the order of 1 ft along and across the model. This node distance produced

adequate accuracy and was therefore used in the GT-STRUDL modeling. In this simplified 3D model, forces and moments were acquired directly from the model and stresses and strains were calculated using formulas to be discussed later.

These are the assumptions upon which the simplified model was developed:

a. The material was assumed to be homogenous and isotropic.
b. Cracking of the bridge was ignored.
c. All the connections were assumed to be rigid (including the girder-diaphragm connection).
d. A small deflection theory was used.
e. Loading was considered to be static.
f. The beams and slab were assumed to act compositely.
g. The effect of stiffening due to beams was taken into consideration, while that of stiffening due to secondary elements was ignored.
h. The effects of cracking, creep, fatigue, and prestressing force were not considered.

3.4 Notation Used to Represent Bridge Configurations

Various bridge configurations were analyzed during parametric studies; therefore, there a need to properly identify them. In order to adequately label these various bridge models with multiple parameter to identify, the following notation was adopted. Girder spacing was identified as S (ft), while L (ft) represents length and D represents the number of intermediate diaphragms. Each letter will be followed by a number defining it. Loading cases were abbreviated as well. These loading cases are abbreviated as “int” or “ext” to indicate the whether the live load is positioned to cause maximum effects in an interior girder or in an exterior one, respectively. Unless otherwise noted, bridge skew angles are 0^{o}, the compressive strength of concrete for girder (f'_{cg}) is 6,000 psi

and the structure is a simple span bridge. Example : A single span bridge with a spacing of 7 ft., a span length of 55 ft, 1 intermediate diaphragms, with the live load positioned in order to create a maximum straining effect in interior girder, skew = 0^{o} , and f'_{cg} = 6,000 psi would be denoted as S7L55D1 (int).

CHAPTER 4. MODELING DESCRIPTION

4.1 Introduction

Finite element methods determine the overall behavior of structures by dividing them into several small (finite) and simple elements with well-defined mechanical and physical properties. The analyses of these simpler elements are done and the overall structure is reassembled, thus producing results that can be studied from a simple element at critical parts of the structures to the behavior of the whole structure.

This method is exemplified below in the modeling of a simple span AASHTO Type II girder, which is later expanded to whole bridge structures where decks, diaphragms, and railings are modeled in a similar way. In order to model these structures, the material properties had to be known and, in some cases, assumed. Some of these properties were acquired from blueprints and others from existing literature. Material properties relevant to this study are described below, followed by the modeling techniques utilized.

4.2 Concrete Modeling

The analysis of reinforced concrete is very complex and time-consuming due to the highly complex behavior of concrete structures. Such structures are, by their nature, non-homogeneous and anisotropic. This is due to the composition of plain concrete, which is a non-homogeneous mixture of coarse aggregate, sand, and hydrated cement paste (figure 4.1)

Concrete has different behavior in tension and compression, such that it is much more resistant to compression than to tension. In general, its tensile strength is in the order of 8% to 15% of its compressive strength. When subjected to compression concrete behaves linearly until approximately 30% to 50% of compressive strength. After this point the compressive stress increases gradually to a maximum, reaching the concrete compressive strength. After reaching the

maximum stress, the stress strain curve descends into a softening region, eventually crushing and failing at an ultimate strain. This phenomenon is illustrated in figure 4.2.

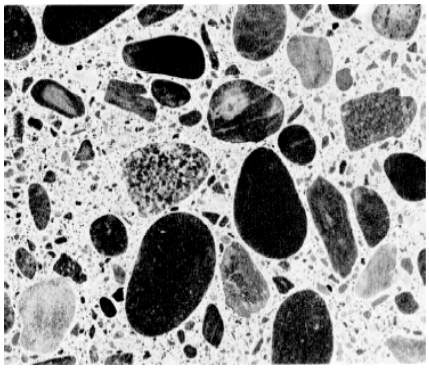

Figure 4.1
Plain concrete composition

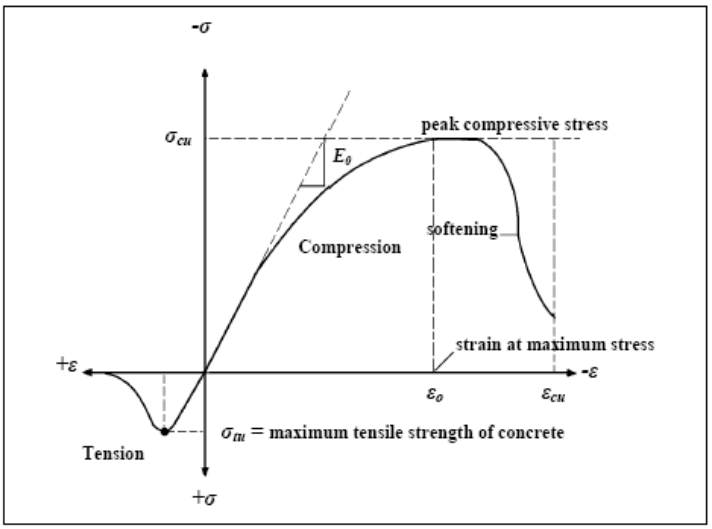

Figure 4.2
Uniaxial compressive and tensile stress-strain curve

In the finite element models developed by the author for these studies the concrete compressive stress-strain relationship was obtained through the following parabolic equation by Lin and Burns (1981) illustrated in figure 4.3:

$$f_c = f_c' \left[\frac{2\varepsilon}{\varepsilon_0} - \left(\frac{\varepsilon}{\varepsilon_0} \right)^2 \right] \qquad \text{Eq. 4.1}$$

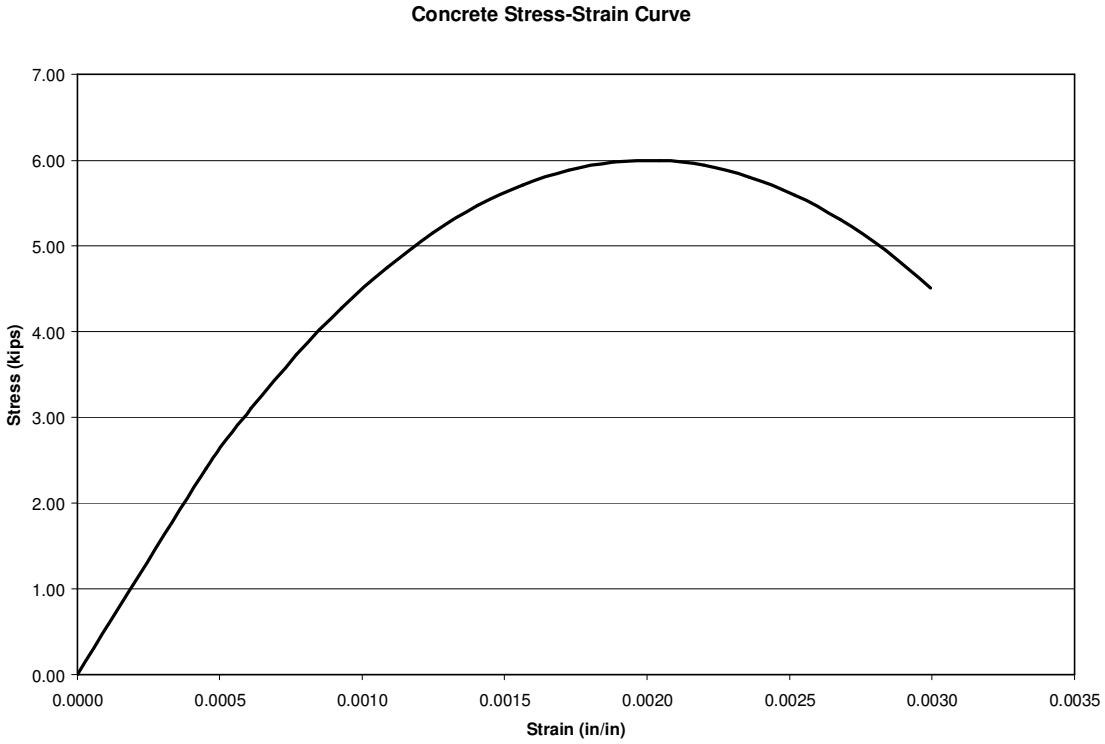

Figure 4.3
Parabolic compressive uniaxial stress-strain curve for concrete

ANSYS element types used in this model to simulate non-linear prestressed concrete with discrete reinforcement are SOLID65 (figure 4.4). These elements have the following characteristics:

a. Eight-node solid element

b. Three degrees of freedom at each node

c. Capable of plastic deformation and cracking (in three orthogonal directions)

d. Reinforcement in three custom adjustable directions

e. Crushing

The smeared reinforcement capability of SOLID65 was disabled because in this model LINK8 elements were used to model the strands. In this case the prestressing strands were simulated through the use of element type LINK8 (figure 4.5) within the SOLID65 elements.

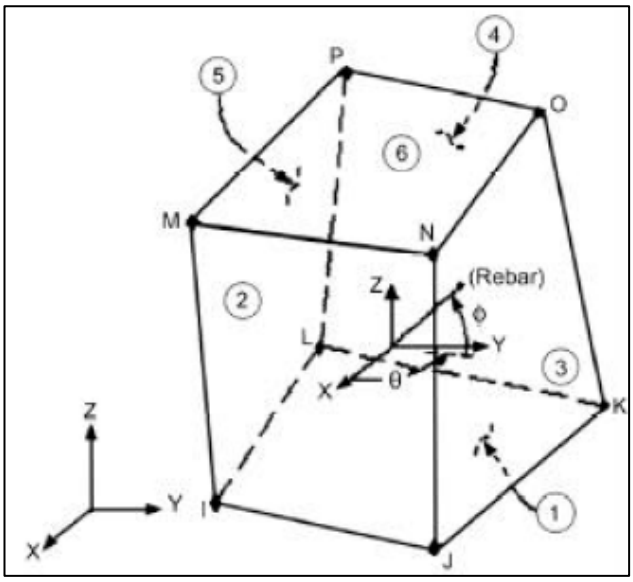

Figure 4.4
SOLID65 – 3D concrete solid element (ANSYS 7.1)

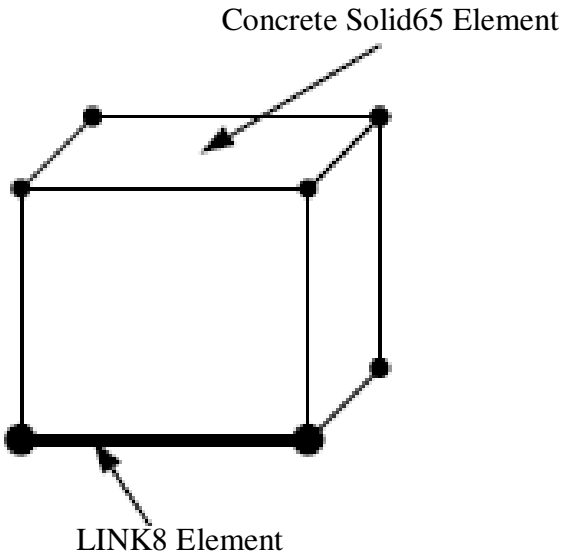

Figure 4.5
Concrete solid and link elements

Both crushing and cracking failures can be accounted for when modeling concrete with element type SOLID65. ANSYS uses the inputted compressive and tensile strengths to define the failure surface. Elements will crack whenever the principal tensile stress in any direction lies

outside this failure surface. Once the element cracks, the elastic modulus parallel to the principal tensile stress is set to zero. Crushing will occur when all principal stresses are compressive and lie outside the failure surface. Once an element crushes, the elastic modulus is set to zero in all directions, and the element ceases to contribute to the results.

The criterion for failure of concrete due to a multiaxial stress state can be expressed in the following equation according to William and Warnke (1975). If equation 4.2 is satisfied, the material will crack or crush.

$$\frac{F}{f_c} - S \geq 0 \qquad \text{Eq. 4.2}$$

F = a function of the principal stress state (σxp, σyp, σzp)

S = failure surface expressed in terms of principal stresses and five input parameters ft, fc, fcb = 1.2*fc , f1 = 1.45*fc and f2 = 1.725*fc

fc = uniaxial crushing strength and σxp, σyp, σzp = principal stresses in principal directions

Figure 4.6 below shows the 3D failure surface for states of stress that are biaxial or nearly biaxial. Cracks can be visualized in the integration points or at the centroid of each Solid65 element cracked and will appear as a sign on the plane perpendicular to the principal stress causing it, as illustrated in figure 4.7.

4.3 Modeling of Prestressing Strands

Equations 4.3 and 4.4 were incorporated into ANSYS to model a stress-strain curve for the 7-wire-low relaxation prestressing strands, according to the Precast/Prestressed Concrete Institute Design Handbook (PCI, 2005), illustrated in Figure 4.8

$$\varepsilon_{ps} \leq 0.0086 : f_{ps} = 28{,}500\varepsilon_{ps}(ksi)$$

$$\varepsilon_{ps} > 0.0086 : f_{ps} = 28{,}500 - \frac{0.04}{\varepsilon_{ps} - 0.007}(ksi)$$

. Eqs. 4.3 and 4.4

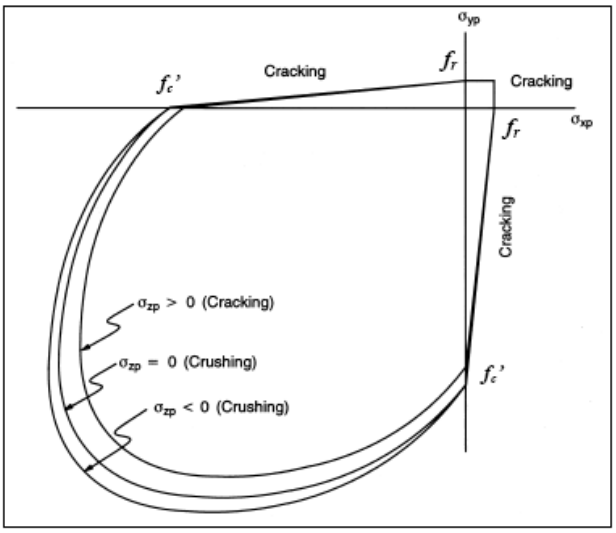

Figure 4.6
3D failure Surface for Concrete

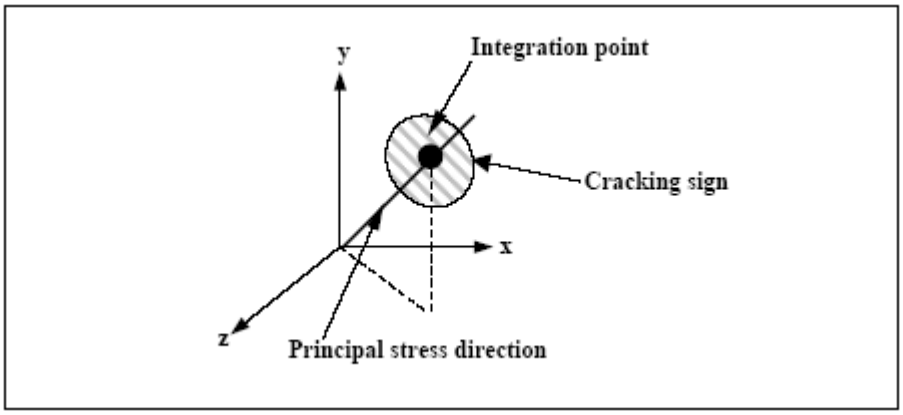

Figure 4.7
Cracking Sign

LINK8 elements were used to model the strands, connected to the concrete elements through their nodes, as illustrated in figure 4.9. This element type has the followings characteristics:

a. Two-node link element

b. Three degrees of freedom at each node

c. Capable of plastic deformation

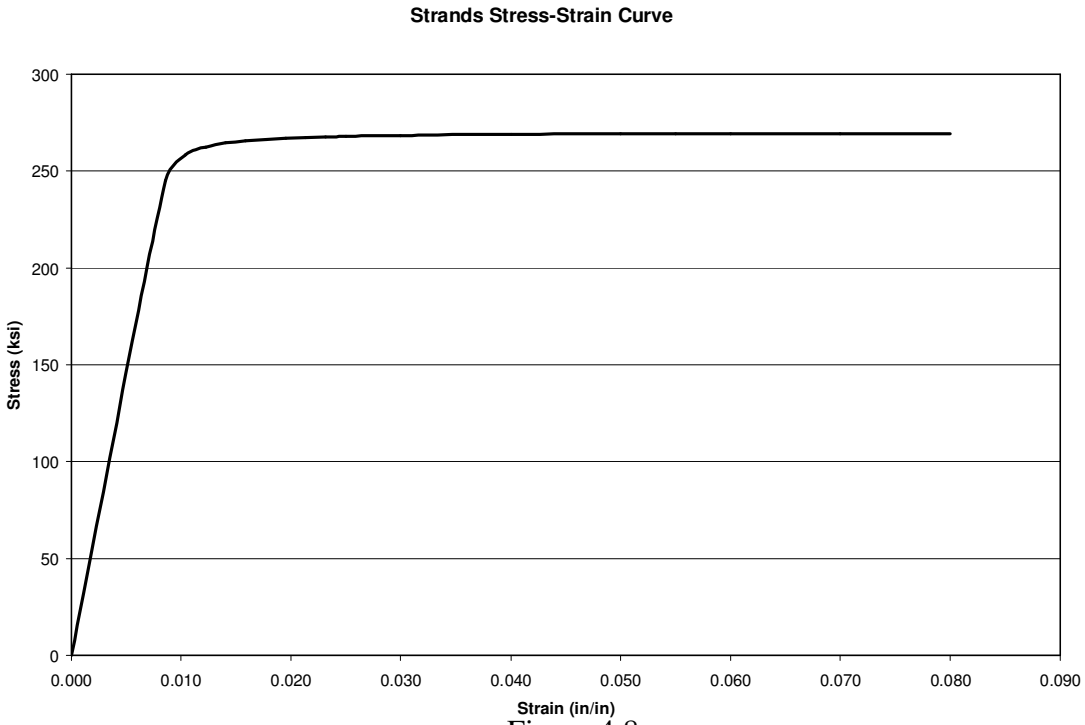

Figure 4.8
Stress-strain curve for reinforcing steel

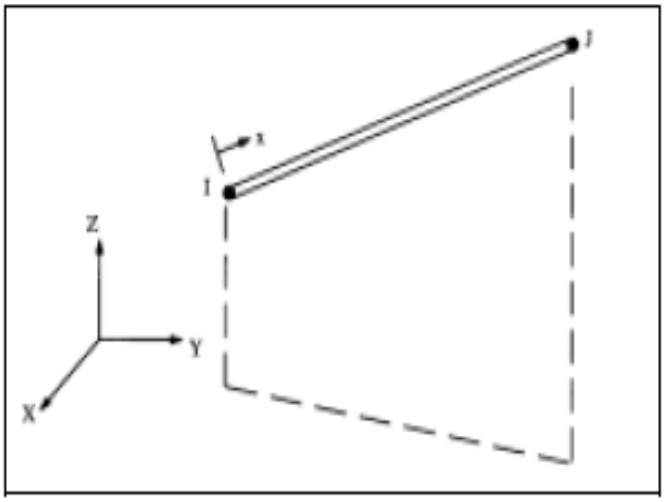

Figure 4.9
LINK8 – 3D reinforcing solid element (ANSYS 7.1)

4.4 Structural Nonlinearity

Structural non-linearity can be grouped into three major types. The first one, changing of status, can be illustrated by cables such as tower guys that are either taut or loose at all times. The

second type is geometric non-linearity, like in a fishing rod which undergoes large rotations at times. The third type is material non-linearity, which occurs in most materials at different levels of importance, being evident in concrete. All three types were considered.

4.5 Non-Linear Solution

In non-linear analysis the total load applied to the model is divided into smaller load increments or load steps. At the end of each load step the stiffness matrix of the model is adjusted to reflect non-linear changes in the structural stiffness before proceeding to the next load step. For this stiffness adjustment ANSYS uses Newton-Raphson equilibrium iterations. In Newton-Raphson method, convergence is checked at the end of each load step with given tolerance limits. A comparison between element forces and applied loads is performed in order to check for convergence. The author used the Newton-Raphson method in this study. An illustration of this method is shown in figure 4.10.

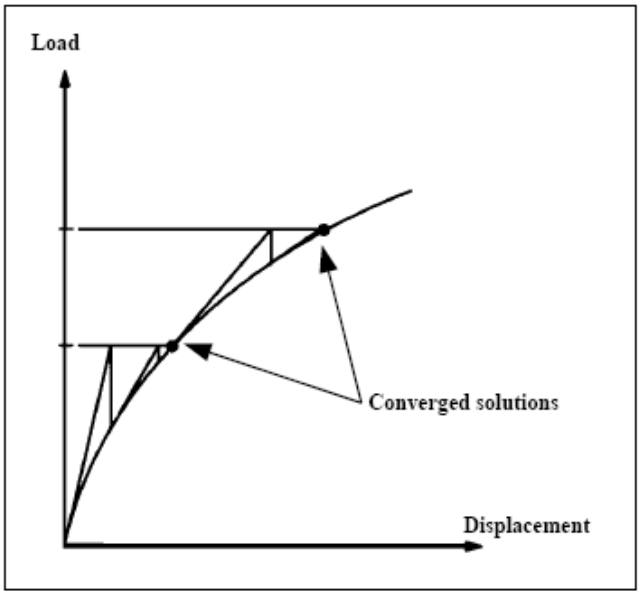

Figure 4.10
Newton-Raphson iteration in a single
degree of freedom nonlinear analysis

CHAPTER 5. MODEL VALIDATION

5.1 Simple Span Girder Modeling

The nonlinear finite element model was initially tested on a girder with dimensions similar to the ones in the prototype bridge experimentally tested, and its accuracy was verified. The girder was modeled using nonlinear concrete elements, and the analysis results were compared to the results of the Precast/Prestressed Concrete Institute Design Handbook (PCI, 2005) in order to establish a qualitative verification of the proposed model.

The analyzed girder is an AASHTO Type II 55 feet in length. The concrete compressive strength was modeled as 6 ksi. A total of eight seven-wire, low-relaxation strands with a yield and ultimate strength of 245 ksi and 270 ksi, respectively, were used as the reinforcement. The cross-sectional dimensions (in inches) of the modeled girders are shown below in figure 5.1.

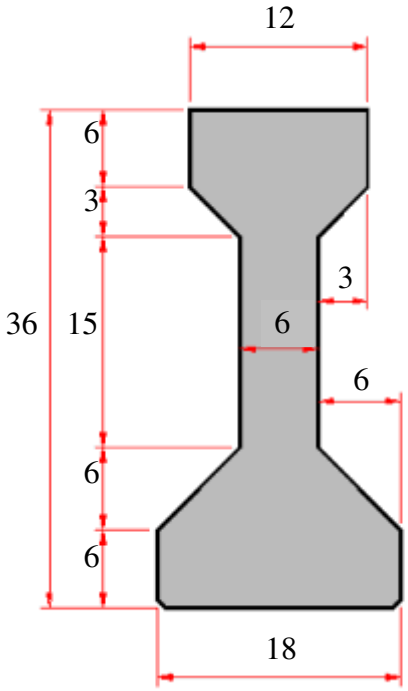

Figure 5.1
AASHTO girder type II

Figure 5.2 illustrates the support boundary conditions for the girder. The stress concentration problem generated by reaction loads and prestressing force at the ends was addressed by making the

girder elements linear at the supports, thus avoiding early divergence due to premature crushing or cracking around the nodes at the supports. This was also done because end girder performance was not a topic of relevant interest in this study.

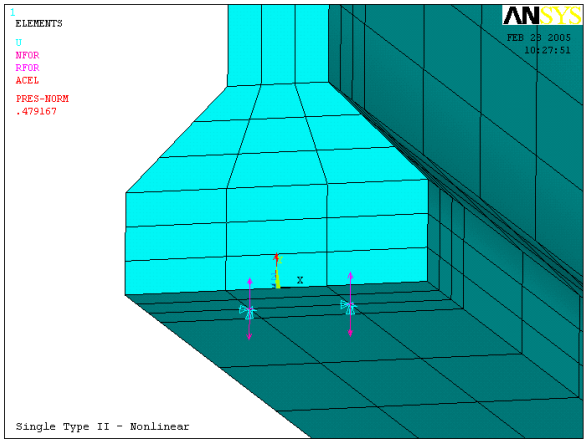

Figure 5.2
Boundary conditions at the supports

Figure 5.3 shows the steel plate modeled at the midspan to reduce the stress concentration caused by the applied load. The loads were applied to the steel plate, which consequently transferred them, uniformly distributed, to the concrete elements. Without the steel plate the concrete elements experienced high concentrated stresses and resulted in early cracking, which generated early divergence.

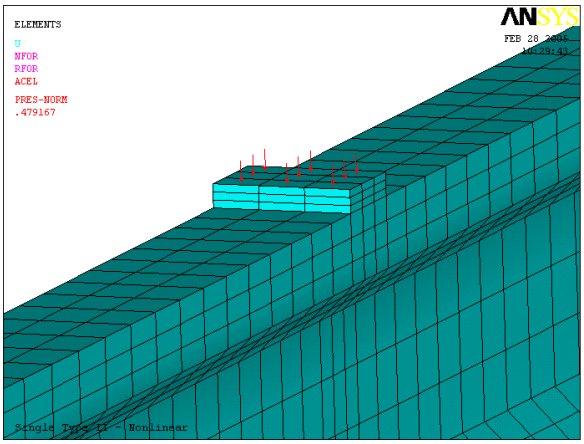

Figure 5.3
Steel plate at the midspan

Figures 5.4 and 5.5 show the girder stress distribution when only self-weight and prestressing forces are acting on it. As expected, the prestressing force in the tendons at the bottom of the girder causes it to hump upwards, resulting in tension stresses at the top and compression at the bottom. Figure 5.5 shows the end of the girder where the stress concentration creates very high stress values. There are a few practical ways recommended to decrease these values in practice; however, these high values are not relevant to this study since the nonlinear part of interest is modeled around the midspan.

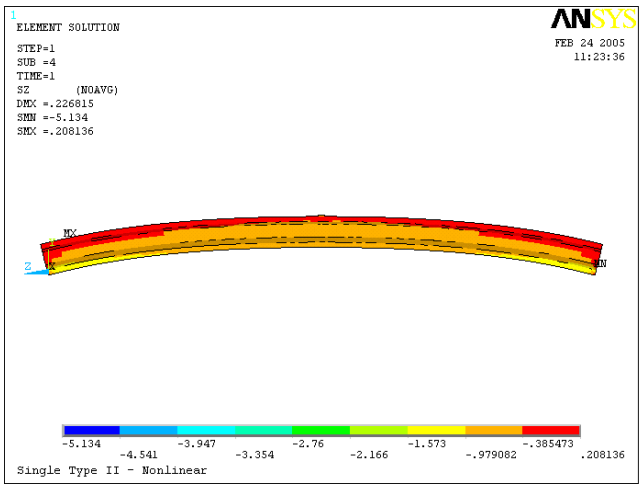

Figure 5.4
Girder stress distribution before vertical load

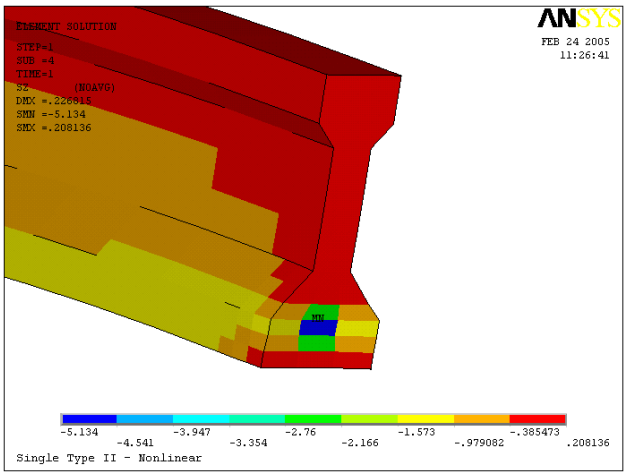

Figure 5.5
Girder end stress distribution before vertical load

A few different cases were analyzed in these simply supported girder analyses, aiming at adjusting the meshing sensitivity and the length of the nonlinear portion of the girder. It was found in the meshing study that element lengths of 4 in long with a length ratio increment of 3 toward the ends of the girder was adequate for the analyses. It was also found that 500 in was satisfactory for the length of the nonlinear portion of the girder. Of the remaining 130 in, 65 in at each end were kept linear.

Initial cracks occurred when the vertical load value was approximately 30.4 kips. Failure took place when the load level was between 35.4 kips and 49 kips for different cases, while the ultimate load result calculated according to the PCI Design Handbook (PCI, 2005) resulted in 44.1 kips. Failure occurred in different cases when the stress level in the tendons was between 219 ksi and 267 ksi, while the maximum deflection was between 0.96 in and 4.4 in. The difference in the cases analyzed was produced by the freedom to deform experienced by nonlinear elements. The more confined the nonlinear concrete elements between linear elements, the earlier they caused the model to diverge.

Figure 5.6 shows the midspan deflection, nonlinear curve produced by the finite element model as a function of the applied load. Figure 5.7 shows the simply supported girder at its ultimate strength, where cracks have propagated throughout the whole cross-section causing the girder to fail.

Once the modeling techniques were verified through an individual girder, the 3D, full finite element, analytical models of the entire bridges for Parts I and II were developed. Preliminary runs for Part II have been performed using ANSYS 9.0. The deck, diaphragms, and edge stiffeners were modeled as nonlinear SOLID65 elements around the midspan, and as linear with SOLID45 elements at the ends; both types had fc' = 3.5 ksi. The strands were modeled as LINK8 elements

with 270 ksi strength. The prestressed girders were modeled as linear toward the supports and nonlinear around the midspan. Similarly, their linear portion was modeled using SOLID45 and the nonlinear using SOLID65; a concrete strength of 6 ksi was considered for all girders.

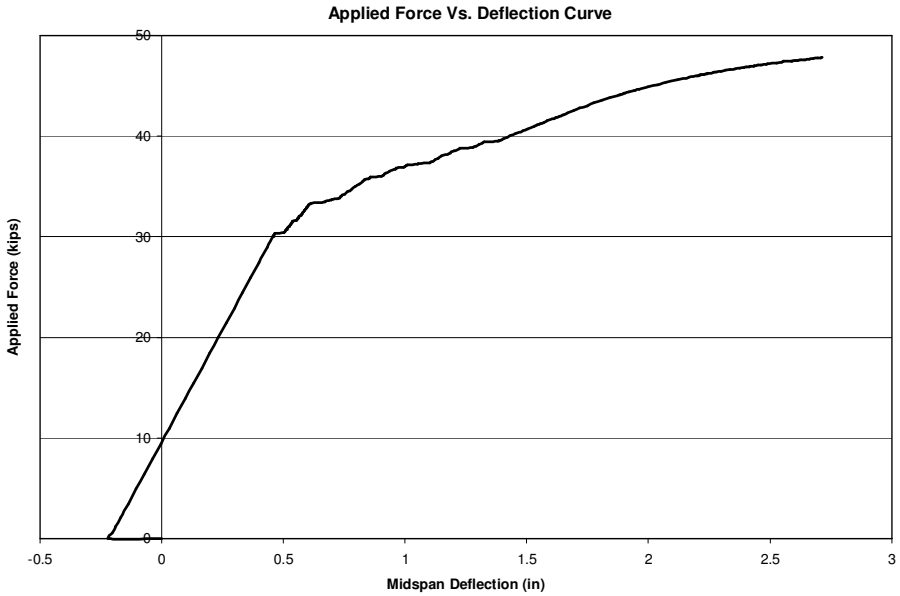

Figure 5.6
Deflection at the midspan vs. applied load

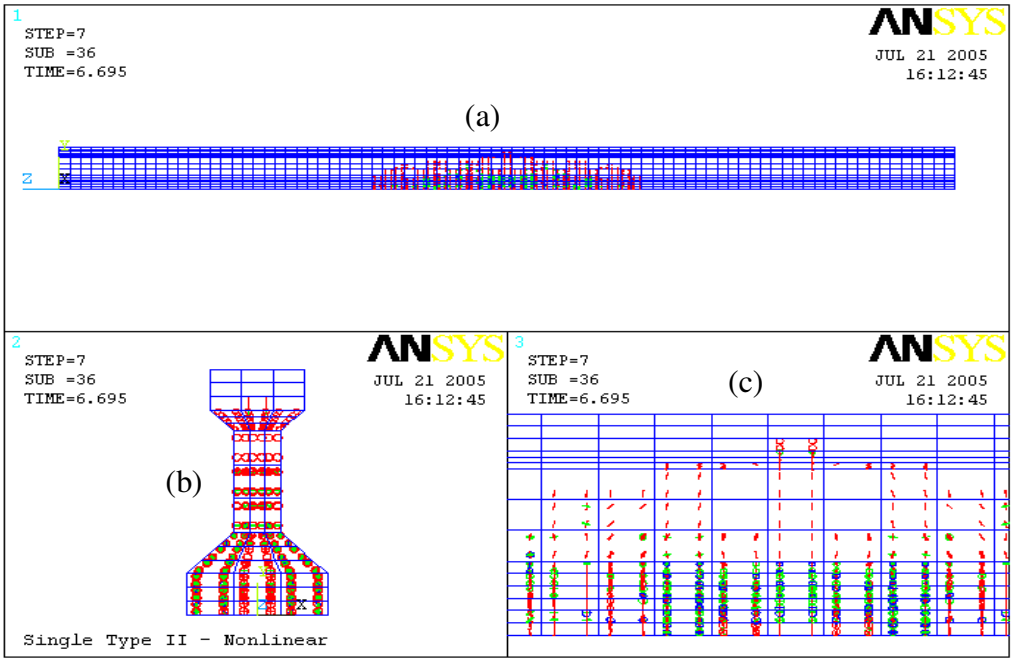

Figure 5.7
Cracks at failure - (a) Side view of girder, (b) Front view, (c) Midspan side view

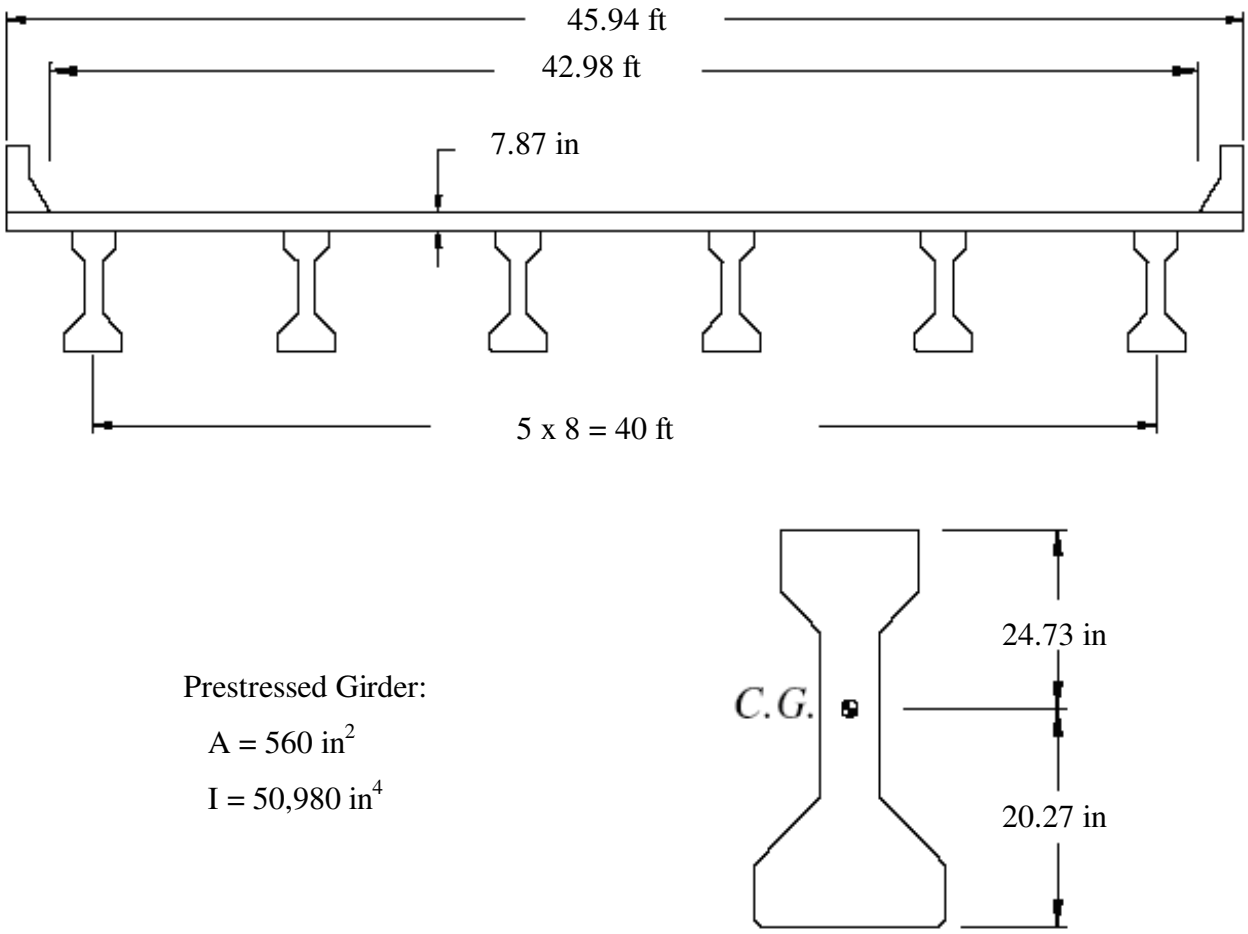

Figure 5.8
Cross-section of analyzed bridge

5.2 Entire Bridge Modeling

The model was further verified while investigating the effects of intermediate and end diaphragms in service range as presented below, with nonlinear results shown and discussed in Chapter 9. Load distribution factor (LDF) comparisons were made between the 3D full finite element model predictions and the LDFs calculated using AASHTO LRFD Bridge Design Specifications (2004) and AASHTO Standard (2002) equations. The bridge modeled is a 82 feet long simply supported slab-on-girder prestressed concrete straight bridge with six AASHTO Type III girders spaced eight feet from center to center. The dimensions of the analyzed bridge are

presented in figure 5.8. The concrete compressive strength is 8,700 psi for the prestressed girders and 4,000 psi for cast-in-place deck. The diaphragms' dimensions and their use are in accordance with the current practice in Louisiana and in agreement with the provisions in the LADOTD Bridge Design Manual (LADOTD, 2002) as discussed in chapter 6.

HS20 trucks were used to load the finite element models. These trucks do not represent actual vehicles, but can be considered umbrella loads. They have two units and three axles comprised of a highway tractor with a semi-trailer. The wheels attached to each of these three axles carry the same load. The front axle weighs 8 kips and the other two axles weigh 32 kips each. The spacing between the first and second axles is 14 ft. The spacing between the second and third axles, however, varies from 14 to 30 ft depending on what distance causes maximum load effects. The width of each of these three axles is 6 ft.

Three different bridge configurations were studied. Two design lanes were loaded at a time, with one HS20 truck each at two transverse loading positions, causing maximum moments in internal and external (INT and EXT) girders for each loading position (figures 5.9 and 5.10). Longitudinally they were positioned with their middle axles 30 inches away from the midspan. Load distribution results from the finite element simulations were compared to AASHTO Standard and AASHTO LRFD, then presented and discussed.

In Configuration 1 (NOED_NOID) the bridge was modeled according to the assumptions made in the AASHTO codes, which do not take into account the effects of diaphragms or edge stiffeners, as shown in figure 5.11. Configuration 2 (ED_NOID) simulates the same bridge with the addition of end diaphragms (EDs), shown in figure 5.12, while in Configuration 3 (ED_ID) the bridge was analyzed using EDs and one intermediate diaphragm (ID) located at the midspan (figure 5.13).

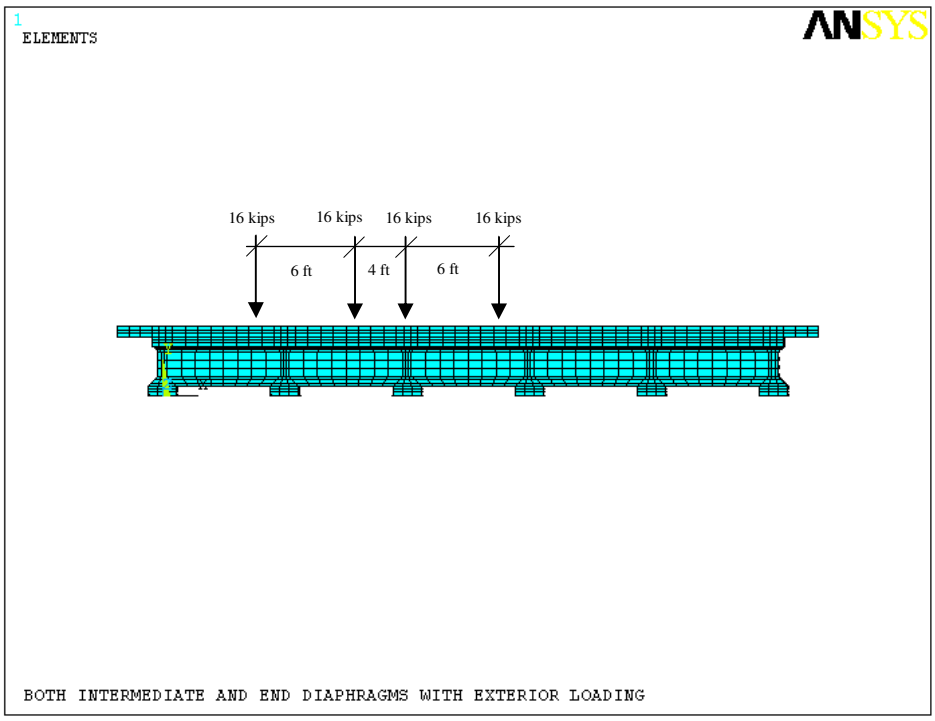

Figure 5.9
Interior girder loading

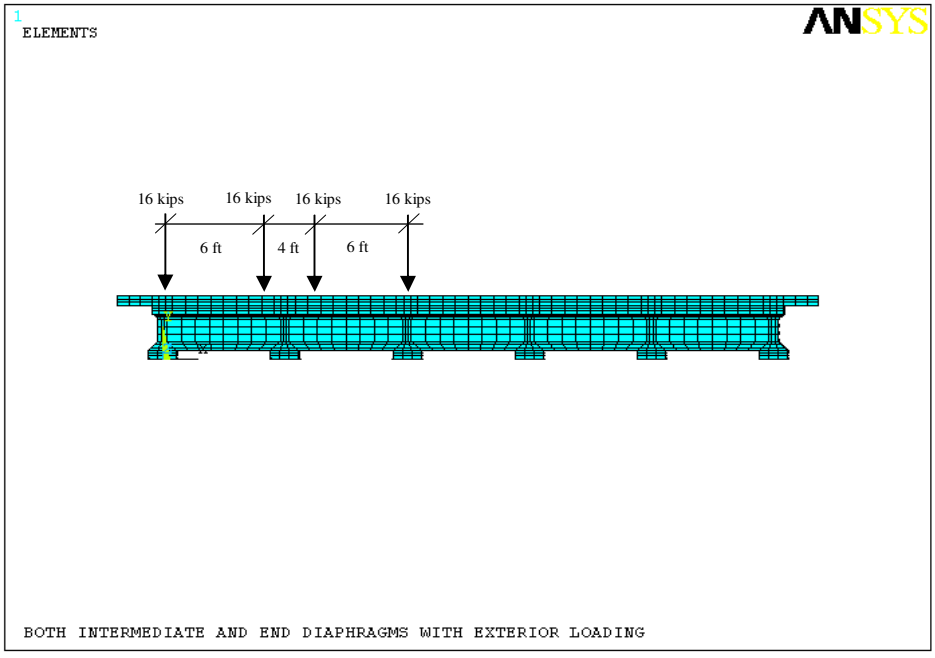

Figure 5.10
Exterior girder loading

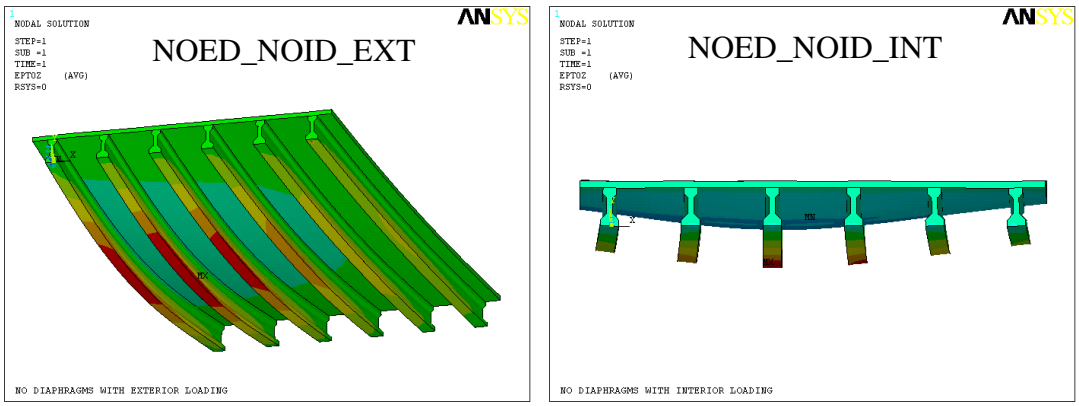

Figure 5.11
Bridge configuration 1

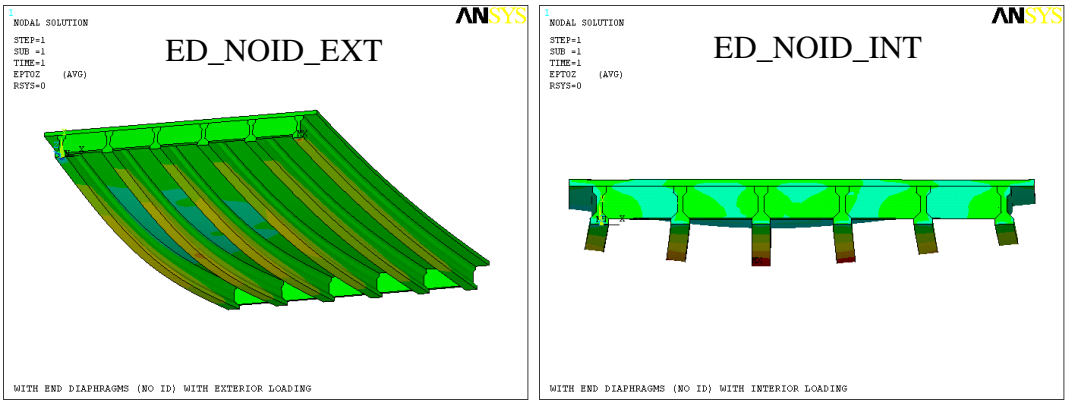

Figure 5.12
Bridge configuration 2

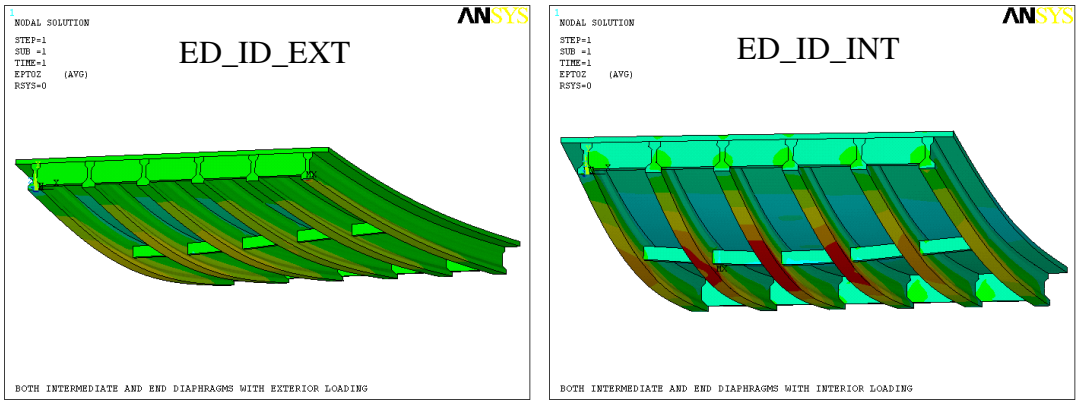

Figure 5.13
Bridge configuration 3

5.3 Verification of Results

Plots of the LDFs calculated in this preliminary full 3D finite element analysis of the bridge described above are presented in figures 5.14 and 5.15. The calculated results were then compared

considering LDFs calculated according to AASHTO LRFD as 100% and all other calculated values as fractions of them for each girder. These LDF values are presented as percentages relative to AASHTO LRFD results in table 5.1. These comparisons are made for exterior and interior loading cases. Percentage comparisons between Configurations 2 and 3 are discussed, as well as the effect caused by the presence of intermediate diaphragms in the structures.

5.3.1 Exterior Loading

In this loading case the maximum interior LDF was found in girder 2 (figure 5.14) for Configuration 1 and its value was 88.7% of the AASHTO LRFD value (table 5.1). The maximum LDF for the exterior girder 1 in the same case was 87.9% of the AASHTO LRFD value.

The addition of EDs in Configuration 2 decreased the maximum interior LDF value in girder 2 to 85.5%, also decreasing the maximum exterior girder 1 LDF to 82.6%.

The addition of the intermediate diaphragm at the midspan caused a shift in the maximum LDF from girder 2 to the exterior girder 1, causing the maximum LDF value in girder 1 to increase from 87.9% in Configuration 1 to 92% in Configuration 3, getting closer to AASHTO LRFD (2004). The addition of the ID caused the LDF in the interior girder 2 to decrease from 88.7% in Configuration 1 to 76.6%.

AASHTO Standard (2002) LDF values were consistently higher than the AASHTO LRFD value (2004), being 15.9% larger for exterior girders and 7.9% larger for interior girders for both exterior and interior loadings.

5.3.2 Interior Loading

In Configuration 1 the maximum exterior LDF of 31.4% was found in girder 1 (table 5.1 and figure 5.15), while the maximum interior LDF of 81.8% in girder 3.

Configuration 2 produced no significant result in either the interior or exterior girders,

whose values are 31% and 81.4%, respectively.

The load distribution was more even in Configuration 3, increasing the LDF in the exterior girders and decreasing it in the most loaded interior ones. The maximum exterior LDF in girder 1 then became 45.1%, and the maximum interior LDF became 67.3% in girder 3.

The effectiveness of the intermediate diaphragm for load distribution in the bridge studied is shown to be twofold. Comparing Configuration 2 and 3, the more realistic ones from a construction standpoint, on one hand the ID presence decreases the maximum interior girder LDF by 8.9% and 14.1% for exterior and interior loadings, respectively. On the other hand, it increases the maximum exterior girder LDF by 9.4% and 14.1% for exterior and interior loadings, respectively. The LDF decrease in interior girders and respective increase in exterior girders are approximately of the same magnitude. Therefore, design moments calculated by using the LDF values produced in Configuration 3 are larger for exterior girders and smaller for interior ones.

From the preliminary model test above we can conclude that AASHTO Standard (2002) LDF values were consistently higher then AASHTO LRFD (2004) ones, being 15.9% larger for exterior girders and 7.9% larger for interior girders for both exterior and interior loadings.

AASHTO LRFD results over predicted the finite element results in interior and exterior loadings by 18.2% and 11.3%, respectively. These results show that AASHTO LRFD predictions are well within the admissible range.

The presence of end diaphragms produced no significant change from Configuration 1 in the maximum LDFs in either interior or exterior girders for interior loading, with value changes of 0.5% and 0.4%, respectively. For exterior loading, the changes were 3.2% and 5.3% for interior and exterior girders, respectively. Greater changes were observed with the addition of intermediate diaphragms when compared to Configuration 2 for interior loading. These maximum changes were

14.4% for interior girders and 14.1% for exterior ones. For external loading, these differences were 7.9% for interior and 9.4% for exterior girders. Further discussion and recommendations are presented in the next few chapters.

Once the results produced by model were verified in service ranges, the truck loads were increased to higher values in order to cause cracking of the concrete and a consequent, nonlinear response.

Table 5.1
Percentage values relative to AASHTO LRFD

LDF RESULTS RELATIVE TO AASHTO LRFD (%)							
	Girder #	1	2	3	4	5	6
AASHTO LRFD	AASHTO Standard	115.9	107.9	107.9	107.9	107.9	115.9
	NOED_NOID_EXT	87.9	88.7	70.4	37.2	14.3	4.3
	ED_NOID_EXT	82.6	85.5	67.6	38.1	17.9	11.2
	ED_ID_EXT	92.0	76.6	59.7	36.6	24.8	13.9
AASHTO LRFD	NOED_NOID_INT	31.4	66.9	81.8	69.2	37.8	12.3
	ED_NOID_INT	31.0	66.4	81.4	69.3	36.4	14.9
	ED_ID_INT	45.1	61.0	67.3	62.7	40.8	24.1

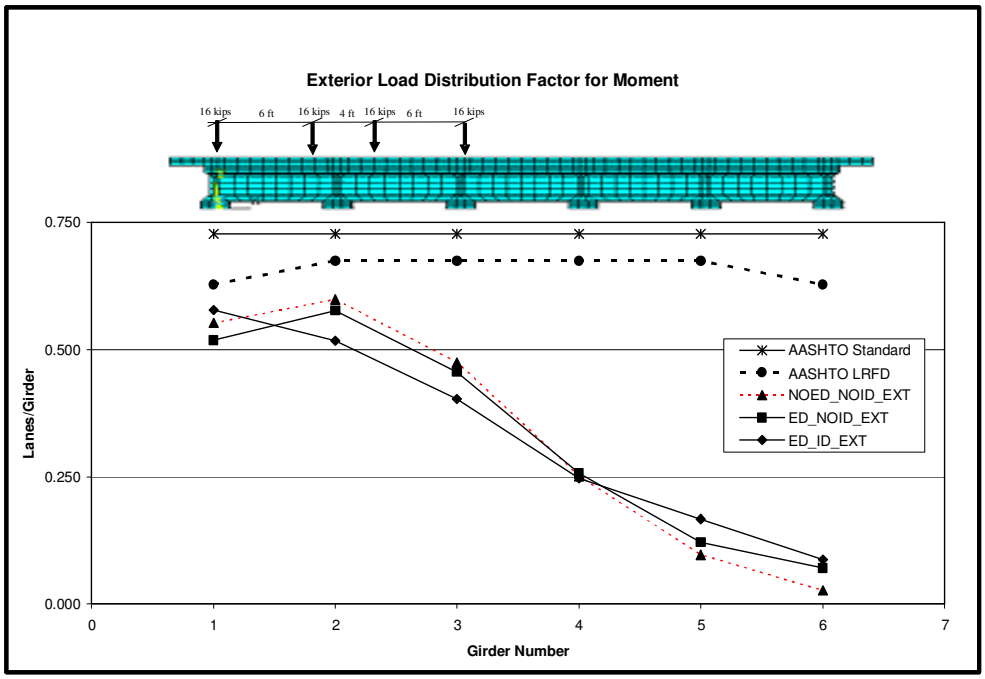

Figure 5.14
LDFs for exterior loading

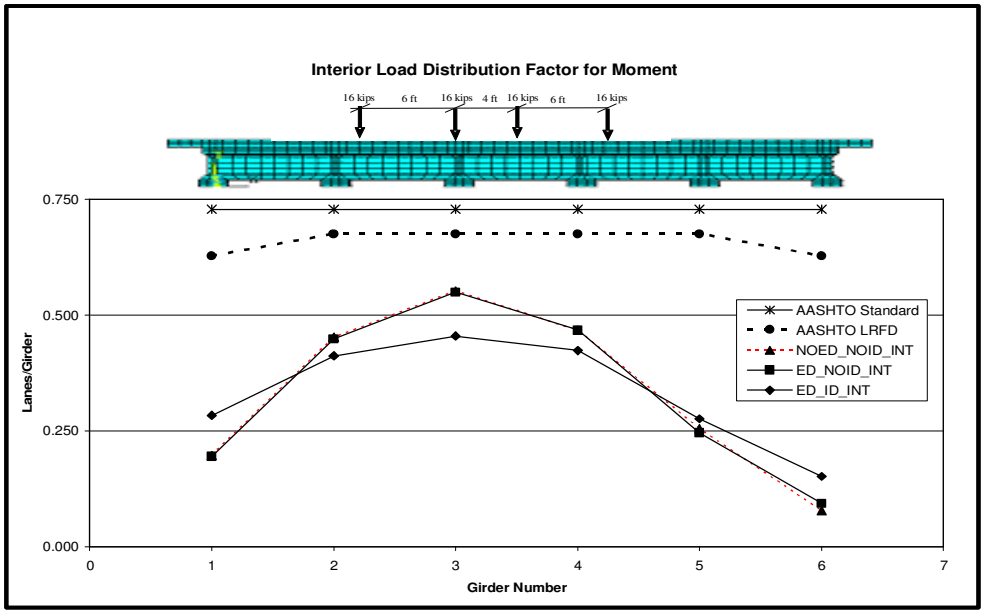

Figure 5.15
LDFs for interior loading

CHAPTER 6. ANALYTICAL ASSESSMENT OF INTERMEDIATE DIAPHRAGMS

6.1 Introduction

As stated earlier, reinforced concrete intermediate diaphragms (IDs) are still used in prestressed concrete (PC) girder bridges in Louisiana. Some of the advantages of providing IDs are disputed in the bridge engineering community. The use of IDs increases the cost and time of construction and there is no consistency in the practice of providing IDs among various states and codes of practice. The overall effectiveness of IDs as well as their need in prestressed concrete bridges is unclear.

In this chapter the assessment of intermediate diaphragm's effectiveness for prestressed concrete bridges is made. The objectives of this study were to:

a) assess the need of reinforced concrete (RC) IDs in PC girder bridges and to determine their effectiveness,

b) search for a possible alternative steel diaphragm configuration that could replace concrete diaphragms if necessary.

Through a survey questionnaire and review of the Louisiana Department of Transportation and Development (LADOTD) Bridge Design Manual (2002), relevant information was obtained regarding ID practices in Louisiana. Questions and answers were summarized and discussed below, and the full survey sheets are included in Appendix A.

Through the LADOTD data base for all state bridges, and from direct interaction with district engineers, several of the bridges of interest for this study were selected for field inspection. From these field trips to various bridge locations, much information has been acquired from the bridges themselves, as well as from LADOTD district engineers.

Systematic parametric studies for various bridge configurations were analyzed through simplified and solid finite element models, as discussed in Chapter 3. These studies represent a

wide range of bridge geometries with different parameters. This study was performed on right and skewed bridges, both simply-supported and continuous. A reduction factor that could be multiplied by the AASHTO load distribution factor (Standard, 2002 and LRFD, 2004) to account for the influence of the diaphragm in load distribution was developed. A finite element analysis was carried out using 3D solid models to assess the effectiveness of various diaphragms in protecting the girders against lateral impact, and to determine the design forces in the steel bracing members during construction of the deck.

Results from parametric studies indicated that several parameters such as skew, span length, spacing, stiffness of diaphragm and girder have different levels of influence on the effectiveness of diaphragms in live load distribution for bridges. Correction factors were developed which could quantify the ID influence on load distribution. A complete list of these factors can be found at "Assessing the Needs for Intermediate Diaphragms in Prestressed Concrete Bridges.", LTRC Project No. 03-3ST, LA State Project No. 736-99-1134, 2006.

The analytical results obtained were verified by load testing a prestressed concrete bridge. This bridge was selected by an inspection team comprised of personnel from FHWA, LADOTD, and the LSU research team and is located over Cypress Bayou on LA 408 East, in LADOTD District 61 in Baton Rouge, Louisiana. A comprehensive instrumentation and loading scheme for the bridge test is presented and illustrated later in chapter 7.

6.2 Current Practice in Louisiana

As discussed earlier, the current diaphragm policy in Louisiana (LADOTD, 2002) is specified as:

a) span $\leq$ 50 ft requires no intermediate diaphragm

b) 50 ft < span $\leq$ 100 ft requires one intermediate diaphragm

c) span > 100 ft requires two intermediate diaphragms

The LADOTD Design Manual (2002) determines that when no intermediate diaphragms are used, a note shall be placed in the plans requiring the contractor to provide temporary bracing during the deck pour. Intermediate diaphragms for skewed spans are usually constructed perpendicular to the girder webs by use of partial span width or stepping the diaphragms. For flared or skewed spans less than about 20°, diaphragms may be constructed at a skew to the web. Diaphragms details are shown in figures 6.1 to 6.6.

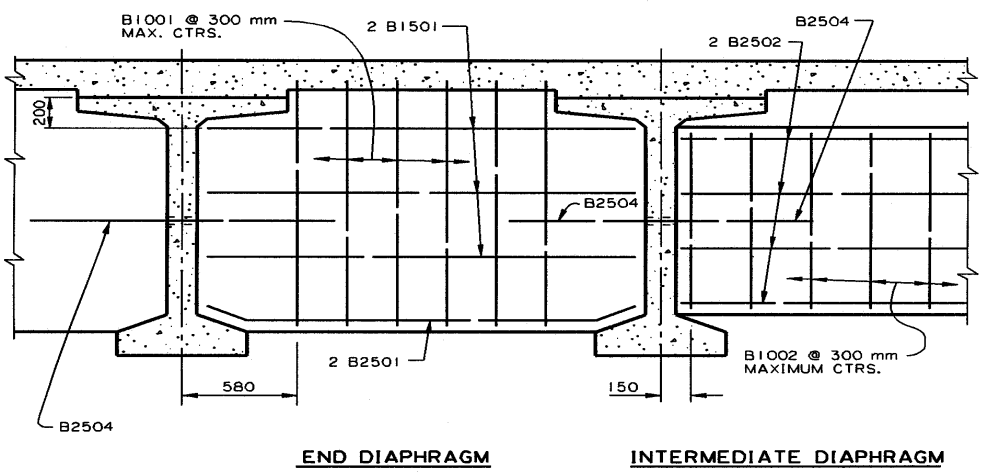

Figure 6.1
Typical detail of CIP diaphragm in Louisiana

6.3 Survey Questionnaire

In order to gather information on ID practices in Louisiana, a questionnaire was created (Appendix A). The first question asked if the district had ever built a precast prestressed slab-on-girder concrete bridge that required the use of IDs. The second was on the district's satisfaction with the use of reinforced concrete diaphragms in all stages. The third was centered on districts' conformity with the LADOTD manual. The fourth related to the consideration of steel IDs. The fifth inquired about the support for the use of steel IDs if justified by research. The sixth was about the complete elimination of IDs if justified by research. Finally, the seventh question asked if any damage or failure related to IDs had been observed. Table 6.1 summarizes the answers obtained.

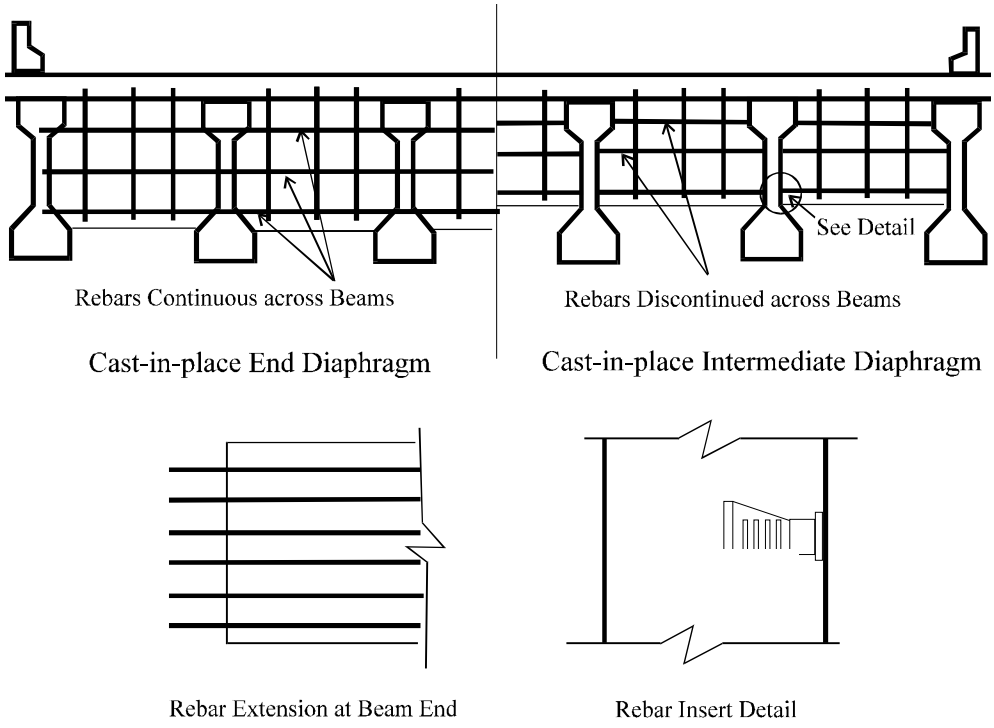

Figure 6.2
Sketch of typical diaphragm detail in Louisiana

According to the answers to the survey, major considerations were given to questions 5 and 6. In question 5, two relevant issues of concern were discussed. The first is the connection between steel diaphragms and concrete girders. If supported by the findings of this study, the proper type of connections will also be proposed along with the recommendation. The second relevant point was the potential maintenance problem due to corrosion of the members. This problem could be addressed if the steel used for the diaphragms had no potential for corrosion, thus conforming to the concern of the LADOTD engineers. Although this point is of great importance, it is beyond the scope of this study.

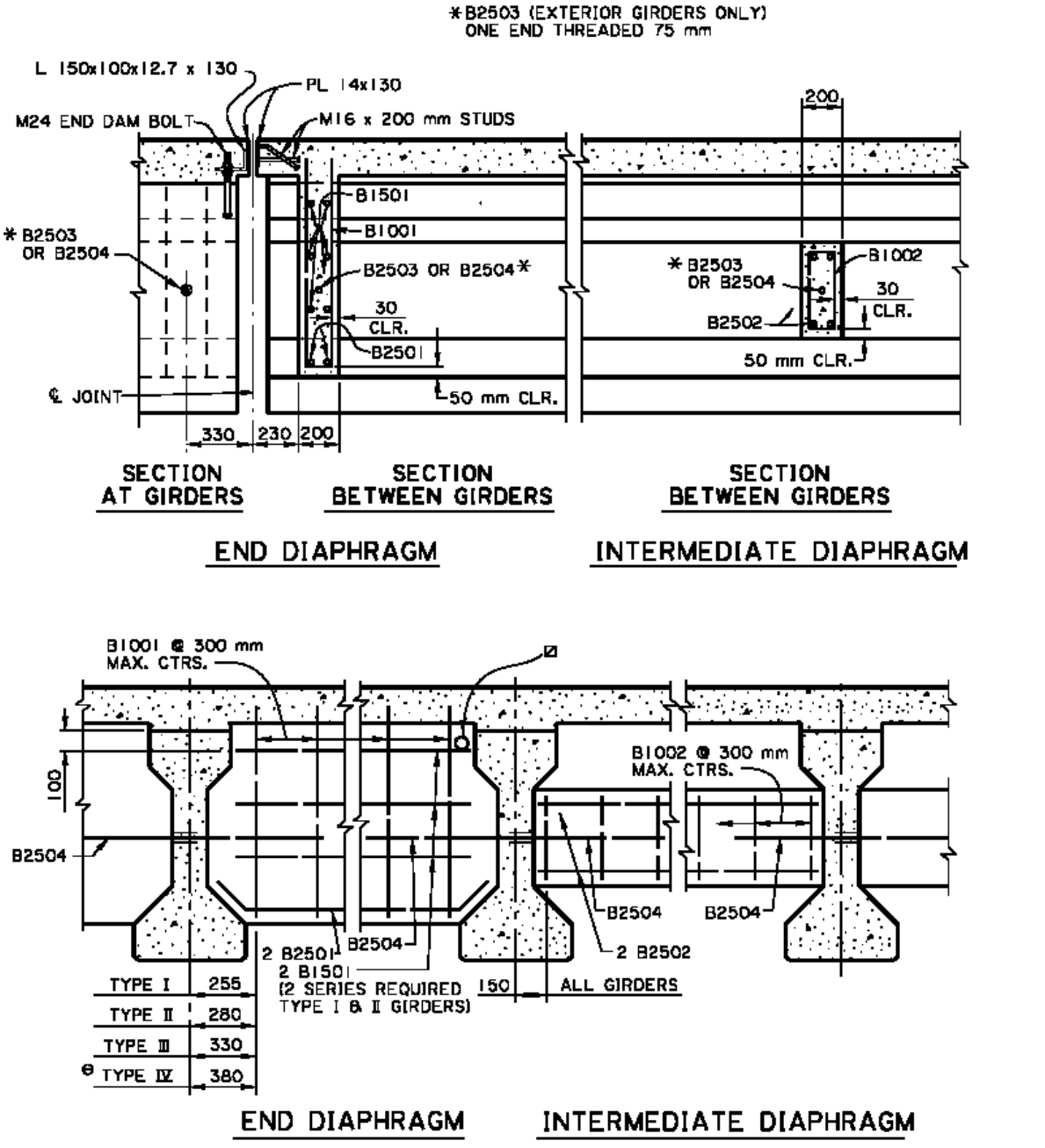

⊖ INCLUDES TYPE IV-MODIFIED

NOTES:

SPANS >15 m REQUIRE ONE INTERMEDIATE DIAPHRAGM.
SPANS >30 m REQUIRE TWO INTERMEDIATE DIAPHRAGMS.

Ø 75 mm ⌖ VENT HOLE IN EACH END DIAPHRAGM WHERE INUNDATION BY FLOOD IS POSSIBLE.

TYPE I-IV (END & INTERMEDIATE DIAPHRAGMS)

Figure 6.3
Current LADOTD intermediate and end diaphragm dimensions for I girders

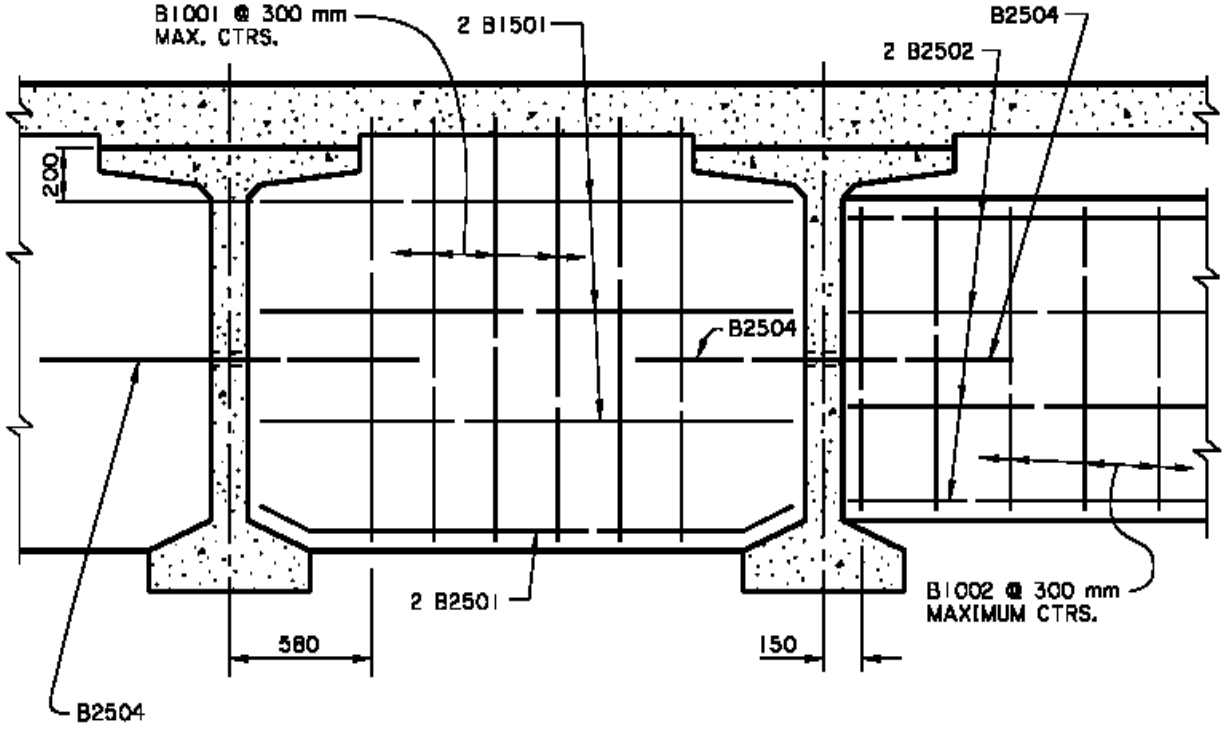

TYPICAL DIAPHRAGM DETAILS
(TYPE BT)

NOTE:

DETAILS NOT SHOWN ARE SIMILAR TO
DETAILS SHOWN ON SHEET 1 OF 8.

Figure 6.4
Current LADOTD intermediate and end diaphragm dimensions for BT girders

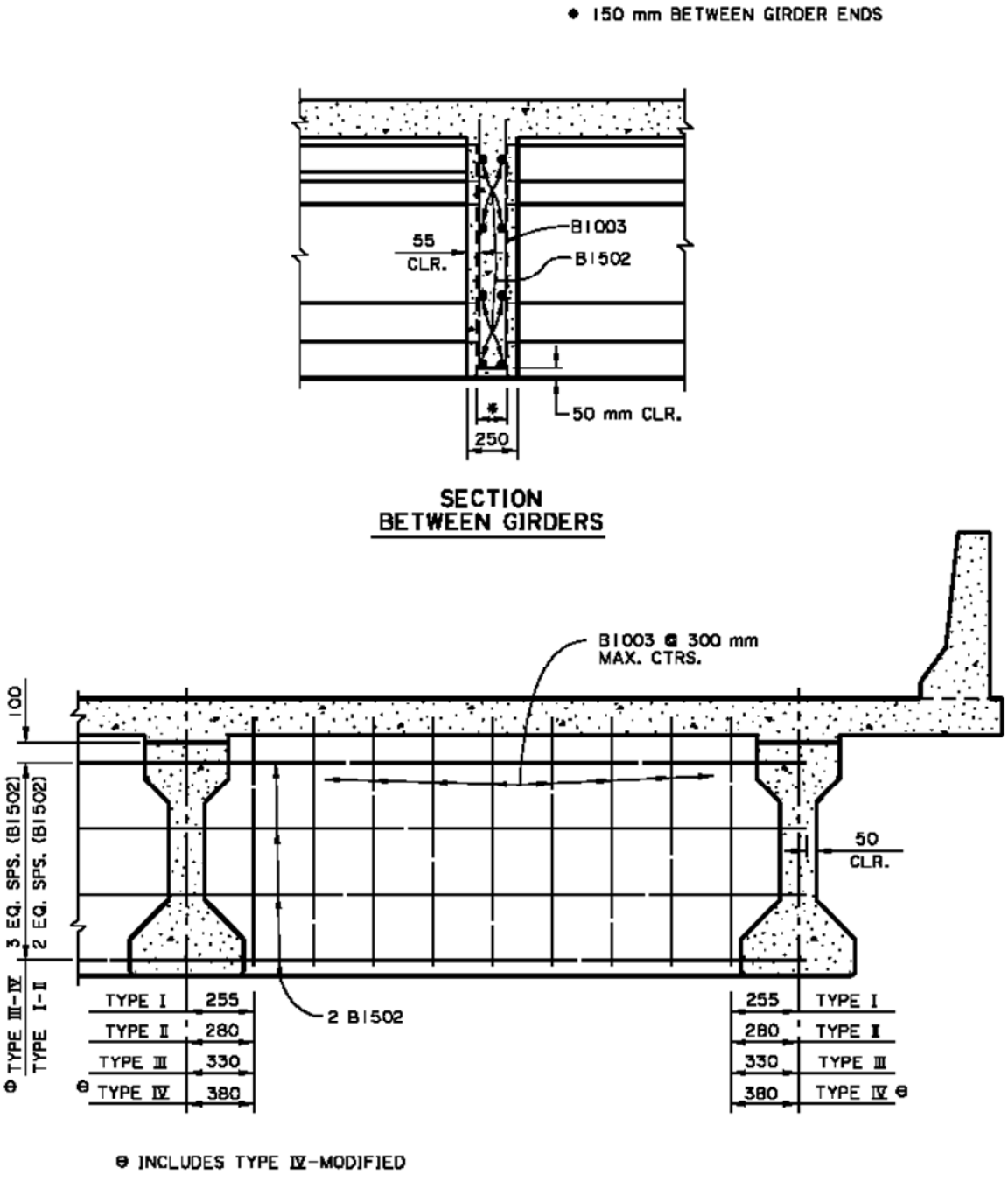

Figure 6.5
Current LADOTD continuity diaphragm dimensions for I girders

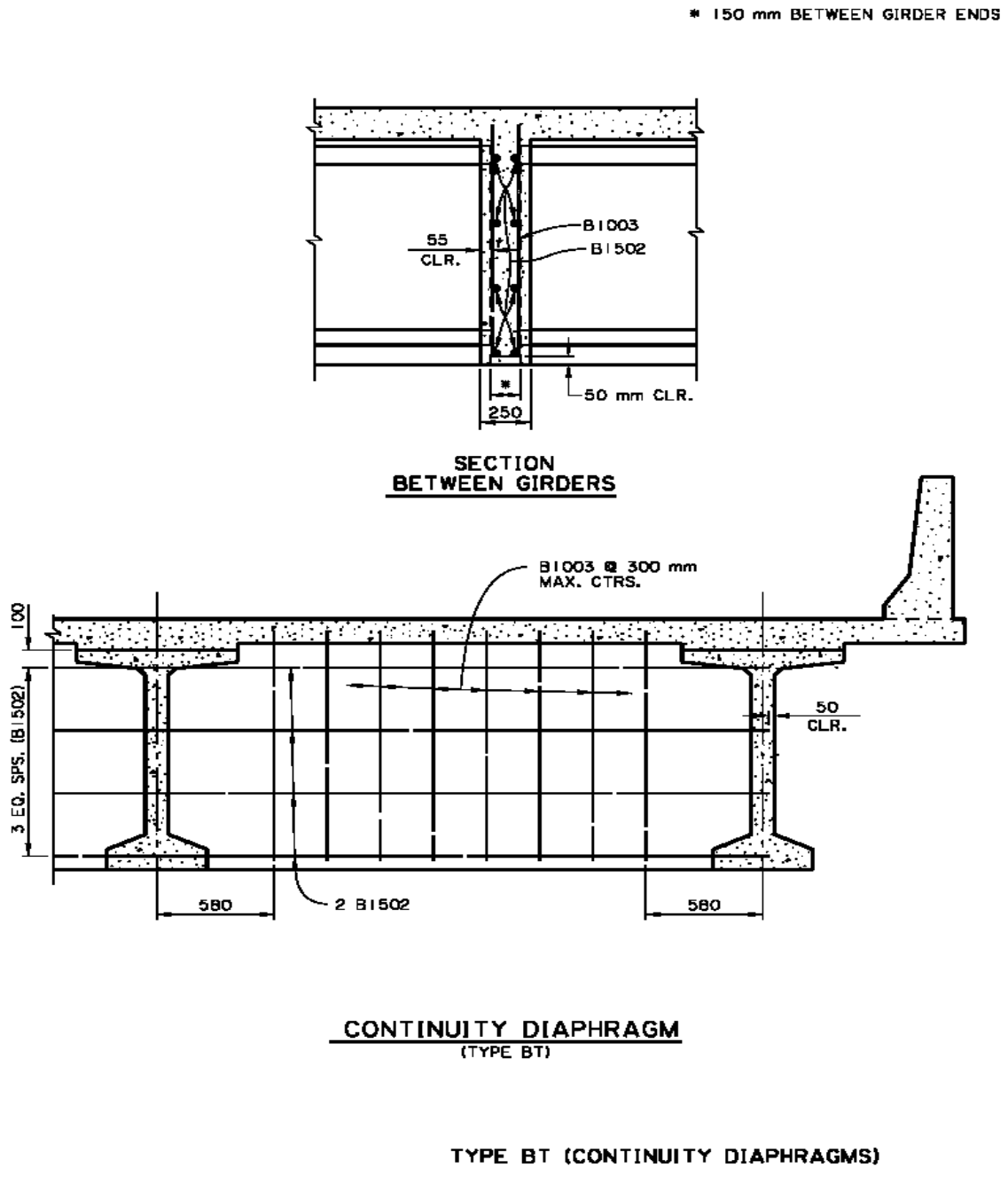

Figure 6.6
Current LADOTD continuity diaphragm dimensions for BT girders

In question 6, the complete elimination of IDs would be accepted by all districts as long as two scenarios are investigated and justified by research: lateral impact due to over-height motor vehicles and lateral stability of girders during construction. Dynamic lateral impacts were simulated using 3D full finite element models. The effects of the impact were investigated considering the

whole bridge structure in various bridge configurations, such as different lengths, girder spacing, number and position of the diaphragms, etc. The lateral stability of girders during construction was investigated and appropriate recommendations were made.

Table 6.1
Intermediate diaphragm survey answers summary

Districts Answers Summary							
	1	2	3	4	5	6	7
District 2	Yes	Yes	Yes	No	*	Yes**	Yes
District 3	Yes	Yes	Yes	*	Yes	Yes	Yes
District 4	Yes	Yes	*	Unknown	No	Over Streams	No
District 5	Yes	Yes	*	*	No	No	*
District 58	Yes	Yes	Yes	No	No	Yes***	No
District 61	*	*	*	*	*	*	*
District 62	*	Yes	*	*	Yes	Yes	No
District 7	*	*	*	*	*	*	*
District 8	Yes	Yes	Yes	No**	Yes	Yes	Yes

* No answer
** Personal answer
*** With construction phase analysis

6.4 Field Investigation

Field investigation and evaluation of typical IDs used in concrete highway bridges in Louisiana were conducted. This investigation assessed the overall bridge condition and focused on areas where cracks are more prone to develop. Some of the bridges inspected were built according to the former LADOTD manual, in which IDs and end diaphragms had exactly the same dimensions. This means these diaphragms extend from the middle of bottom flange to the bottom of the deck. Other diaphragms were built conforming to the new recommendations, in which the IDs are connected only to the web of adjacent girders.

Interestingly, some of the diaphragms of inspected bridges, both end and intermediate, did not conform to any known specification. Some IDs were not connected to the slab, stopping a few inches from it. As for the end diaphragms, some were not connected to the slab and their bottoms did not end at the specified position, ending at the top of the girders' web. After a first comparison, no definite correlation has been established, except that no difference in performance or structural behavior has been observed between the bridges that followed the manuals and the ones that did not.

Information was gathered from three sources: inspection records from existing LADOTD files, field visits to various bridges, and interviews with experienced LADOTD engineers. Some pictures that illustrate the observations made during field investigations are presented below. These pictures reveal the great variety of forms and shapes of diaphragms that were found throughout the state. The types of IDs encountered during the field trips, as well as the damages observed in the bridges along with miscellaneous observations, are presented below.

6.4.1 Types of IDs Observed

In this phase of the study, several bridges in all 9 LADOTD districts were inspected with the purpose of evaluating the types of IDs used. The criteria of selection for these bridges involved location, recorded damages, skew angle, year of construction, presence of IDs, and type of girders.

The location of the structures determined the amount of traffic to which they were subjected and their accessibility in relation to other selected bridges. Bridges with more traffic were preferred because of their straining conditions, which lead to a better exposure of the actual effects of IDs. This exposure is also more evident as structures age; therefore, many older bridges were selected as well.

Damages recorded in the inspection files were also an important source of information during the selection process. The damages sought after were deck cracks, ID cracks, and most

importantly the cracks caused in girders due to lateral impacts by over-height trucks. According to the scope of this study, only AASHTO types II, III, and IV and BT-72 pre-stressed concrete girders were considered. Different skew angles were selected in order to correlate them to ID performance.

Although the LADOTD bridge design specifications manual suggested only one ID type before its revision and one after, a total of 6 different types were found among the bridges visited. These types are shown in figures B1 to B6 in Appendix B; note that ID type II is monolithic with the deck and ID type III is not. The locations of the bridges with their respective ID types and other study related information are listed in table 6.2. ID Type I is the one recommended by the current manual, while ID type II was recommended previously.

6.4.2 Types of Damage Observed

Some of the most common types of damage encountered during field inspections are presented in figures B7 to B14 in Appendix B. These damages are multiple cracks on decks, cracked ID bottom tips at external girders, cracked cold joints between IDs and girders, and spalled concrete on girders due to lateral impact by over-height trucks. Some spallings were deep enough to expose some of the pre-stressing tendons, even revealing a few broken tendons in some cases.

6.4.3 Miscellaneous Observations

During the field investigation phase of this study, a few peculiarities related to the use of diaphragms were observed.

a) For some of the bridges inspected, the internal and external girders were of different types. In these cases, two different ID configurations were observed. In the first configuration, the ID would taper in a straight line from the smaller girder to the larger. In the second configuration, it would come horizontally towards the external girder and drop suddenly, forming a sharp tip that was cracked most of the time due to the high stress concentration. They are illustrated in figures B15 and B16.

Table 6.2
Bridge Classification by ID Type

ID TYPE	BRIDGES LOCATIONS	DISTRICT	MAX. SPAN (ft.)	YEAR BUILT
I	I-10 over Loyola Ave	2	85	1971
	LA 33 over I-20	5	110	1991
	LA 562 over Macon Bayou	58	-	-
	LA 577 over Crockett Point	58	-	-
	I-10 over LA 27	7	under construction	
	I-49 over LA 498	8	106	1992
II	I-10 over Williams Blvd	2	87	1968
	US 90 over LA 182	2	-	-
	US 90 over LA 316	2	90	1980
	I-10 over Essen Ln	61	90	1974
	I-10 over Bluebonnet Rd	61	95	1974
	I-10 over Siegen Ln	61	95	1974
	I-49 over LA 119	8	106	1985
III	LA 154 over I-20	4	80	1964
	US 80 over I-20	4	75	1964
	I-20 over LA 17	5	75	1970
	LA 133 over I-20	5	75	1968
	I-20 over LA 137	5	70	1968
	LA 577 over I-20	5	93	1971
	LA 1026 over I-12	62	70	1970
	LA 1032 over I-12	62	50	1970
	LA 441 over I-12	62	70	1968
	LA 442 over I-55	62	70	1970
	LA 1064 over I-55	62	70	1970
	LA 63 over I-12	62	77	1975
	US 51 over I-12	62	70	1995
	LA 40 over I-55	62	80	1970
	I-10 over LA 26	7	50	1965
IV	I-49 over LA 182	3	90	1971
	LA 183-SR over I-49	3	95	1978
	US 90 over LA 83	3	-	1978
	US 80 over I-220	4	111	1985
	LA 15 at Turkey Creek	58	-	-
	I-10 over Highland Rd	61	73.5	1974
	I-12 over LA 21	62	77	1975
	I-10 over US 90	7	75	1967
	I-210 over Louisiana St	7	86	1975
	I-210 over Ryan St	7	98	1975
	I-49 over LA 120	8	87	1988
	I-49 over LA 3276	8	-	-
	I-49 over LA 181	8	77	1985
	LA 8 over I-49	8	90	1984
V	I-10 over LA 182	3	56	1968
VI	US 90 over I-55	62	-	-

b) In the second configuration, it would come horizontally towards the external girder and drop suddenly, forming a sharp tip that was cracked most of the time due to the high stress concentration. They are illustrated in figures B15 and B16.

c) Although uncommon, the authors observed that precast IDs were used in at least one of the bridges inspected, as shown in figure B17.

d) Another peculiarity was the use of IDs on large skew bridges; in these cases, the IDs are not in a straight line, but offset across the girders, as shown in figure B18.

e) The author had the opportunity to observe firsthand the labor work required to construct diaphragms. All the work related to building and placing the steel cage and formwork, and casting and curing of the concrete is illustrated from figure B19 to B21 (for end diaphragms and IDs). It was interesting to compare this bridge to another one built at the Texas-Louisiana border. The second bridge was built according to the Texas DOT specifications and has no intermediate or end diaphragms, as in figures B22 and B23. Since there are no end diaphragms, deck edges require extra reinforcement to avoid warping. This extra reinforcement, in this case, is provided by the steel plates observed in figure B23. Interestingly, this same concept was applied in one of the bridges inspected in Louisiana, where the extra reinforcement was provided by a thicker deck edge instead, as shown in figure B24.

f) The ID and the cantilever supporting the sidewalk built in 1937 are shown in figures B25 and B26, respectively.

6.5 Scope of Parametric Studies

This section includes a discussion of the parameters and cases considered for parametric studies, various geometric configurations, the loading configurations adopted for bridges,

computation of load distribution factor for girders, and a comparison of the results obtained from the two finite element models. The results of interest in this study are strain at the girder bottom, girder deflection under live loads, and the load distribution factor (LDF) at the mid-span.

The parameters adopted in this study were the type of girder, girder spacing, span length, ID type, skew angle, number of spans, and compressive concrete strength of girders. All these parameters were varied to observe the influence of each of them on load distribution and on the effectiveness of diaphragms. For a successful study, numerous cases of bridges and loading configurations are required. The parameters in this study were suitably chosen from a reasonable range of these variables so as to quantitatively represent bridges of as many configurations as possible in the defined range.

6.5.1 Geometric Configuration of Bridges

Typical two-lane highway bridges with two shoulders were considered in the parametric study. The width of the bridge was taken as 50 ft, with each lane, shoulder, and cantilever being 12, 10, and 3 ft, respectively. In order to place the loading system close to the edge, an 18-inch thick barrier was assumed along the edges. These barriers, however, were not considered in the actual analyses of the studied bridges. The slab thickness was taken as 8 in. and the compressive strength of concrete for slab and diaphragm was taken as 3,500 psi. Parameters involved in the study are

a. Four types of girders, AASHTO Type II, III, IV, and Bulb T, were chosen, as these are the predominantly used prestressed concrete girders in Louisiana.
b. Normal concrete compressive strength in the girder was taken as 6,000 psi, and for high strength concrete, this was taken as 10,000 psi. For all the configurations of bridges, an analysis was performed using normal concrete compressive strength while the study on the influence of using girders of high strength concrete was limited to a few cases.

c. Girder spacings of 5 and 9 ft were chosen; these are the minimum and maximum spacings specified by the LADOTD Manual (2003).

d. Minimum and maximum values of the span length for each type of girder were chosen as specified in LADOTD Manual with slight modification.

e. All bridge configurations were analyzed without IDs and then with IDs. The number of IDs was chosen based on LADOTD specifications.

f. In addition to analyzing right bridges, skew bridges with skew angles of 30^o and 50^o were also analyzed. Bridge continuity was also investigated. Some of these results, however, are presented but not extensively discussed; they can be found in detail in LTRC Project No. 03-3ST (2006).

g. For a limited number of cases, an analysis was performed for bridges with different steel diaphragm configurations.

6.5.2 Diaphragm Configurations

At the locations of supports for all the bridges considered in the parametric study, end diaphragms were provided parallel to the direction of support. The end diaphragms extend from the bottom of the slab to the bottom flange of the girders.

Intermediate diaphragms type, number, spacing, and location were provided as per the LADOTD specifications (2002). All RC diaphragms were considered to be 8-inch thick.

For bridges with a single diaphragm, the ID is provided at the midspan and for bridges with two diaphragms, these are located at the third points of the span length. The current practice in Louisiana is to connect girders with IDs at the girder web; this was adopted modeling the studied bridges.

In the case of skew bridges, ID construction is a difficult task and there are various possible geometric configurations of IDs in skew bridges. The diaphragms can be parallel to the support,

perpendicular to the girder line, or perpendicular to the girder line but discontinuous with the staggered IDs to maintain equal distances from the support. The third type of configuration described above is predominantly used in Louisiana; hence this configuration of IDs has been used for modeling diaphragms in skewed bridges. For small skew angles, the orientation of IDs does not influence the results since the distance between the positions of IDs for different configurations would be small.

One of the objectives of this study was to search for alternative steel configurations which could replace RC diaphragms. A parametric study was made by analyzing bridge configurations where appropriate steel diaphragms were chosen for the corresponding bridges.

6.5.3 Loading Configurations

A HS20 standard truck that is a common truck used for design loading was used to load the bridge. The lane loading was not considered in this study, since the difference between the load distribution of lane and truck loading is insignificant, as observed by previous researchers (Chen, 1995, Chen, 1995, and Chen and Aswad, 1996). Meanwhile, Barr *et al.* (2001) concluded that using truck load distribution for lane load is more conservative. Therefore, only the effect of truck loading on the bridges was studied. This is also consistent with the methodology used in developing the AASHTO LRFD Code Specifications (2004) where only truck loads were considered in determining the load distribution factors (LDFs).

As to be described in Chapter 8, the truck loading used in the finite element models have two units and three axles. The front axle weighs 8 kips, while the other two weigh 32 kips each. The wheels on each of the posterior axles bare the same load. A minimum spacing of 2 ft was provided between the curb and the wheel line of the truck, and the closest wheel lines of the two trucks were placed no closer than 4 ft. as per AASHTO specifications.

Since all bridges in this study were two-lane bridges, two-lane loading was applied

throughout. The truck was moved parallel to the direction of the bridge. The spacing between the second axle and third axle was taken as 14 ft for all cases because this configuration of truck generated the maximum load effect for all bridge configurations. The loading was intended to generate maximum straining action at the mid-span section of the bridge; this was achieved by placing the middle axle of the truck at the mid-span for right bridges. Two kinds of loading positions were adopted to obtain the maximum straining action in exterior girders and in an interior one.

To obtain the maximum straining action for the exterior girder, the trucks were placed as close as possible to the exterior girder. Unless specified, the distance between the exterior girder and the edge was taken as 30 in. The maximum straining action for an exterior girder may be the case where the wheel line of the first truck is applied on the exterior girder. However, since the minimum spacing between the curb and the wheel line must be 2 ft, the first wheel line was placed 42 in from the bridge edge (18 in of barrier width + 24 in of minimum distance of barrier to the wheel line) by default. In order to obtain the maximum straining action for the interior girder, the second wheel line of the first truck is placed above the innermost girder (third girder in the case of 9-foot girder spacing and fifth girder for 5-foot girder spacing) and the first wheel line of the second truck is placed 4 ft away from the first truck (figure 6.7).

The loading configuration was the similar for skew bridges, except that both wheels of an axle could not be at the mid-span since the sections under consideration were not in line with the loading axles. Hence, only the first wheel of the second axle of both trucks was placed at the mid-span, as shown in figure 6.8.

6.6 Cases for Parametric Studies

Cases show in tables 6.3 and 6.4 were simulated by varying the parameters believed to influence the ID effectiveness. These parameters are spacing, span length, girder type, skew angle,

continuity, and strength of the concrete. The parametric study was done for loading configurations generating the maximum straining action for both interior and exterior girders.

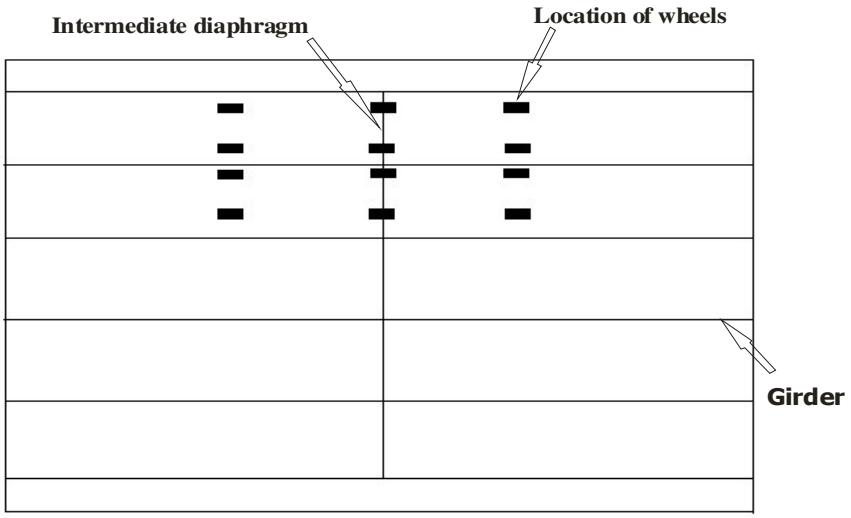

Figure 6.7
Loading to obtain maximum straining action for exterior girder in zero-skew bridges

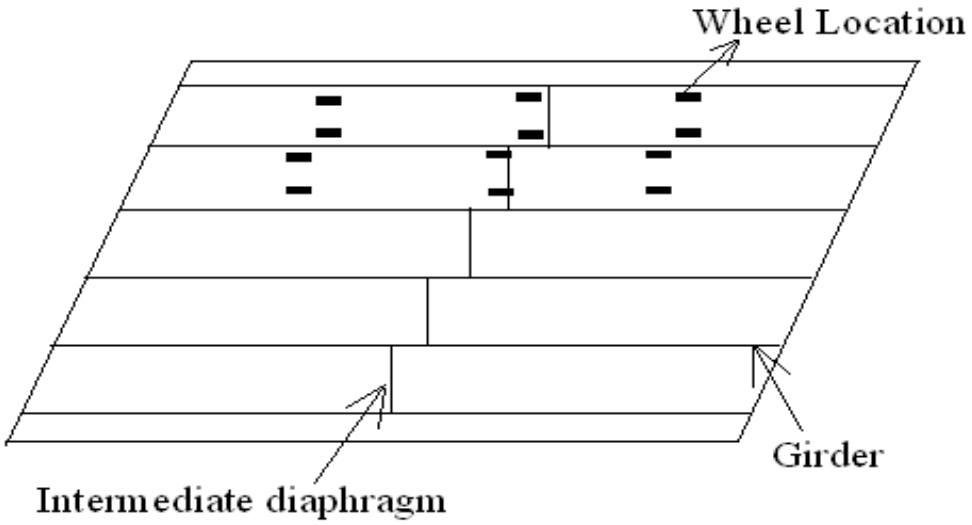

Figure 6.8
Loading to generate maximum straining action for exterior girder in skewed bridges

Table 6.3
Proposed cases for parametric study for bridges with RC diaphragms

Concrete Diaphragm								
Girder Type	Girder Concrete Strength (psi)	Girder Spacing (ft.)	Span Length (ft.)	Number of IDs	ID Type	Skew Angle (degree)	Number of Spans	Total Case Number
II	6000	5, 9	50, 65	0, 1	1	0, 30, 50	1, 3	48
III	6000	5, 9	70, 90	0, 1	1	0, 30, 50	1, 3	48
IV	6000 (10,000)	5, 9 (9)	95, 110 (110)	0, 2	1	0, 30, 50	1, 3	60
Bulb T	6000 (10,000)	5, 9 (9)	105, 130 (130)	0, 2	1	0, 30, 50	1, 3	60
							Sub Total =	216

Table 6.4
Proposed cases for parametric study for bridges with steel diaphragms

Steel Diaphragm								
Girder Type	Girder Concrete Strength (psi)	Girder Spacing (ft.)	Span Length (ft.)	Number of IDs	ID Type	Skew Angle (degree)	Number of Spans	Total Case Number
II*	6000	9	65	0, 1	2	0, 30, 50	1, 3	18
IV	6000 (10000)	9	110	0, 2	2	0, 30, 50	1, 3	36
Bulb T	6000 (10000)	9	130	0, 2	2	0, 30, 50	1, 3	36
							Sub Total =	90

Note*: Case number = 3 ID cases (no ID, ID Type 1, and ID Type 2) x 3 Skew Angle x 2 Number of Spans = 18

6.7 Load Distribution Factors

Girder stresses were calculated based on axial and bending stresses at the sections of interest, which were in turn calculated from the simplified model's output expressed in terms of axial force (P) and bending moment (M). This is indicated in equation 6.1.

$$\sigma = P/A + M/S \qquad \text{Eq. 6.1}$$

A = area of the beam cross-section

S = section modulus at the bottom of the beam cross-section

Maximum strain for this corresponding stress was obtained by dividing the maximum stress by Young's modulus of elasticity.

$$\varepsilon = \sigma / E \qquad \text{Eq. 6.2}$$

E = Young's modulus of elasticity

ε = Strain

Load distributions were obtained by dividing the strain of each girder by the summation of strains of all the girders of the bridge at the same section. This value was then multiplied by the number of wheel lines or the number of trucks, depending on whether it was defined in terms of wheel lines or lanes (axles or trucks). For all cases, the load distribution and respective LDF was determined at the mid-span. This method is only valid for cases where all beams have the same section properties and as long as no cracking occurs. This can be represented in the form of the equation as follows:

$$LDF = \text{Max}\left((\varepsilon_i / \Sigma \varepsilon_i) * N\right) \qquad \text{Eq. 6.3}$$

ε_i = Strain in girder number i at the section considered.

$\Sigma \varepsilon_i$ = Sum of the strains in all the girders along the section considered; "i" is the girder number.

N = Number of wheel lines.

6.8 Comparison between Simplified and Solid Models

The simplified model was also used by Cai and Shahawy (2004) to perform sensitivity studies to find the influence of various field factors, such as flange stiffening, parapet stiffening, and bearing stiffening, on the load distributions. This previous study justifies the applicability of this model in the current study. To make sure that a simplified model could be used for the current studies, the results obtained from this model were compared to the results from the solid model. The comparison was limited to strains and load distribution.

The bridge modeled for this comparison is 110 ft. (L) with girder spacing (S) equal to 9 ft., modeled with and without IDs (D) for the two loading configurations described earlier. Comparison results are presented in Tables 6.5 to 6.8 and figures 6.9 to 6.12. In these tables, although the percentage variation in results is larger for girders away from the loading system, the actual difference between the results is very small. Therefore, the percentage difference between the results for these girders has been highlighted in tables 6.5 to 6.8. For interior girders, the difference was 2%. For exterior girders, the maximum difference was 4%. Figures 6.9 and 6.10 show how IDs affect the load distribution for interior and exterior girders, respectively. ID effects on girder strains for interior and exterior girders are presented in figures 6.11 and 6.12, respectively. This comparison proved that the effect of IDs on load distribution obtained from both models were comparable.

Table 6.5
Comparison of results between simplified model and solid 3D model for bridge S9L110D0 (int)

3D Solid Model						
Girder #	**1**	**2**	**3**	**4**	**5**	**6**
Maximum Microstrain	60	128	160	127	64	24
LD (Wheels/girder)	0.43	0.91	1.14	0.90	0.46	0.17
Results from simplified model						
Maximum Microstrain	63	127.5	162.8	127.3	62.5	17.9
LD (Wheels/girder)	0.45	0.91	1.16	0.91	0.45	0.13
Difference between simplified model and 3D model						
% difference in strain	5	0	2	0	-2	-34
% change in LD	5	0	2.1	1	-2	-34

Note: The load distribution (LD) numbers shown were rounded. The % change is based on actual results.

Table 6.6
Comparison of results between simplified model and solid 3D model for bridge S9L110D1(int)

3D Solid Model						
Girder #	**1**	**2**	**3**	**4**	**5**	**6**
Maximum Microstrain	83	120	136	114	69	43
LD (Wheels/girder)	0.59	0.85	0.96	0.81	0.49	0.30
Results from simplified model						
Maximum Microstrain	73.6	108.5	138.2	121.1	74.2	44.5
LD (Wheels/girder)	0.53	0.77	0.99	0.87	0.53	0.32
Difference between simplified model and 3D model						
% difference in strain	-13	-11	2	6	7	3
% change in LD	-12	-10	2.4	7	8	4

Note: Load distribution (LD) numbers were rounded. The % change is based on actual results.

Table 6.7
Comparison of results between simplified model and solid 3D model for bridge S9L110D0 (ext)

3D Solid Model						
Girder #	**1**	**2**	**3**	**4**	**5**	**6**
Maximum Microstrain	156	168	127	63	32	20
LD (Wheels/girder)	1.102	1.187	0.898	0.445	0.226	0.141
Results from simplified model						
Maximum Microstrain	150	171	134	66	25	2
LD (Wheels/girder)	1.095	1.25	0.976	0.485	0.182	0.011
Difference between simplified model and 3D model						
% difference in strain	-4	2	5	5	-29	-1222
% change in LD	-1	5	8	8	-24	-1179

Note: Load distribution (LD) numbers were rounded. The % change is based on actual results.

Table 6.8
Comparison of results between simplified model and solid 3D model for bridge S9L110D2 (ext)

3D Solid Model						
Girder #	**1**	**2**	**3**	**4**	**5**	**6**
Maximum Microstrain	162	157	120	68	40	20
LD (Wheels/girder)	1.14	1.11	0.85	0.48	0.28	0.14
Results from simplified model						
Maximum Microstrain	165.9	167	126	67.8	31	9.5
LD (Wheels/girder)	1.17	1.18	0.89	0.48	0.22	0.07
Difference between simplified model and 3D model						
% difference in strain	2	6	5	0	-29	-111
% change in LD	2	6	5	0	-29	-111

Note: Load distribution (LD) numbers were rounded. The % change is based on actual results.

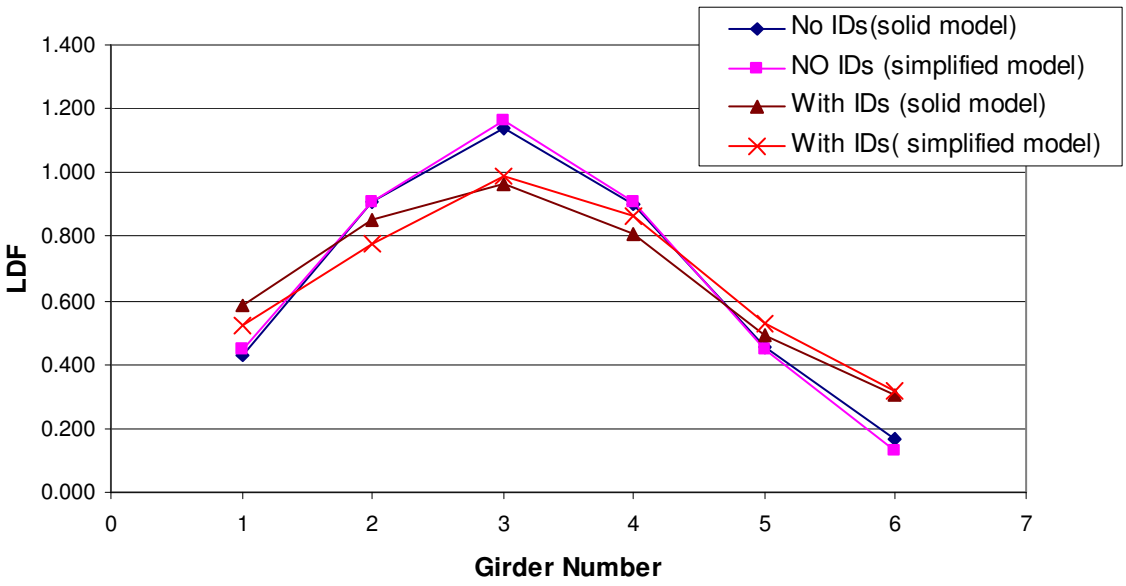

Figure 6.9
Comparison of LD values between the two FEM models (loading generating maximum straining action for interior girder for bridge S9L110)

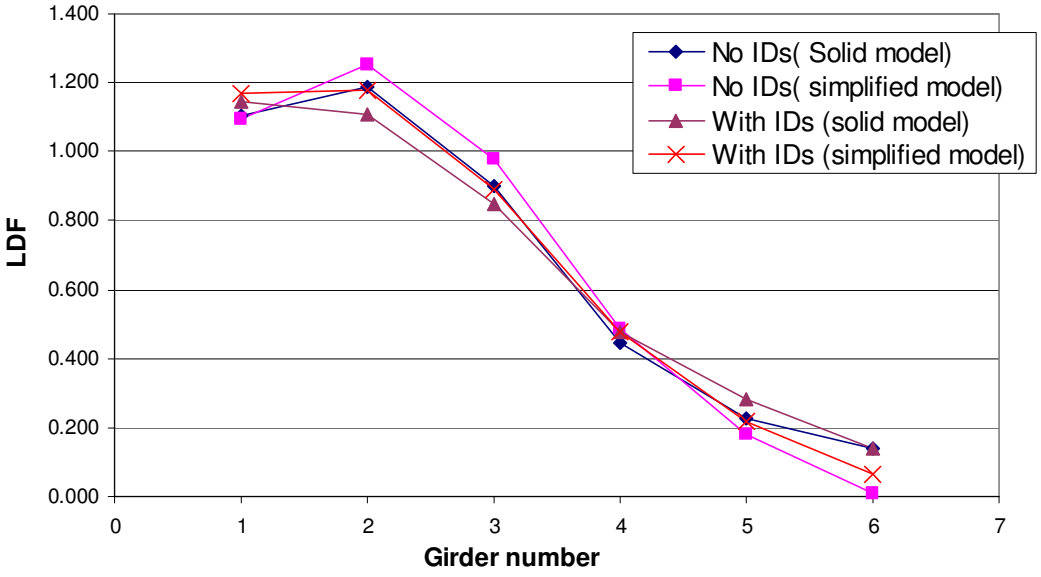

Figure 6.10
Comparison of LD values between the two FEM models (loading generating maximum straining action for exterior girder for bridge S9L110)

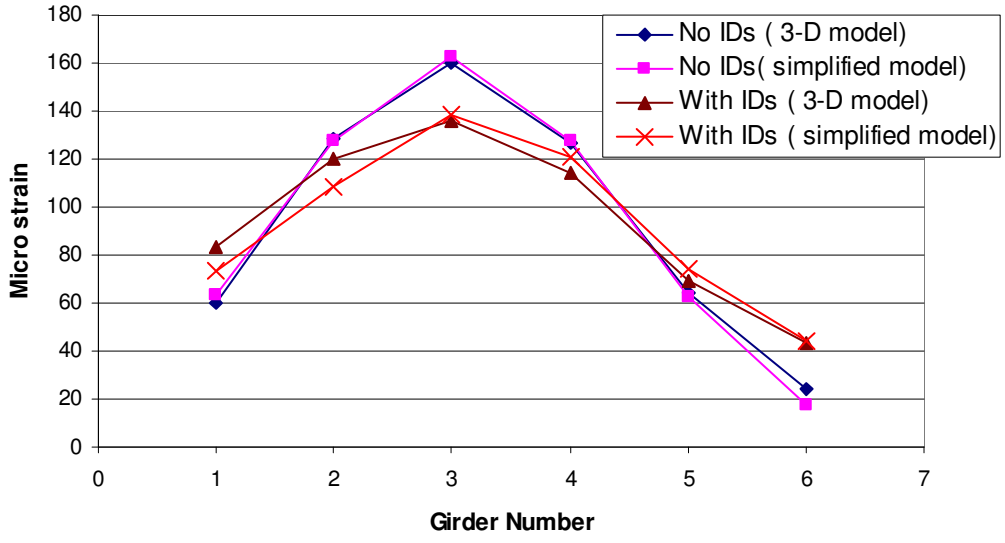

Figure 6.11
Comparison of strain values between the two FEM models (loading generating maximum straining action for interior girder for bridge S9L110)

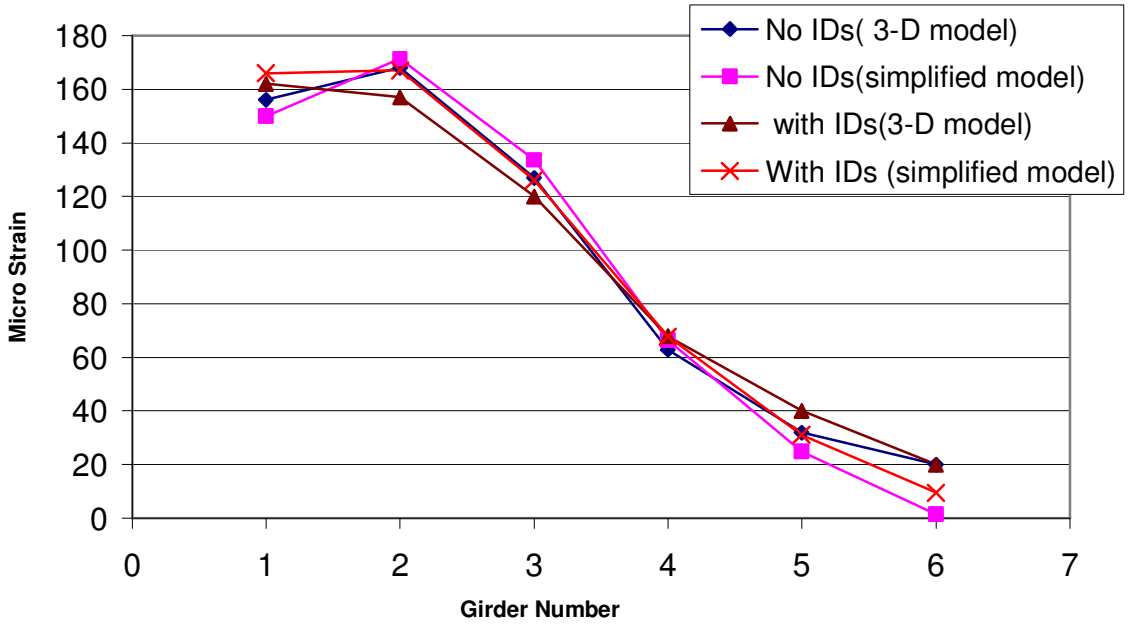

Figure 6.12
Comparison of strain values between the two FEM models (loading generating maximum straining action for exterior girder for bridge S9L110)

6.9 Intermediate Diaphragms Modeling

Proper diaphragm stiffness consideration will lead to reasonable results. It has been observed that the connection between the girder and the diaphragm is essentially a cold joint and is structurally "weak," with usually one or two reinforcement bars connecting these elements. The stiffness at the connection is variable and is based on the load levels (Cai and Shahawy, 2204). At low loads, the connection is close to full moment connection. As loads increase up to the ultimate stage, the cold joint may crack and open, leaving only the steel reinforcement effective in the tension region of the ID girder interface. Therefore, it is necessary to model IDs rationally to simulate its actual behavior and to appropriately estimate its effectiveness.

Intermediate diaphragms were modeled using different stiffnesses in two bridges in order to better understand this phenomenon and its effect on bridge behavior. The bridge configurations chosen for this study were S9L110 and S9L130. Strains, deflections, and load distribution factor

from the finite element model, AASHTO Standard (2002) and LRFD (2004) and the strains in diaphragms were calculated. These results are presented in table 6.9. Table 6.9 also shows the difference a particular diaphragm modeling creates in the values of strains, load distribution, and deflections when compared with the respective values for the same bridge without diaphragms. This difference between the results is expressed in terms of the percentage change in respective values of results for the case without a diaphragm to that with a diaphragm. The load distribution factor by AASHTO LRFD is the number of design lanes per girder, while other load distribution factors are in terms of the number of wheel lines per girder. Therefore, while comparing the various load factors, the AASHTO LRFD load distribution factor is multiplied by a factor of two. The same procedure was adopted throughout this work wherever a comparison between different load distribution factors is made.

Diaphragms were modeled for these bridges in a few different ways. The ones relevant to this dissertation are presented below, as labeled in table 6.9:

1) Case1- Rigid diaphragm connection with full stiffness (100 percent)

   In this case, IDs are modeled as a rigid element offset from the slab to the location of the geometric centroidal axis of the ID, between the girders. Full diaphragm stiffness is considered, which is equivalent to elastic solid modeling (Green et al., 2002). In reality, heavy loads create the possibility of cracks at the diaphragm-girder connection, and only a part of the diaphragm stiffness effectively contributes to load distributions. Diaphragm effectiveness obtained is an upper result boundary since maximum diaphragm stiffness contribution is taken into account (Cai and Shahawy, 2004).

2) Case 2- Diaphragm stiffness equal to 30 percent of full stiffness

   In the case of cracking at diaphragm-girder interface, the full diaphragm stiffness does not affect the load distribution. To model this condition the diaphragm stiffness was taken as 30

percent of the full stiffness by taking the Young's Modulus as 30 percent of its original value for concrete in diaphragms.

3) Case 5- Only rebar connection between the diaphragm and girder

In this case, the stiffness contribution of concrete in the diaphragm was ignored completely and the girders were assumed to be connected only through rebars in the diaphragm. The rebars were modeled as truss elements, and the results obtained from this case would be the lower boundary values.

6.9.1 Discussion of Results

Table 6.9 shows that modeling the diaphragm differently yields different results. Case 1 simulates the maximum contribution of diaphragm, while Case 5 predicts the least contribution by diaphragms; results for other cases lie in-between these extreme values. By reducing the stiffness of IDs to 30 percent from the full (100 percent) diaphragm stiffness, the effectiveness of the diaphragm in reducing load distribution decreases by about 6 percent for the interior girder. The effect of diaphragm stiffness has greater impact on interior girders. These results ratify the need to quantify the effective stiffness of the diaphragm properly. tensile stresses due to live loads in the diaphragms for Case 1 may exceed or reach a value close to the rupture modulus ($7.5\sqrt{f_c^{'}} = 7.5\sqrt{3500} = 444\,psi$), resulting in concrete cracking. The stresses listed in the table are only due to action of live loads. If the influence of dead loads and temperature stresses are also included stresses could reach much beyond the rupture stress. The stress contour diagrams in figures 13 to 15, which were obtained from solid model analysis in ANSYS 9.0, show that there is a significant stress concentration at the diaphragm-girder interface. This stress is alleviated by concrete cracking after the rupture stress is reached.

6.10 Parametric Analyses

A few of the parameters considered had more influence in the effectiveness of intermediate

diaphragms and are discussed below based on a reduced parametric investigation.

Table 6.9
Diaphragm stiffness effect on bridge performance

Model of diaphragm	Girder Case	Strain	%change in strain	Deflection (in)	%change in deflection	FEM LDF	%change in LDF	AASHTO STD LDF	LRFD LDF	Stress in diaph. (psi)
	(a) Type 4 AASHTO girder with span length 110 ft, fc' = 6000 psi, girder spacing = 9 ft									
No Diaphragm	Interior	160.0		0.568		1.14		1.64	1.42	
	Exterior	177.3		0.707		1.26		1.64	1.25	
Case 1	Interior	138.2	13.7	0.482	15.2	0.99	13.7	1.64	1.42	690.5(T)
Rigid Moment	Exterior	182.2	-2.8	0.706	0.0	1.30	-2.8	1.64	1.25	376.5(T)
Case 2	Interior	147.8	7.6	0.520	8.5	1.06	7.6	1.64	1.42	348.7(T)
30% stiffness of Case 1	Exterior	180.8	-2.0	0.722	-2.1	1.29	-2.0	1.64	1.25	195(T)
Case 3	Interior	156.9	2.0	0.555	2.3	1.12	2.0	1.64	1.42	564.3(T)
Rigid without offset	Exterior	178.2	-0.5	0.710	-0.5	1.27	-0.5	1.64	1.25	383.0(T)
Case 4	Interior	140.0	12.5	0.492	13.5	1.00	12.5	1.64	1.42	372.6(T)
As truss element	Exterior	182.7	-3.1	0.729	-3.1	1.30	-3.1	1.64	1.25	144.8(T)
Case 5	Interior	157.8	1.4	0.559	1.6	1.13	1.4	1.64	1.42	N.A.
Only steel connection	Exterior	179.0	-1.0	0.715	-1.1	1.27	-1.0	1.64	1.25	N.A.
	(b) BT-72 girder with span length 130 ft, fc' = 6000 psi, girder spacing = 9 ft									
No Diaphragm	Interior	167.4		0.597		1.20		1.64	1.41	
	Exterior	182.9		0.739		1.30		1.64	1.24	
Case 1	Interior	129.5	22.6	0.444	25.6	0.93	22.7	1.64	1.41	438(T)
Rigid Moment	Exterior	190.3	-4.0	0.773	-4.6	1.36	-4.0	1.64	1.24	168.2(T)
Case 2	Interior	138.5	17.3	0.481	19.5	1.0	17.3	1.64	1.41	318.5(T)
30% stiffness of Case 1	Exterior	189.6	-3.6	0.769	-4.1	1.4	-3.6	1.64	1.24	128.2(T)
Case 3	Interior	143.0	14.6	0.50	16.6	1.02	14.7	1.64	1.41	407(T)
Rigid without offset	Exterior	188.3	-2.9	0.76	-3.4	1.34	-2.9	1.64	1.24	197.4(T)
Case 4	Interior	138.4	17.3	0.484	19.0	0.99	17.4	1.64	1.41	273.4(T)
As truss element	Exterior	189.9	-3.8	0.769	-4.1	1.4	-3.8	1.64	1.24	82.5(T)
Case 5	Interior	162.9	2.7	0.579	3.0	1.16	2.7	1.64	1.41	N.A.
Only steel connection	Exterior	185.3	-1.3	0.750	-1.5	1.32	-1.3	1.64	1.24	N.A.

6.10.1 Span Length Effect on ID Effectiveness

Span length is one of the major parameters affecting load distribution. An attempt was made to understand the influence of span length on diaphragm effectiveness. Analyses were performed for bridges of two different span lengths for different girder types while keeping all other parameters in the group constant. Results are presented in table 6.10, which shows that span length

has a significant effect on ID effectiveness.

6.10.2 Girder Spacing Effect on ID Effectiveness

Three groups of bridges were analyzed differing in their span length and girder type, with spacing being the only difference between the bridges within each group. Results shown in table 6.11 indicate that girder spacing does not seem to have a significant impact on the diaphragm's influence on load distribution.

6.10.3 Effect of High Strength Concrete Girders on ID Effectiveness

AASHTO standard specifications (2002) do not account for the influence of the compressive strength of concrete in girders, while AASHTO LRFD takes this factor into account through the inclusion of modular ratio in load distribution formulas.

Bridges with high compressive strength concrete girders were modeled and are differentiated from bridges with normal compressive strength concrete girders by adding a suffix H in parenthesis at the end of the bridge geometry definition. The difference in LDF due to the use of high strength concrete in bridge girders is of an order of 1 percent (comparing the group with high strength concrete and that with regular concrete). The average difference of interior and exterior girders in LDF values obtained from AASHTO LRFD (2004) for girders with normal and high compressive strength of concrete is also listed in table 6.12, and this difference is about 2 percent. These results indicate that concrete strength do not cause a significant difference in the ID influence on LDF.

A complete parametric study was then conducted for the remaining cases listed in table 6.3, keeping results from these sample results in view. The results are presented in tables 6.13 and 6.14.

6.11 Parametric Study Observations

The influence of significant parameters on ID effect on load distributions was observed based on a broader parametric investigation. These observations are discussed below.

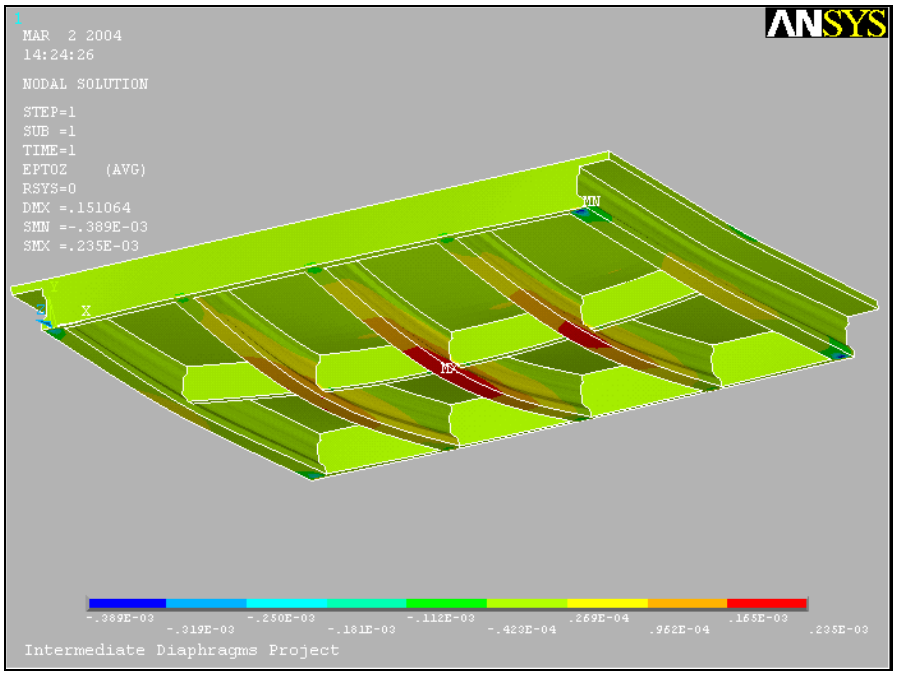

Figure 6.13
Stress contour for solid model under live load (full model)

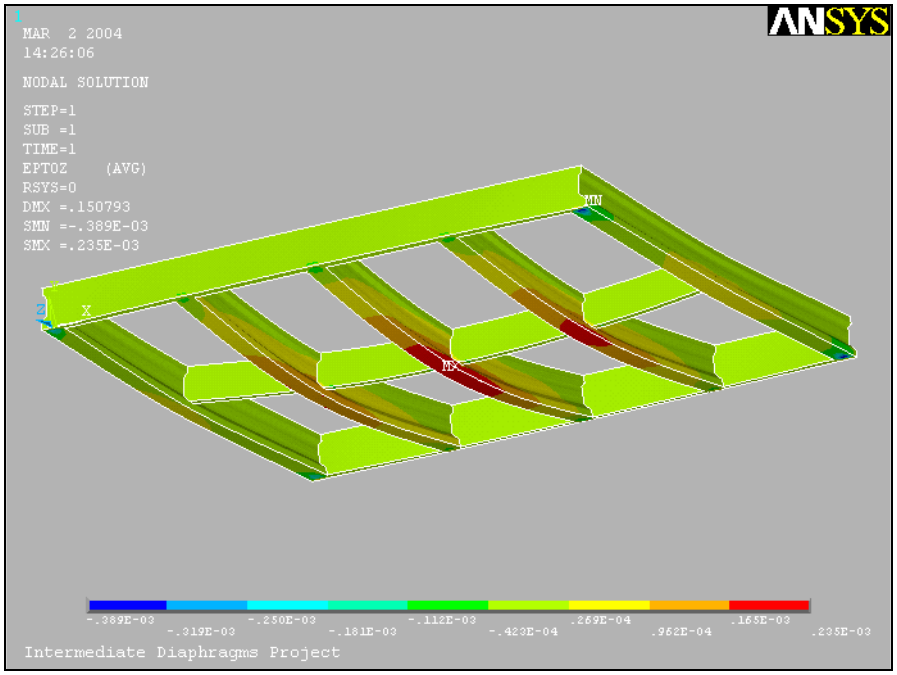

Figure 6.14
Stress contours in girders and diaphragms

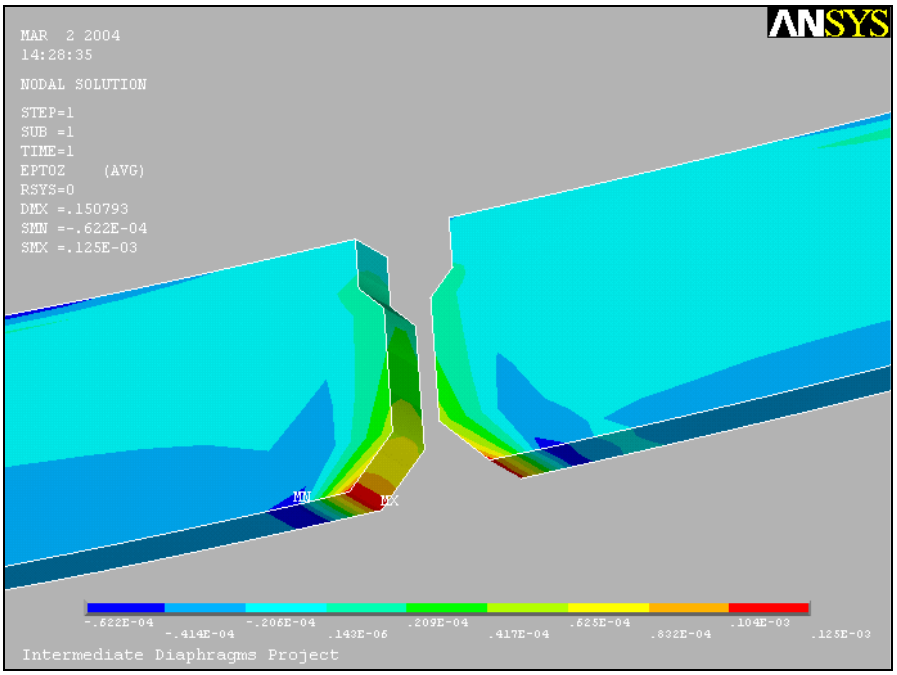

Figure 6.15
Stress contour at the diaphragm-girder joint

6.11.1 Influence of Girder Type on ID Effectiveness - Interior Girders

The percentage reduction in LDF due to ID and the span length for bridges having different girder sections with girder spacing equal to 9 ft. is shown in figure 6.16. These results indicate that a significant difference exists between the ID effects on load distributions for different girder types. It could occur because of the existing difference in the stiffness of the girder and the ID due to geometry of the sections. In bridges with Type III girders, the reduction in LDF due to the ID is greater than for bridges with Type II girders because Type III girders require greater ID stiffness (table 6.13). Though diaphragms in bridges with type IV girders have greater stiffness compared to the diaphragms for bridges with type III girders, there is a significant drop in percentage reduction in load distributions, which is possibly due to the location of diaphragms.

On bridges with Type IV girders, the diaphragms are located at mid-third locations; on bridges with Type III girders, the diaphragm is located at the mid-span. Since the LDF is calculated

at the critical mid-span section, the influence of diaphragms located at a significant distance from the section considered would be less, which could be the reason behind the lesser reduction in load distribution due to diaphragms for bridges with type IV girders. This was confirmed by considering a bridge configuration of S9L90, with one and two diaphragms, where diaphragms are located at the mid-span (one ID Case) and mid-third-span (two ID case), respectively. The percentage reductions in load distribution values for bridges due to single and two IDs are 18 percent and 13.2 percent, respectively. This behavior also leads to the conclusion that the results obtained for the cases with a single diaphragm would be quite different than those obtained for bridges with two diaphragms, and should be considered separately. Although the diaphragms are away from the mid-span for bridges with BT girders, the percentage reduction in LDF due to the diaphragm is large when compared to bridges with other girders because of its large diaphragm section (table 6.14).

6.11.2 Influence of Girder Spacing on ID Effectiveness - Interior Girders

From the preliminary parametric analysis, the influence of girder spacing on diaphragm effect on load distribution is minimal; this can be observed clearly from the results in table 6.15 and 6.16. The difference between the reduction in LDF and strain between 5 ft. and 9 ft. spacing is about 3 percent for all the cases considered.

6.11.3 Influence of Span Length on ID Effectiveness - Interior Girders

The results in tables 6.13 and 6.14 and figure 6.16 show that span length significantly affects the diaphragm's effectiveness in load distribution. Although the range of span length used was small, the difference between the reduction in LDF is as high as 6 percent.

6.11.4 Effect of Studied Parameters on Exterior Girders

Percentage change in strain and LDF of exterior girders due to IDs are discussed and summarized in tables 6.17 and 6.18. As observed from various studies (Sithichaikasem and Gamble, 1972), the use of diaphragms increases the strain and LDF values for the exterior girder. The influence of the

diaphragm on the LDF and strain was smaller numerically, when compared to theLDF and strain for interior girders in tables 6.15 and 6.16. With the results in tables 6.17 and 6.18 being similar,

Table 6.10
Preliminary study to understand the effect of span length on load distribution

case	Interior(In) or Exterior(Ex)	strain	%change in strain	Deflection (in)	%change in deflection	FEM LDF	%fem change	AASHTO STD LDF	LRFD LDF
S9L70D0	In	167.6		0.289		1.33		1.64	1.51
	Ex	158.2		0.305		1.25		1.64	1.33
S9L70D1	In	140.0	16.5	0.253	12.4	1.11	16.4	1.64	1.51
	Ex	171.1	-8.2	0.319	-4.7	1.35	-8.1	1.64	1.33
S9L90D0	In	203.3		0.562		1.18		1.64	1.41
	Ex	221.6		0.679		1.28		1.64	1.24
S9L90D1	In	166.7	18.0	0.491	12.5	0.97	18.0	1.64	1.41
	Ex	235.5	-6.3	0.700	-3.0	1.36	-6.2	1.64	1.24
S9L95D0	In	144.4		0.389		1.23		1.64	1.48
	Ex	140.5		0.431		1.19		1.64	1.30
S9L95D2	In	122.3	15.3	0.325	16.5	1.04	15.2	1.64	1.48
	Ex	148.3	-5.6	0.453	-5.1	1.26	-5.6	1.64	1.30
S9L110D0	In	160.0		0.568		1.14		1.64	1.42
	Ex	177.3		0.707		1.26		1.64	1.25
S9L110D2	In	138.2	13.7	0.482	15.2	0.99	13.7	1.64	1.42
	Ex	182.2	-2.8	0.706	0.0	1.30	-2.8	1.64	1.25
S9L105D0	In	144.8		0.335		1.34		1.64	1.49
	Ex	138.9		0.378		1.27		1.64	1.31
S9L105D2	In	105.2	27.4	0.243	27.4	0.96	28.4	1.64	1.49
	Ex	150.3	-8.2	0.408	-8.1	1.37	-8.2	1.64	1.31
S9L130D0	In	167.4		0.597		1.20		1.64	1.41
	Ex	182.9		0.739		1.30		1.64	1.24
S9L130D2	In	129.5	22.6	0.444	25.6	0.93	22.7	1.64	1.41
	Ex	190.3	-4.0	0.773	-4.6	1.36	-4.0	1.64	1.24

the influence of each individual parameter is understood less clearly than they were for interior girders. For girders Type II and Type III, there was no significant difference in the results. But in the case of bridges with Type IV girders, the influence of the diaphragm was very small (less than 3.0 percent) when compared to the results for bridges with Type II and III girders. This occurred because the diaphragm was located away from the mid-span where the strains and LDF values are

Table 6.11
Preliminary study to understand the effect of spacing

case	Interior(In) or Exterior(Ex)	strain	%change in strain	Deflection (in)	%change in deflection	FEM LDF	%fem change	AASHTO STD LDF	LRFD LDF
S5L65D0	In	153.3		0.288		0.733		0.91	0.95
	Ex	177.8		0.357		0.849		0.91	0.84
S5L65D1	In	131.0	14.6	0.260	9.8	0.628	14.4	0.91	0.95
	Ex	190.9	-7.3	0.370	-3.5	0.912	-7.3	0.91	0.84
S9L65D0	In	247.4		0.431		1.263		1.64	1.44
	Ex	252.1		0.480		1.277		1.64	1.26
S9L65D1	In	214.1	13.5	0.387	10.2	1.092	13.5	1.64	1.44
	Ex	267.6	-6.1	0.496	-3.4	1.355	-6.1	1.64	1.26
S5L90D0	In	125.6		0.380		0.68		0.91	0.94
	Ex	155.3		0.505		0.84		0.91	0.82
S5L90D1	In	102.2	18.621	0.335	11.7	0.55	18.4	0.91	0.94
	Ex	166.4	-7.126	0.519	-2.7	0.92	-9.2	0.91	0.82
S9L90D0	In	203.3		0.562		1.18		1.64	1.41
	Ex	221.6		0.679		1.28		1.64	1.24
S9L90D1	In	166.7	18.0	0.491	12.5	0.97	18.0	1.64	1.41
	Ex	235.5	-6.3	0.700	-3.0	1.36	-6.2	1.64	1.24
S5L110D0	In	98.7		0.385		0.65		0.91	0.94
	Ex	130.0		0.545		0.86		0.91	0.83
S5L110D2	In	85.9	12.928	0.331	13.9	0.57	12.9	0.91	0.94
	Ex	131.0	-0.763	0.552	-1.3	0.87	-0.7	0.91	0.83
S9L110D0	In	160.0		0.568		1.14		1.64	1.42
	Ex	177.3		0.707		1.26		1.64	1.25
S9L110D2	In	138.2	13.652	0.482	15.2	0.99	13.7	1.64	1.42
	Ex	182.2	-2.795	0.719	-1.8	1.30	-2.8	1.64	1.25

compared. The same behavior was reflected by BT girders, but with the stiffness of diaphragm in bridges with Type BT girders being larger, its influence on load distribution and strain was higher

than that of bridges with Type IV girders.

Span length seemed to be an important parameter that could be quantified, and its influence was observed to be significant, with a maximum difference of about 4 percent for two different span lengths, with other parameters remaining the same. The IDs increased the deflection of the exterior girder marginally, but the deflections were still in permissible limits given by the AASHTO Standard (2002) and AASHTO LRFD (2004).

Table 6.12
Preliminary study to understand the effect of high strength concrete

case	Interior(In) or Exterior(Ex)	strain	%change in strain	Deflection (in)	%change in deflection	FEM LDF	%fem change	AASHTO STD LDF	LRFD LDF	% LRFD
S5L95D0(H)	In	72.1		0.2215		0.71		0.91	1.00	
	Ex	82.8		0.2807		0.82		0.91	0.88	
S5L95D2(H)	In	62.2	13.7	0.1902	14.1	0.61	13.6	0.91	1.00	
	Ex	86.5	-4.4	0.2906	-3.5	0.85	-3.5	0.91	0.88	
S5L95D0	In	88.5		0.2613		0.70		0.91	0.98	2.14
	Ex	104.1		0.3357		0.82		0.91	0.86	
S5L95D2	In	75.8	14.4	0.2219	15.1	0.60	14.3	0.91	0.98	
	Ex	108.0	-3.8	0.3477	-3.6	0.85	-3.8	0.91	0.86	
S9L95D0(H)	In	117.7		0.3306		1.25		1.64	1.51	
	Ex	111.4		0.3595		1.18		1.64	1.33	
S9L95D2(H)	In	100.3	14.8	0.2789	15.7	1.06	14.7	1.64	1.51	
	Ex	118.0	-5.9	0.3769	-4.8	1.25	-6.0	1.64	1.33	
S9L95D0	In	144.4		0.3895		1.23		1.64	1.48	2.27
	Ex	140.5		0.4307		1.19		1.64	1.30	
S9L95D2	In	122.3	15.3	0.3253	16.5	1.04	15.2	1.64	1.48	
	Ex	148.3	-5.6	0.4526	-5.1	1.26	-5.6	1.64	1.30	
S9L110D0(H)	In	130.8		0.4837		1.16		1.64	1.45	
	Ex	140.8		0.5898		1.25		1.64	1.27	
S9L110D2(H)	In	113.1	13.5	0.4132	14.6	1.01	13.5	1.64	1.45	
	Ex	145.4	-3.2	0.6076	-3.0	1.29	-3.2	1.64	1.27	
S9L110D0	In	160.0		0.5682		1.14		1.64	1.42	2.26
	Ex	177.3		0.7066		1.26		1.64	1.25	
S9L110D2	In	138.2	13.7	0.4820	15.2	0.99	13.7	1.64	1.42	
	Ex	182.2	-2.8	0.7064	0.0	1.30	-2.8	1.64	1.25	

Table 6.13
Results for bridges with Type II and III girders for skew 0^o skew

S.No	case	Girder Type	Interior(In) or Exterior(Ex)	strain	%change in strain	Deflection (in)	%change in deflection	FEM LDF	%fem change	AASHTO STD LDF	LRFD LDF
1	S5L50D0	II	In	119.4		0.136		0.82		0.91	1.02
			Ex	119.7		0.147		0.82		0.91	0.90
2	S5L50D1	II	In	104.9	12.2	0.124	9.3	0.72	12.0	0.91	1.02
			Ex	130.4	-9.2	0.155	-5.4	0.90	-9.0	0.91	0.90
3	S5L65D0	II	In	153.3		0.288		0.73		0.91	0.95
			Ex	177.8		0.357		0.85		0.91	0.84
4	S5L65D1	II	In	131.0	14.6	0.260	9.8	0.63	14.4	0.91	0.95
			Ex	190.9	-7.3	0.370	-3.5	0.91	-7.3	0.91	0.84
5	S9L50D0	II	In	194.5		0.207		1.43		1.64	1.54
			Ex	167.9		0.196		1.23		1.64	1.36
6	S9L50D1	II	In	172.4	11.4	0.188	9.4	1.27	11.3	1.64	1.54
			Ex	180.3	-7.4	0.205	-5.0	1.31	-7.3	1.64	1.36
7	S9L65D0	II	In	247.4		0.431		1.26		1.64	1.44
			Ex	252.1		0.480		1.28		1.64	1.26
8	S9L65D1	II	In	214.1	13.5	0.387	10.2	1.09	13.5	1.64	1.44
			Ex	267.6	-6.1	0.496	-3.4	1.35	-6.1	1.64	1.26
9	S5L70D0	III	In	102.8		0.193		0.76		0.91	1.00
			Ex	112.2		0.229		0.83		0.91	0.88
10	S5L70D1	III	In	85.3	17.0	0.170	11.9	0.63	16.8	0.91	1.00
			Ex	122.8	-9.5	0.240	-4.8	0.91	-10.2	0.91	0.88
11	S5L90D0	III	In	125.6		0.380		0.68		0.91	0.94
			Ex	155.3		0.505		0.84		0.91	0.82
12	S5L90D1	III	In	102.2	18.6	0.335	11.7	0.55	18.4	0.91	0.94
			Ex	166.4	-7.1	0.519	-2.7	0.92	-9.2	0.91	0.82
13	S9L70D0	III	In	167.6		0.289		1.33		1.64	1.51
			Ex	158.2		0.305		1.25		1.64	1.33
14	S9L70D1	III	In	140.0	16.5	0.253	12.4	1.11	16.4	1.64	1.51
			Ex	171.1	-8.2	0.319	-4.7	1.35	-8.1	1.64	1.33
15	S9L90D0	III	In	203.3		0.562		1.18		1.64	1.41
			Ex	221.6		0.679		1.28		1.64	1.24
16	S9L90D1	III	In	166.7	18.0	0.491	12.5	0.97	18.0	1.64	1.41
			Ex	235.5	-6.3	0.700	-3.0	1.36	-6.2	1.64	1.24

Table 6.14
Results for bridges with type IV and BT girders for 0° skew

S.No	case	Girder Type	Interior(In) or Exterior(Ex)	strain	%change in strain	Deflection (in)	%change in deflection	FEM LDF	%fem change	AASHTO STD LDF	LRFD LDF
17	S5L95D0	IV	In	88.5		0.261		0.70		0.91	0.98
			Ex	104.1		0.336		0.82		0.91	0.86
18	S5L95D2	IV	In	75.8	14.4	0.222	15.1	0.60	14.3	0.91	0.98
			Ex	108.0	-3.8	0.348	-3.6	0.85	-3.8	0.91	0.86
19	S5L110D0	IV	In	98.7		0.385		0.65		0.91	0.94
			Ex	130.0		0.545		0.86		0.91	0.83
20	S5L110D2	IV	In	85.9	12.9	0.331	13.9	0.57	12.9	0.91	0.94
			Ex	131.0	-0.8	0.552	-1.3	0.87	-0.7	0.91	0.83
21	S9L95D0	IV	In	144.4		0.389		1.23		1.64	1.48
			Ex	140.5		0.431		1.19		1.64	1.30
22	S9L95D2	IV	In	122.3	15.3	0.325	16.5	1.04	15.2	1.64	1.48
			Ex	148.3	-5.6	0.453	-5.1	1.26	-5.6	1.64	1.30
23	S9L110D0	IV	In	160.0		0.568		1.14		1.64	1.42
			Ex	177.3		0.707		1.26		1.64	1.25
24	S9L110D2	IV	In	138.2	13.7	0.482	15.2	0.99	13.7	1.64	1.42
			Ex	182.2	-2.8	0.706	0.0	1.30	-2.8	1.64	1.25
25	S5L105D0	BT	In	88.4		0.227		0.76		0.91	0.99
			Ex	97.7		0.279		0.85		0.91	0.87
26	S5L105D2	BT	In	64.6	26.9	0.164	28.1	0.56	26.8	0.91	0.99
			Ex	103.5	-5.9	0.294	-5.7	0.89	-5.0	0.91	0.87
27	S5L130D0	BT	In	103.1		0.397		0.70		0.91	0.94
			Ex	127.8		0.540		0.86		0.91	0.82
28	S5L130D2	BT	In	79.1	23.3	0.298	24.8	0.54	23.3	0.91	0.94
			Ex	130.1	-1.8	0.553	-2.5	0.88	-1.8	0.91	0.82
29	S9L105D0	BT	In	144.8		0.335		1.34		1.64	1.49
			Ex	138.9		0.378		1.27		1.64	1.31
30	S9L105D2	BT	In	105.2	27.4	0.243	27.4	0.96	28.4	1.64	1.49
			Ex	150.3	-8.2	0.408	-8.1	1.37	-8.2	1.64	1.31
31	S9L130D0	BT	In	167.4		0.597		1.20		1.64	1.41
			Ex	182.9		0.739		1.30		1.64	1.24
32	S9L130D2	BT	In	129.5	22.6	0.444	25.6	0.93	22.7	1.64	1.41
			Ex	190.3	-4.0	0.773	-4.6	1.36	-4.0	1.64	1.24

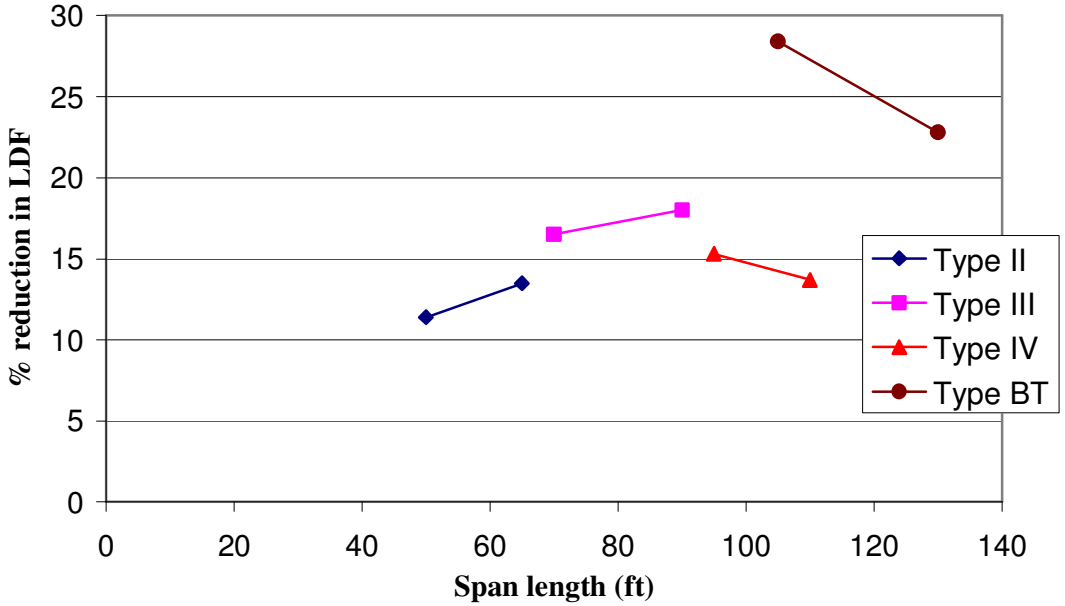

Figure 6.16
Percentage reduction in LDF for bridges with different girder types and span lengths

Table 6.15
Percentage decrease in strain for different bridge configurations

Span length (ft.)	Skew=0		Skew=30		Skew=50	
	Spacing (ft.)					
	5	9	5	9	5	9
50	12.2	11.4	10.9	9.9	9.4	12.1
65	14.6	13.5	12.6	8.3	16	12.9
70	17	16.5	13.9	12.6	15.6	13.4
90	18.6	18	15.3	13.6	17	13.6
95	14.4	15.3	9.6	11.2	8.4	12.3
105	26.9	27.4	14.1	13.6	9.2	11.2
110	12.9	13.7	8.6	10	7.3	10.2
130	23.3	22.6	13	11.5	8.3	8.9

Table 6.16
Percentage decrease in LDF for different bridge configurations

Span length (ft.)	Skew=0		Skew=30		Skew=50	
	Spacing (ft.)					
	5	9	5	9	5	9
50	12	11.3	9.9	7.2	4	5.2
65	14.4	13.5	6	7.9	6.8	5.8
70	16.8	16.4	9.2	9.8	8.3	7
90	18.4	18	10.1	10.7	8.2	7.5
95	14.3	15.2	7.8	11.3	8	11.3
105	26.8	28.4	13.8	13.9	9	11.2
110	12.9	13.7	8.5	10.2	7.2	10.1
130	23.3	22.7	13.2	11.8	8.5	9.6

Table 6.17
Percentage change in strain due to diaphragm for exterior girder in different bridges

Span length (ft.)	Skew=0^o		Skew =30^o		Skew = 50^o	
	Spacing (ft.)					
	5	9	5	9	5	9
50	-9.2	-7.4	-4.3	-4.9	-4.8	-3.1
65	-7.3	-6.1	-4	-3.8	-2.4	-2.4
70	-9.5	-8.2	-5.9	-5.6	-4	-3.9
90	-7.1	-6.3	-4.6	-4.3	-3.2	-3.1
95	-3.8	-5.6	-3.2	-3.3	-2.9	-3.3
110	-0.8	-2.8	-1.4	-1.9	-1.6	-1.4
105	-5.9	-8.2	-4.7	-4.9	-3.8	-3.6
130	-1.8	-4	-1.2	-1.7	-1.3	-0.9

Table 6.18
Percentage change in LDF due to diaphragm for exterior girder in different bridges

Span Length (ft.)	Skew=0^o		Skew =30^o		Skew = 50^o	
	Spacing (ft.)					
	5	9	5	9	5	9
50	-9	-7.3	-4.9	-5.8	-6.5	-6.1
65	-7.3	-6.1	-4.4	-4.7	-6.1	-5.1
70	-10.2	-8.1	-6.1	-6.4	-7	-6.5
90	-9.2	-6.2	-4.7	-5	-5.9	-5.2
95	-3.8	-5.6	-2.7	-3.3	-2.8	-4
110	-0.7	-2.8	-1.5	-1.8	-1.4	-1.7
105	-5	-8.2	-4.6	-4.8	-3.5	-3.9
130	-1.8	-4	-1.2	-1.6	-1.3	-0.7

6.12 Steel Intermediate Diaphragms and Lateral Loading

6.12.1 Introduction

One of the important objectives of this study was to identify steel diaphragm configurations that could have similar performance as that of RC IDs in PC PS girder bridges, as it would be more economical to provide steel IDs. This section discusses: (1) the possible configurations of steel IDs that could replace RC IDs; (2) the stability these diaphragms provide when compared to RC IDs during the construction of the deck; (3) how much these steel sections contribute to load distributions by doing a parametric study for bridge configurations listed in table 6.2; and (4) the performance of various IDs under impact loads.

6.12.2 Selection of Appropriate Steel Diaphragm Section

Diaphragm configurations were chosen based on the geometry of the girder section. For girder Types II, III, and IV, since the depth of the web region of the girders is small, a channel section is appropriate to fit in the girder web region. For a BT girder, the possibility of providing a channel and X type bracing with a bottom strut was explored.

Three different bridge configurations for Type II, III, IV, and BT girders were analyzed by modeling a diaphragm as a beam element and another as an axial truss element. Table 6.19 shows the percentage reduction in LDF for interior girders caused by IDs from these two different forms of diaphragm modeling. The results indicated that the ID influence on reducing LDF for interior girders is predominantly due to the transfer of axial forces through the diaphragm. Therefore, different sections having nearly the same axial stiffness would generate nearly equal ID effectiveness, and this criterion was used for choosing steel ID sections. For bridges with Type II, III, and IV girders, a channel section was chosen that could be used for all bridges with these three girder types. Girder Type II had the smallest web depth of all three girder types; therefore, it was decided that a channel section with a depth no greater than 15 in. would be used.

Providing a steel channel that has the exact same axial stiffness as the RC diaphragm is not possible, as the section would be very heavy and no single channel section can provide the desired stiffness. It has been discussed earlier that only a portion of the RC diaphragm section is effective in load distributions because of the possible cracking at the diaphragm-girder interface. Keeping this in mind, a minimum target ID stiffness of 40 percent of the RC ID was set up, based on which an appropriate steel channel section was chosen. It was thought that rather than providing three different diaphragm sections for the three girder types, it would be better to choose a common section for the purpose of uniformity. For the three girders discussed here, the ID for a bridge with type IV girder had the maximum stiffness. Therefore, a channel section was chosen as the diaphragm for these three girder types. The channel section could provide equivalent stiffness greater than 40 percent of the axial stiffness contributed by a RC ID for Type IV girders. This was done to make sure that for all the girder types, the diaphragm stiffness was greater than the target stiffness.

Finally, a channel section C15X33.9 was chosen as the diaphragm since it satisfied all the limiting conditions defined earlier. The depth of the channel was 15 in. and the axial stiffness of this section was 46.7 percent of the absolute stiffness of the RC diaphragm for a Type IV girder. In calculating the equivalent axial stiffness for the steel section, the area of steel section is multiplied by a modular ratio ($m = E_{steel} / E_{concrete} = 8.6$). For an ID with girder Types II and III, the ratio of axial stiffness of the C15X33.9 section to the RC diaphragm axial stiffness is about 71 percent and 56.5 percent, respectively. For the purpose of maintaining uniformity in the diaphragm sections provided, the same section was adopted for Type II and Type III girders, though a smaller section would have been sufficient to provide the target stiffness of 40 percent of ID stiffness for the respective girders. In table 6.19, a value comparison is made for $\mathbf{R_d}$.

Table 6.19
Comparison between R_d obtained by modeling diaphragm as an axial truss element and beam element

Bridge configuration	R_d	
	Axial element	Beam element
S9L65	11.7	13.5
S9L90	15.2	18
S9L110	12.5	13.7

For the BT section, the depth of the web was 54 in., making the concrete section area 432 $in.^2$. This would mean that to provide a stiffness equivalent to about 40 percent of the axial stiffness of the RC diaphragm, a steel section of 20 in^2 would be required, which no single steel section can provide. Also, since the channel depth was small compared to the depth of the 54 in. web, the lateral stability provided by this section might not be adequate for BT girders. Providing an X type bracing with a bottom strut for BT bridges seemed to be a possible alternative. Initial study was done by choosing a MC8X20 channel section for all its bracing members.

In table 6.20, a comparison was done between percent reduction in LDF due to RC IDs considering the absolute stiffness of diaphragm contributing to load distributions and steel IDs of X-plus-bottom-strut configuration for bridge S9L105 and S9L130 with bulb T girders. The results showed that reduction in LDF due to IDs of X-plus-bottom-strut configuration is about 0.8 times that provided by RC IDs, which is a very significant contribution. From the relation obtained between the stiffness of RC IDs and the R_d due to ID for interior girders in the previous section, it was found that for 40 percent of the absolute stiffness contribution of RC IDs yielded an R_d value of about 80 percent of that of the R_d value obtained from absolute ID stiffness (S_t $=0.3024*40^{0.2641}=0.801$). This implies that the assumed steel ID configuration is providing an axial

stiffness of about 40 percent of the absolute diaphragm stiffness of the corresponding RC diaphragms, which was our target stiffness. Hence, steel IDs of X-plus-bottom-strut configuration with all its members of the MC 8X20 section was found to be appropriate for BT girders, in terms of contribution of diaphragm in load distributions.

Table 6.20
Comparison of R_d values for X plus bottom strut and RC diaphragm

Bridge configuration	% reduction in LDF for RC ID (1)	% reduction in LDF for X + bottom strut (2)	Ratio of (2)/(1)
S9L105	27.4	22.1	0.8
S9L130	22.6	19.3	0.85

6.12.3 Stability Provided by Steel Diaphragm during Deck Construction

One of the reasons for providing diaphragms is to provide stability to girders during deck construction. During this process, the concrete in the deck, being wet, cannot transmit lateral loads that are induced during the construction process and other sources of lateral loading. The diaphragms are provided to transfer these loads from one girder to another and to provide lateral restraint. The present study was limited to comparing the stability provided by steel diaphragms relative to that provided by RC diaphragms rather than determining the absolute stability provided by each of these diaphragms. This was achieved by comparing the principal tensile stresses developed in the girder web region for the bridges with different ID configurations. This analysis was done using a 3-D solid FEM model built in ANSYS.

6.12.4 Calculation of Construction Loads

It was assumed that steel sheets provided as formwork during the construction of the deck were of negligible stiffness. Initial studies indicated that the load carried by the bracing was

maximum when the formwork was loaded up to the center of the innermost girder along the length of the span. Hence, the loading was done in this manner and was applied as pressure on the surface of the formwork (figure 6.17). Three components of load were applied on the formwork, these being dead load of the wet concrete, dead load of the formwork, and construction loads due to equipment. The load values for construction loads and formwork were adopted from the values used in the design of formwork for the deck for some bridges designed earlier.

Dead load due to wet concrete = ρ* thickness = 150 *9/12 = 112.5 psf (assuming the thickness of deck to be 9 in.)

Assuming dead load of formwork = 4 psf

Construction loads = 50 psf

Sum of all the components of construction load = 166.5 psf ≈ 170 psf

Therefore, the loading was done as shown in figure 6.17 on formwork with a load of 170 psf to determine the stability provided by the diaphragm and also to determine the forces generated in the bracing.

A comparison of stability provided by the RC ID to that provided by the steel ID was done for a S9L130 bridge with BT girders. As mentioned earlier, for BT girders providing X plus bottom strut with all its members of MC 8X20 section seemed to be appropriate; hence, this section was adopted as the steel ID for this bridge in this study. The study of relative stability provided was done by comparing the largest principal stress at the inner face of the web at the location of the diaphragm and the mid-span. The results show that for both RC and steel diaphragms, the principal stresses obtained from the FEM analysis were nearly the same (table 6.21), thereby indicating that both diaphragms provide nearly the same order of stability to the girder.

Similar investigation was carried out for bridge configuration S9L90 with Type III girders. For these bridges, using a channel section of C15X33.9 was found to be appropriate, as discussed

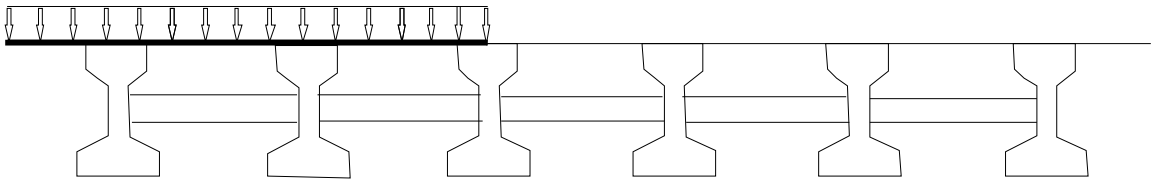

Figure 6.17
Construction loading, generating maximum forces in bracing

Table 6.21
Comparison of principal stresses (ksi) due to construction load in S9L130 bridge with different diaphragm configuration

Girder no.	Steel ID		RC ID		No diaphragm	
	ID section (one third span)	Mid-span	ID section (one third span)	Mid-span	one third span	Mid-span
2	0.933	1.7	0.948	1.67	1.31	2.2
3	0.668	1.4	0.7	1.37	0.98	1.7

Table 6.22
Principal stresses (ksi) due to construction load in S9L90 bridge with different diaphragm configuration

Girder no.	Steel ID		RC ID		no diaphragm	
	Quarter span	ID section (Mid-span)	Quarter span	ID section (Mid-span)	Quarter span	Mid-span
2	0.4015	0.2973	0.407	0.3045	0.6126	0.49085
3	0.2975	0.2452	0.2871	0.2339	0.2831	0.2375

earlier. Therefore, the stability provided by this diaphragm was compared to that provided by the RC ID. In this case, the principal stresses in the bottom portion of web on the inner face were

compared at the location of the diaphragm (which is at the mid-span) and quarter span. The diaphragm was modeled using shell elements (SHELL 41 in ANSYS). The results of this study are presented in table 6.22, and the observations were similar to the case of BT girders.

From the results obtained in this study, it was concluded that the lateral stability provided by the steel ID was equivalent to that provided by the RC ID as well.

6.12.5 Loads Carried by Bracing

The load carried by bracing under various loading conditions was determined, and the steel diaphragm members were checked for load carrying capability. The maximum loads in members were determined for each of the three different loading conditions: under uniform construction loading, concentrated load on girder during the process of construction, and due to live load. The study was carried out for two bridge configurations, S9L90 with a channel diaphragm of section C15X33.9 and bridge S9L130 (with BT girders) with an X plus bottom strut diaphragm.

The forces in the bracing were determined for a uniformly distributed construction load of 170 psf, applied from the edge of the bridge to the center of the innermost girder as shown in figure 6.17. Since the possible maximum concentrated load coming on the formwork during construction was unknown, a load of 50 kips was applied as the concentrated load on the edge of the interior girder. For this loading the stresses and forces in the diaphragm members were determined by analyzing 3-D solid models. The forces in the bracing generated under live load were also determined. These were obtained by analyzing models in GT STRUDL for the same live load configuration used in determining LDF.

The values of forces and the stresses in the ID members for bridges S9L90 and S9L130 for the above mentioned loading are listed in tables 6.23 and 6.24. The member capacity of the MC8X20 was in order of 220 kips in tension and 110 kips in compression, which was significantly larger than all the maximum forces obtained under the three loads added together in table 6.23.

Similarly, the C15X33.9 had a tensile and compressive load carrying capacity of about 380 kips and 200 kips, respectively, which is again larger than all the forces in the braces added together under the three loads in table 6.24. The slenderness ratio of these bracing members provided was about 120, which was less than the maximum slenderness ratio of 140 - the limiting value used in the design of bracings. From these results, it was concluded that the bracing members considered could carry the forces induced in the bracing.

6.13 Assessing the Influence of IDs in Limiting Impact Damage of Over-height Trucks

In many instances, prestressed concrete girder bridges have collided with over-height trucks passing under them. The effectiveness of diaphragms in limiting damage during collision is controversial. To get a better understanding of this issue and to know how different diaphragms affect the performance of bridges during collision, an analytical study was carried out with a 3-D solid model built in ANSYS. Simulating the actual collision is a difficult task and beyond the scope of this study. This study was limited to the comparison of the relative performance of bridges with different diaphragm configurations under lateral impact loading, which was applied as a concentrated static load.

6.13.1 Comparison with Previous Experimental Results

To see if the proposed finite element model could be used for studying bridge performance under lateral loading, the results obtained by analyzing the model were compared to the experimental results obtained under the lateral loading of the bridge. As no experimental tests were carried out in this study, the comparison was done for results obtained from the experimental work carried out by Abendroth et al. (2003) on bridges under lateral loading. The details of the experiment and its results were obtained from the thesis work of Andrawes (2001). A comparison was also made between the results of the present study and the finite element model by Andrawes.

Table 6.23
Maximum forces and stresses in bracing members for S9L130 bridge under different loading conditions

Loading condition	Force (Kips)	Stress (ksi)
Uniform const. load	33.7 (T) 34.1 (C)	5.73 (T) 5.79 (C)
Concentrated const. load (at midspan)	23.93 (T) 16.26 (C)	4.07 (T) 2.77 (C)
Concentrated const. load (at diaphragm section)	38.6 (T) 24.5 (C)	6.57 (T) 4.16 (C)
Live load (at midspan)	29.4 (T) 3.6 (C)	5.03 (T) 0.61 (C)
Live load (at diaphragm section)	30.9 (T) 2.4 (C)	5.26 (T) 0.41 (C)

Table 6.24
Maximum forces and stresses in bracing members for S9L90 bridge under different loading conditions

Loading condition	Force (kips)	Stress (ksi)
Uniform const. load	24 (T) 5.1 (C)	2.43 (T) 0.52 (C)
Concentrated const. load	15.81 (T) 6.83 (C)	1.6 (T) 0.7 (C)
Live load	63.2 (T) 9.3 (C)	6.4 (T) 0.95 (C)

The experimental bridge is a slab over girder bridge with 3 Iowa “A38” prestressed concrete girders spaced 6 ft. apart with a 3 ft. overhang measured from the center of the exterior girder. The span of the bridge is 40 ft. and 4 in. and is an un-skewed bridge. The thickness of the deck was 4 in. and was limited to this amount intentionally so as to make the structure flexible. At each end of the bridge, a 42 in. deep by 18 in. wide reinforced concrete abutment supported the PC girders, and

each girder was placed on elastomeric bearing pads. The end diaphragms were of 8 in. thickness, and different ID configurations were used. Strain gauges and direct current displacement transducers were placed near the mid-span location of the girders. The tests were done for three ID configurations - RC diaphragms, X type bracing configuration with a bottom strut of steel diaphragm, and a steel channel section. They also studied a case without diaphragms. The RC diaphragm was 6 in. thick. All the steel members were of MC8x20 section and were held between the girders by fixing these steel members to the gusset plates, which in turn were attached to the girder through anchor bolts.

A comparison was made between the strains and displacements obtained from the experiments, the current finite element model, and the FEM by Andrawes for different diaphragm configurations tabulated in the columns under the title E, C, and A, respectively (tables 6.25 and 6.26). This comparison was done for a lateral load value of 75 kips. The locations where results were compared were referred by the girder number followed by suffix 'R' or 'L' indicating the right or left side of the girder. The last two columns indicate the levels of difference between the results obtained from the current model and Andrawes' model and the experimental results.

Table 6.25
Strains (μ) for bridge with RC diaphragm with loading on girder 1

Location	E	C	A	(E-C)/E*100	(E-A)/E*100
1R	-8.9	26.5	-22	397.8	-147.2
1L	110.7	121	91	-9.3	17.8
2R	-59	-56	-49	5.1	16.9
2L	12.1	33.1	18	-173.6	-48.8
3R	-38.9	-91	-48	-133.9	-23.4
3L	7.8	-3.3	-9	142.3	215.4

From the results, it was observed that the performance of the current finite element model was similar to that of the experimental bridge and also Andrawes' Model. In the case of deflections,

as shown in table 6.27, the variation is in the order of -25 percent to 5 percent, which is within the permissible limits. While the strain variation was large percentage wise for the small strains, the maximum values were close. These results provided the confidence needed to perform studies on lateral loading using the current 3-D solid finite element model.

Table 6.26
Strains (μ) for bridge with X plus strut diaphragm with loading on girder 1

Location	E	C	A	(E-C)/E*100	(E-A)/E*100
1R	-67.5	-30	-35	55.6	48.1
1L	148.7	175	127	-17.7	14.6
2R	-57.6	-67.5	-58	-17.2	-0.7
2L	32.5	57.5	41	-76.9	-26.2
3R	-43.7	-90	-69	-105.9	-57.9
3L	17.4	12	4	31.0	77.0

Table 6.27
Deflection (in) for X plus Strut diaphragm configuration with loading on Girder 1

Diaphragm type	Load position	EXP(E)	C	A	(E-C)/E*100	(E-A)/E*100
RC Diaphragm	1	0.075	0.089	0.08	-18.7	-6.7
	2	0.075	0.079	0.065	-5.3	13.3
No diaphragm	1	0.225	0.2128	0.21	5.4	6.7
	2	0.2	0.238	0.16	-19	20
X plus Strut	1	0.095	0.107	0.08	-12.6	15.8
	2	0.075	0.095	0.065	-26.7	13.3

6.13.2 Diaphragm Influence on Bridge Performance under Impact Loading

The study of impact on bridge behavior with different ID configurations was done for two bridges. The two bridges chosen were S9L90 and S9L130, for which the study was done with steel ID, RC ID, and without ID. Steel ID configurations used for S9L90 and S9L130 were channel section and X plus bottom strut, respectively, as proposed earlier. For X plus bottom strut

diaphragm members, the elements were modeled as 3-D LINK-8 elements (line element), while a channel section diaphragm was modeled as SHELL 28 elements (two dimensional shell elements) in ANSYS (figures 6.18 and 6.19).

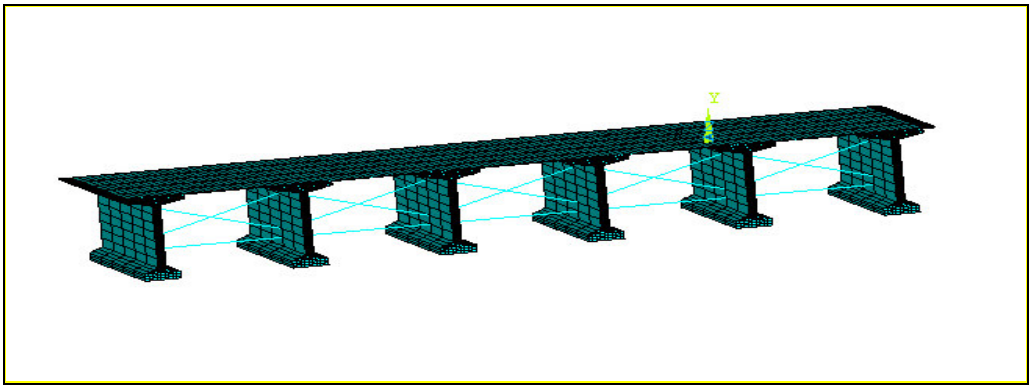

Figure 6.18
Section showing X plus bottom strut in ANSYS

The magnitude of impact is a function of several parameters such as mass, speed, geometrical configuration, and hardness (Abendroth et al., 2003), and there is no available literature which gives information on issues related to impact loading. A numerical value of impact load was assumed, which was applied as a concentrated static load. This value was taken as 120 kips, the same value which was used by Abendroth et al. (2003). This study was done for impact at the bottom flange of the girder.

6.13.3 Different Cases Considered in Study of Lateral Impact

For both bridges, the impact load was applied at two locations - one at the location of the ID and another midway between two diaphragms. For S9L130, where there are two diaphragms, impact load was applied midway between the two IDs (which is the midspan) and at one of the IDs. For S9L90, the loading was applied midway between the ID and the end diaphragm (one fourth span length) and at the location of the ID (midspan).

The comparison was done between the maximum values of the first principal stresses in the

girder undergoing impact and the two girders next to it in the regions of interest. For each impact case, the results were extracted at the location of impact and also at the other location where the impact load was intended to be applied. That is, for S9L90, the results were extracted at the mid-span and quarter span; for S9L130, it was at the mid-span and location of the ID. Results from the small regions of stress concentrations along the bridge were eliminated, as taking these results into account might lead to erroneous conclusions. Therefore, caution was taken to filter out these results with the aid of contour plots for the first principal stresses in ANSYS. These regions existed at the location of loading, at connections between different elements, and at the location of the supports. This could be observed in figure 6.20, where a small region of stress concentration exists which is in red color at the location of impact on the girder undergoing collision for the S9L130 bridge.

6.13.4 Results for Impact Studies

Values of principal stresses for S9L90 and S9L130 at regions of interest for different impact loading conditions are presented in tables 6.28 and 6.29. For bridge configuration S9L90, when the impact occurred at the diaphragm location, the RC ID provided the most protection to the girder. The principal stresses developed at the ID location were about one-third of the principal stress developed in the girder for the case without IDs in the region of impact. In contrast, the presence of steel IDs created a 40 percent reduction in principal stresses. When the impact occurred at quarter span, which is 22.5 ft. away from both the end and the ID, there was no significant difference in principal stress developed for bridges with different ID types and the bridge without IDs.

Similar results were observed in bridge configuration S9L130. In this case, the mid-span was midway between the two IDs at a distance of 21.6 ft. from each. When the impact occurred at mid-span, there was no significant difference in principal stresses for the bridges with both ID types and the one without IDs. When the impact occurred at the ID location, the principal stresses developed were 0.5, 0.9, and 3.5 for bridges with RC, steel, and without ID, respectively.

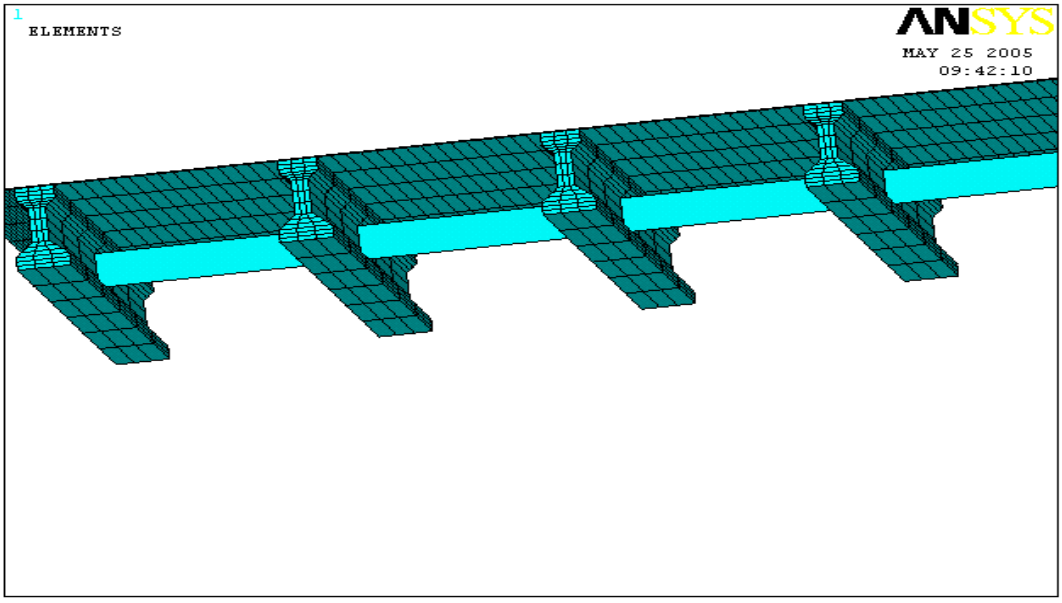

Figure 6.19
Section showing channel ID in ANSYS

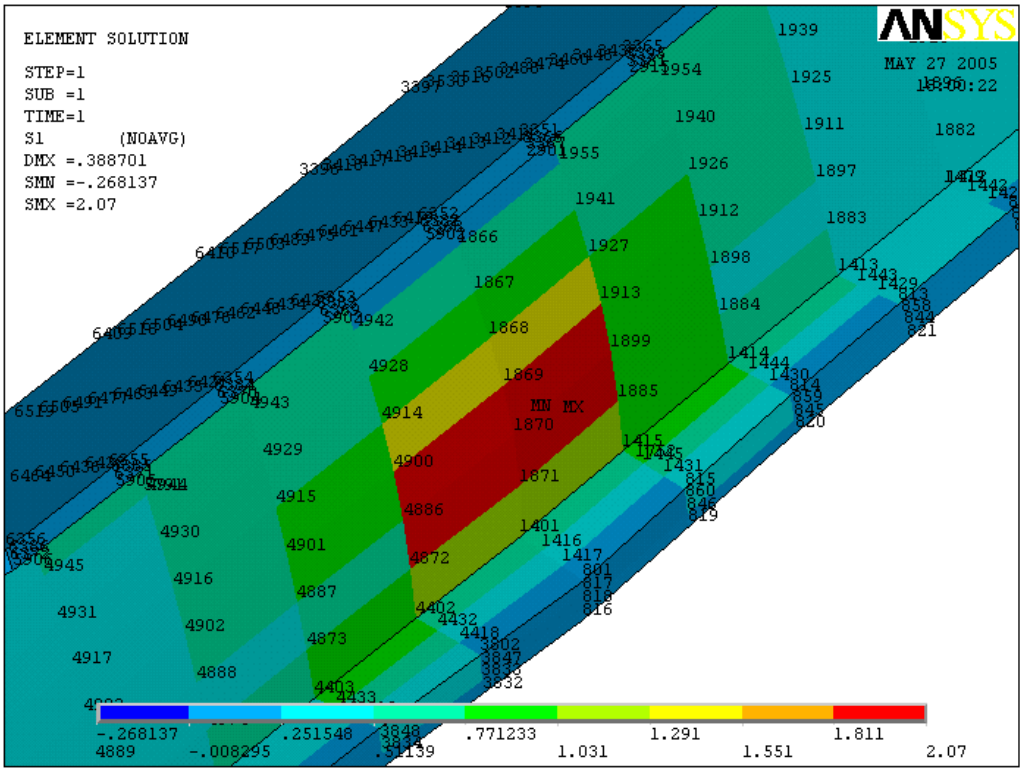

Figure 6.20
Contour for principal stress on outer face of exterior girder which underwent impact for S9L130 bridge

Table 6.28
Principal stresses (in ksi) in region of interest for S9L90 bridge with different diaphragm configuration

Location of impact load	Results region	Girder no.	Diaphragm section		
			RC	channel	no ID
Diaphragm location	Diaphragm location	1	0.45	0.8	1.4
		2	0.11	0.45	0.05
		3	0.07	0.2	0.005
	quarter span	1	0.15	0.3	0.33
		2	0.035	0.07	0.06
		3	0.015	0.01	0.01
quarter span	Diaphragm location	1	0.3	0.23	0.25
		2	0.09	0.06	0.03
		3	0.04	0.03	0.008
	quarter span	1	1.2	1.3	1.3
		2	0.07	0.08	0.07
		3	0.03	0.025	0.025

These results show that when the impact occurred at the location where IDs are located, different IDs reduced the impact stresses to a different extent with respect to the case without IDs. Since the magnitude of the real future impact load is unknown, it could not be concluded if the diaphragm would be in a position to transfer the impact load successfully to other girders, as the structural performance may be nonlinear under large impact loads. A more detailed study is needed to reach a conclusion on how diaphragms affect the performance of a bridge when the impact occurs at the location of the diaphragm. But when the impact takes place at a significant distance from the ID, the ID and its type have no effect on the behavior of the bridge under impact. If the IDs are provided for the purpose of protecting the girders under impact, they must be provided above each lane of the road under the bridge. Therefore, the current ID locations that are based upon the purpose of providing stability are not sufficient for protecting the girder under impact.

6.13.5 Parametric Study for Bridges with Steel IDs

After selecting the diaphragms and confirming that those diaphragms chosen were adequate,

a parametric study was carried out for the bridges listed in table 6.4 with corresponding steel diaphragms for those bridges. Only those parameters that could affect the LDF were considered. The results of this study are listed in table 6.31. In this table, the values of strain, deflection, and LDF values are presented for interior and exterior girders of bridges, both with and without IDs. Percentage reduction in these values caused due to the steel IDs are presented, and the value of R_d calculated from the formulas developed for RC diaphragms is also included.

The ratio of the axial stiffness of steel ID to the axial stiffness of RC ID was used to determine the stiffness reduction factor, which was used in calculating R_d values. The axial stiffness ratio was considered, as it was already known that the reduction in LDF due to IDs is significantly dependent on the axial stiffness of IDs. But for X-plus-strut steel IDs, with the axial stiffness being unknown, the stiffness ratio was taken as 40 percent (discussed earlier), since this value of stiffness ratio gave nearly the same value of R_d obtained from the formulae and the results obtained from FEM analysis. The stiffness ratio for the steel diaphragms used in calculating R_d values, corresponding to each girder type, is presented in table 6.30. Although the expression for R_d for exterior girders does not include the influence of ID stiffness, the expression would yield an R_d value which is on the upper side since the stiffness ratio is always less than 1.

By comparing the R_d values obtained from the FEM to those obtained from the formulae, it was concluded that the R_d formula developed for RC diaphragms could be used for steel diaphragms also by taking the axial stiffness ratio of steel to RC ID into consideration in determining the stiffness reduction factor.

Table 6.29
Principal stresses (in ksi) in region of interest for S9L130 bridge with different diaphragm configuration

Location of impact	Results region	Girder no.	Diaphragm section		
			RC	X + strut	no ID
Mid-span	Mid-span	1	3.3	3.33	3.5
		2	0.125	0.128	0.07
		3	0.017	0.059	0.015
	Diaphragm location	1	1	1.11	0.95
		2	0.26	0.18	0.065
		3	0.1	0.11	0.013
Diaphragm location	Mid-span	1	0.12	0.2161	0.78
		2	0.058	0.057	0.05
		3	0.01	0.023	0.01
	Diaphragm location	1	0.5	0.9	3.5
		2	0.05	0.215	0.08
		3	0.05	0.19	0.013

Table 6.30
Stiffness ratio of steel ID to RC ID for particular girder type

Girder Type	Stiffness ratio (%)
II	71
III	56.5
IV	46.7
BT	40

Table 6.31
Parametric study for bridges with steel diaphragms

S.No	case	Girder Type	Skew	Interior(In) or Exterior(Ex)	strain	%change in strain	Deflection (in)	%change in deflectio	FEM LDF	%fem change	Rd
1	S9L65D0	II	0	In	247.45		0.4311		1.26		
				Ex	252.08		0.4796		1.28		
	S9L65D1	II	0	In	218.22	11.81	0.3944	8.50	1.11	11.74	11
				Ex	265.32	-5.25	0.4948	-3.18	1.34	-5.28	-7.2
2	S9L65D0	II	30	In	224.24		0.3996		1.24		
				Ex	240.53		0.4457		1.31		
	S9L65D1	II	30	In	201.75	10.03	0.3710	7.16	1.15	7.39	6.1
				Ex	245.40	-2.03	0.4581	-2.78	1.35	-2.70	-5.06
3	S9L65D0	II	50	In	179.37		0.3281		1.19		
				Ex	218.91		0.3953		1.43		
	S9L65D1	II	50	In	158.20	11.80	0.3022	7.89	1.13	5.39	4.4
				Ex	223.95	-2.30	0.4048	-2.41	1.47	-2.93	-5.06
4	S9L110D0	lV		In	160.00		0.5682		1.14		
				Ex	177.26		0.7066		1.26		
	S9L110D2	lV		In	143.90	10.06	0.5071	10.75	1.03	10.07	9.2
				Ex	181.47	-2.37	0.6857	2.96	1.29	-2.36	-2.9
5	S9L110D0	IV	30	In	152.61		0.5504		1.14		
				Ex	172.71		0.6624		1.28		
	S9L110D2	IV	30	In	140.54	7.91	0.5015	8.88	1.05	8.07	4.6
				Ex	175.44	-1.58	0.6730	-1.59	1.30	-1.52	-1.7
6	S9L110D0	IV	50	In	135.27		0.4960		1.12		
				Ex	162.83		0.5995		1.33		
	S9L110D2	IV	50	In	123.45	8.73	0.4480	9.68	1.02	8.59	3.2
				Ex	165.02	-1.34	0.6072	-1.27	1.35	-1.55	-1.7
7	S9L130D0	BT	0	In	167.40		0.5970		1.20		
				Ex	182.90		0.7390		1.30		
	S9L130D2	BT	0	in	136.91	18.22	0.4670	21.78	0.98	18.52	17.8
				ex	189.51	-3.61	0.7686	-4.01	1.35	-3.84	-3.9
8	S9L130D0	BT	30	In	160.36		0.5804		1.18		
				Ex	179.00		0.6988		1.31		
	S9L130D2	BT	30	In	143.68	10.40	0.5027	13.38	1.05	10.66	8.9
				Ex	182.03	-1.69	0.7136	-2.12	1.34	-1.64	-2.4
9	S9L130D0	BT	50	In	145.71		0.5370		1.15		
				Ex	172.09		0.6496		1.34		
	S9L130D2	BT	50	In	133.25	8.55	0.4831	10.03	1.04	9.11	6.2
				Ex	173.75	-0.96	0.6566	-1.08	1.35	-0.88	-2.4

CHAPTER 7. BRIDGE LOAD TESTING - PLANNING AND INSTRUMENTATION

7.1 Introduction

Static and dynamic load tests were conducted on the bridge structure described below on February 20, 21, and 22, 2006. These tests were conducted on the original bridge configuration. Plans for similar load tests after the removal of its intermediate diaphragm (ID) were in place, pending approval by the LADOTD. Approval was not granted by the time of completion of this investigation. The bridge span located east of Cypress Bayou was instrumented and tested, and numerically analyzed using the ANSYS full 3D finite element model developed by the research team.

The results obtained from field tests were compiled, analyzed, and compared to finite element predictions, AASHTO Standard (2002) and AASHTO LRFD (2004) bridge design codes. These comparisons are presented in chapter 8 in the form of tables, graphs, and plots. Preliminary finite element predictions were conducted before the bridge tests and used to guide the testing process in order to ensure personnel safety and bridge integrity.

7.2 Bridge Description

The tested bridge is located over Cypress Bayou in District 61, on LA 408 East. The location of this bridge and its easy accessibility were some of the factors that were considered. According to its last bridge inspection data recorded on March 11, 2002, the total average daily traffic (ADT) for the structure was 11,473. This bridge structure is representative of the large majority of prestressed concrete slab-on-girder highway bridges in the state of Louisiana and was selected by an inspection team comprised of personnel from FHWA, LADOTD, and LSU research team.

This bridge was built in 1984 and has three straight simple spans, each measuring 55 ft in length with zero skew angles (figure 7.1). Its cross section has seven AASHTO Type II prestressed

concrete girders, spaced 7 ft from center to center. All girders are anchored to the supports at both ends with anchor bolts on both sides of them. Each span has one intermediate diaphragm (ID) located at the midspan. This ID is not connected to the deck, which is essential for its removal without damaging the deck structure (figure 7.2). The bridge structure number on LADOTD records is 255 02 02.08.1.

7.3 Data Acquisition

Strains were acquired by a 16-channel Structural Testing System II (BDI-STS II) manufactured by Bridge Diagnostics, Inc (figure 7.3). The STS II is a cutting edge system especially developed for bridge tests. The system's water resistant "Intelligent" strain transducers (or intelliducers) have full Wheatstone bridge and four active 350-Ohm foil gauges.

These intelliducers are automatically detected by the BDI-STS II after being connected. Through the Automatic Vehicle Position Indicator (AVPI, figure 7.4) attached to the testing truck, the longitudinal position of the truck can be determined at any time during the tests, which is essential while analyzing and comparing the strains and deflections obtained. Mid-span deflections and accelerations were acquired for all seven girders using a Gould DAStarNet 32-channel data acquisition system (figure 7.5).

Acoustic emissions were acquired using a state-of-the-art DiSP Acoustic Emissions workstation system along with a set of four Physical Acoustics Corporation (PAC) sensors to facilitate non-destructive inspection of structures. These sensors were used to detect cracking on both sides of the middle girder and the intermediate diaphragm. Acquisition of acoustic emission signals and their digital processing is enabled with the implementation of the PCI/DSP cards in the DiSP workstation. This enhances the performance and the multiple DSP technology as a single PCI/DSP card caters to process information from four sensors simultaneously. The master PCI/DSP-4 board also has eight parametric channels built-in. This DiSP-16 system also includes a

PC with the latest version of AEWin data processing software, 16 Hit LED on the front panel, and an on-board Ethernet 10/100 Mbit interface developed by PAC. This system also has remote monitoring capabilities enabled with the software PAC AE system viewer provided along with the system. All four sensors (R6I) are resonant frequency sensors (figure 7.6). They have integral 40 dB pre-amplifiers and auto sensor testing (AST) capabilities. AST capacity of these sensors enables them to pulse as well as receive signals. This feature ensures sensitivity of the sensor throughout the test. The post-processing of the AE data was done using the AEWin software, which has exceptional graphing capabilities that were attuned to this specific bridge test. The results of this collaboration are presented in Cai *et al.* (State Project No. 736-99-1134, 2006).

7.4 Bridge Loading

The bridge was loaded with two dump trucks (figure 7.7) weighing 61.1 kips (Truck 1) and 61.3 kips (Truck 2). Their weights were acquired using portable scales. The weight values in the front axles were 18 kips and 17.8 kips, with back axle weights equal to 43.1 kips and 43.5 kips, respectively.

Figure 7.1
Lateral view of test bridge

Figure 7.2
Intermediate diaphragm on load-tested bridge

Figure 7.3
STS II data acquisition system and intelliducer

7.4.1 Static Loading

During the static load tests, the trucks were driven at a constant crawling speed of about 5 mph on three longitudinal loading paths, as shown in figures 7.8, 7.9, and 7.10. After each crawling speed test, each truck was backed up and stopped with its middle axle at the mid-span. Each of the crawling speed and crawling stopping tests were performed twice for verification of results. Each

traffic lane and the shoulder were first loaded with a single truck; Lane 1 was then loaded simultaneously with Lane 2 and the shoulder, respectively. On the first day of tests, only the shoulder and traffic Lane 1 were loaded separately and together because the objective was to cause maximum effects on the exterior girder and, consequently, strain gauges were installed only on the intermediate diaphragm segments E and F. On the second day, traffic Lanes 1 and 2 and the shoulder were loaded separately, and the shoulder and traffic Lane 1 were loaded together because strain gauges were attached to the girders. On the third day, only traffic Lanes 1 and 2 were loaded before and after relocating the strain gauges from the girders to the intermediate diaphragm segments C and D. Simultaneous loading of the traffic lanes represented the routine service condition causing the maximum effect on the central girder, while loading traffic Lane 1 and the shoulder produced the worst case scenario for the exterior girder. The design lanes coincided with the traffic lanes and the shoulder, and the trucks were positioned according to AASHTO bridge design specification (LRFD, 2004), in which the design lanes can be more toward the edge or center of the bridge. These loading paths were chosen to cause maximum effects in the fascia girder (figure 7.8) and normal traffic effects in an interior girder (figure 7.10). Strain, deflections, and acoustic emissions were continuously acquired from the static tests.

Figure 7.4
Automatic vehicle position indicator

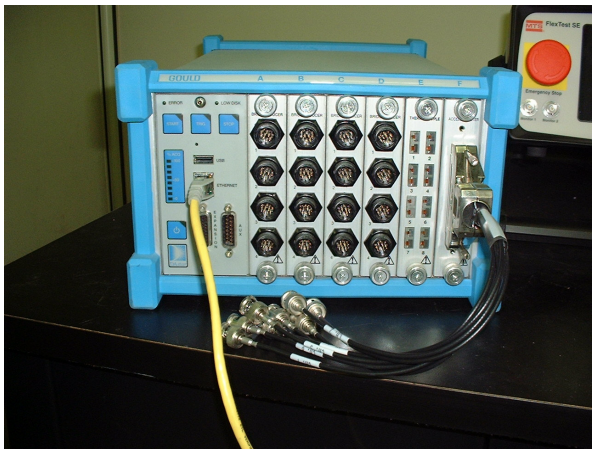

Figure 7.5
Gould data acquisition system

Figure 7.6
Acoustic emissions R6I-AST sensor

Figure 7.7
Trucks used in field loading tests

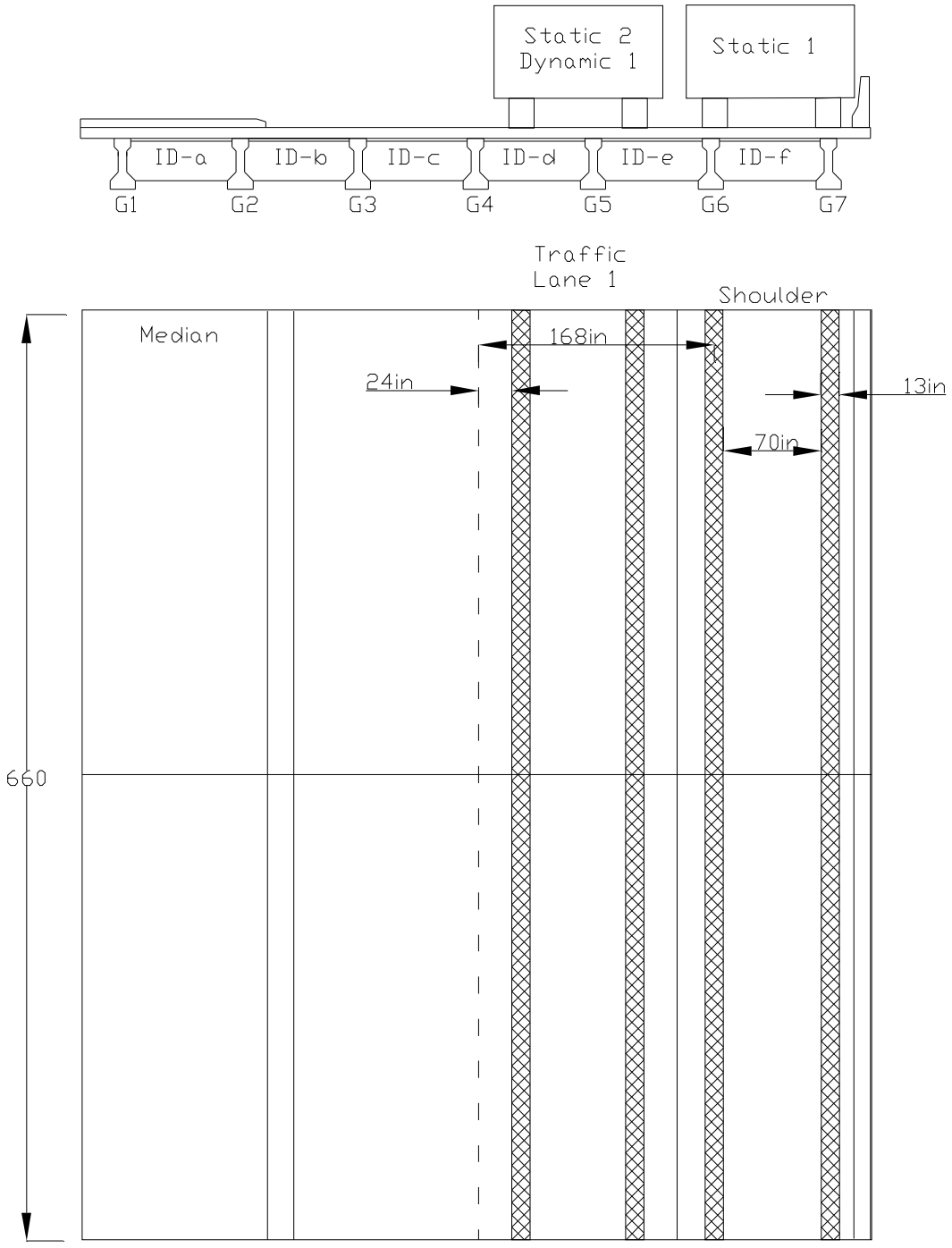

Figure 7.8
Loading paths for strain gauges on diaphragm segments E and F

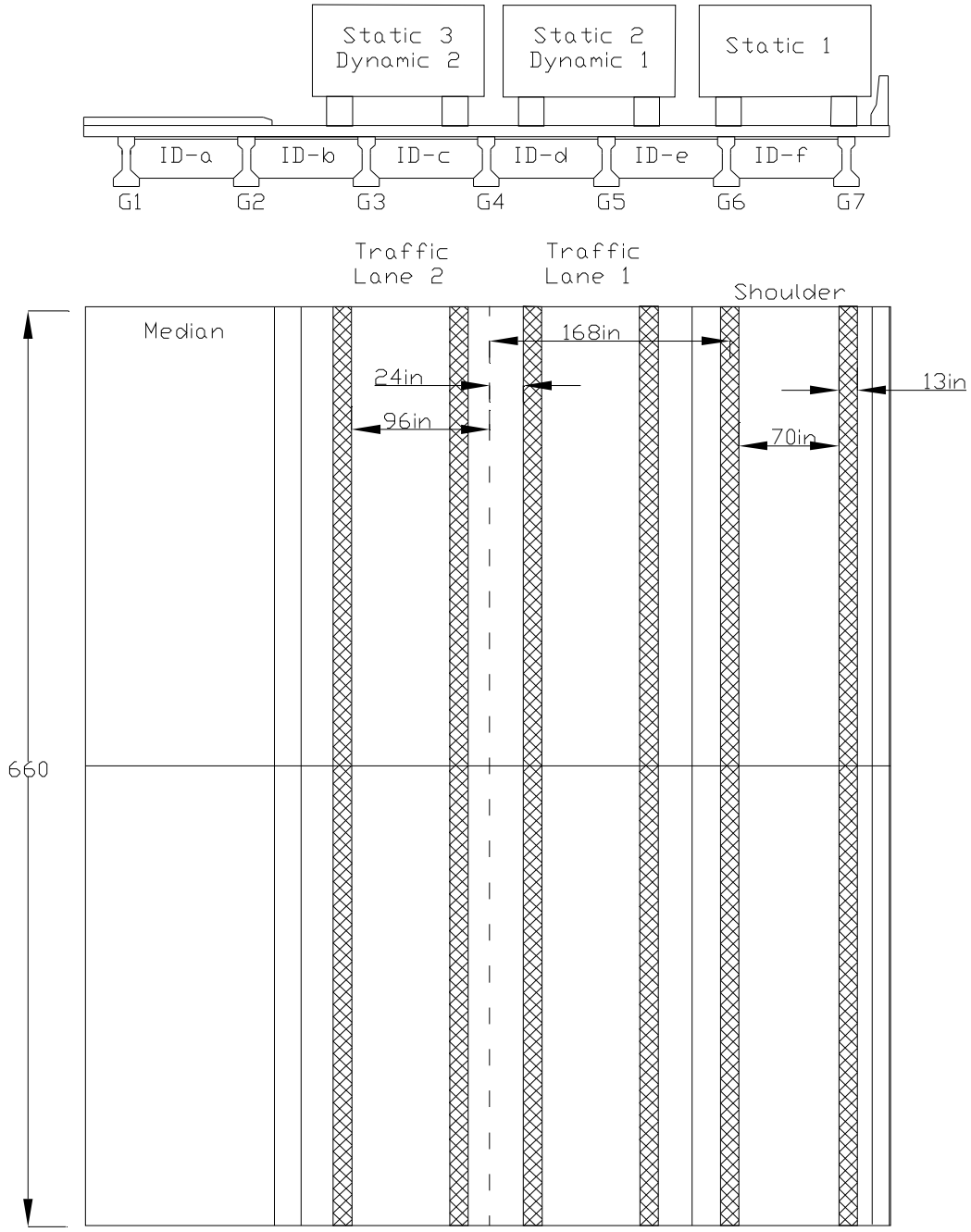

Figure 7.9
Loading paths for strain gauges on girders

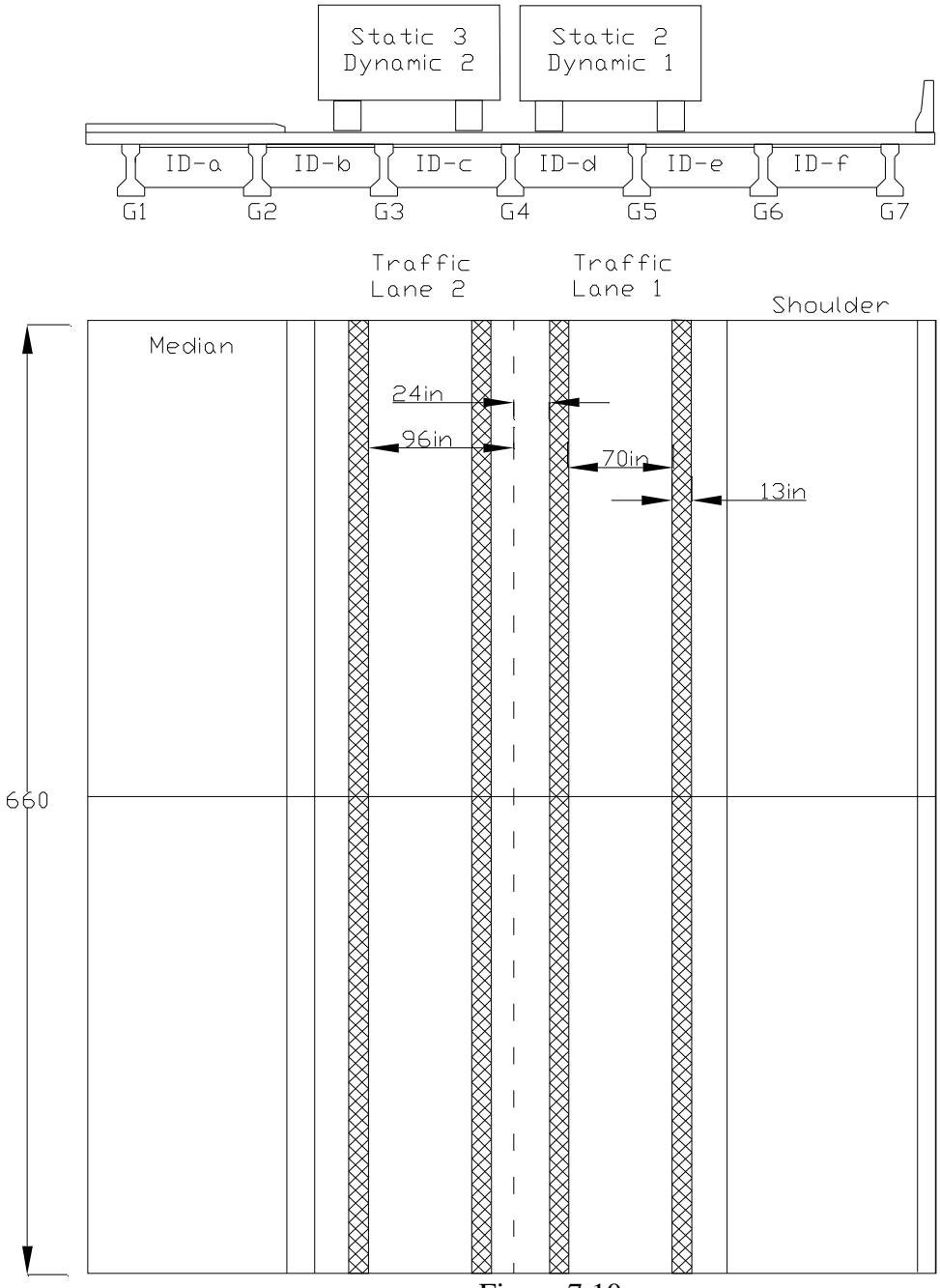

Figure 7.10
Loading paths for strain gauges on diaphragm segments C and D

7.4.2 Dynamic Loading

Dynamic loading tests were performed on traffic lanes with the truck at speeds of 30, 38.5, 40, and 43 mph. In addition to strains, deflections, and acoustic emissions, accelerations were also continuously acquired as the truck passed over both traffic lanes at the above-mentioned speeds, one

lane at a time (figure 7.9). For safety reasons, dynamic tests were carried out only on traffic lanes. Dynamic results are presented in chapter 8.

7.5 Loading Tests Description

All tests were performed on the bridge as built in its original configuration, i.e., with the ID still in place. In these tests, all girders and ID segments C, D, E, and F were instrumented according to figures 7.11, 7.12, 7.13, 7.14, and 7.15, later discussed. In order to acquire strains in the girders and diaphragms, the tests were repeated after the strain gauges were relocated, or three sets of test were performed for three instrumentation positions. Within each set of tests, every truck pass was repeated for results verification. These truck passes are presented in table 7.1, in which their names are labeled as follows. If the test was dynamic, the label shows "D" followed by the truck speed (Dynamic at 40 mph or D40); if static, it was either rolling (Static Rolling or SR) along the bridge at about 5 mph or stopped with the middle axle at the mid-span (Static Stopping or SS). The next label describes the truck and its position. For example, if Truck 1 was on Lane 1 the label reads T1L1; if Truck 1 was on Lane 1 and Truck 2 on the Shoulder the label reads T1L1_T2Sh. Since each pass was repeated within the same strain gauges configuration, the first pass reads P1 and its repetition reads P2 for result verification. The last label depicts the strain gauges configuration - if they were on the girders, it reads GIRDERS; if on ID segments C and D, they read ID_CD. For example, the second slow rolling pass of Truck 1 on the shoulder when the strain gauges were placed on ID segments E and F is named SR_T1Sh_P2_ID_EF. To simulate the bump effect at the bridge end, wooden boards with different heights were placed near the bridge end during the dynamic test, which is labeled as B1 to B3.

For the first set of tests, 12 strain gauges and four acoustic emission sensors on ID segments E and F (figure 7.11) and five accelerometers on girders G3 to G7 were installed. The various sensors positions are illustrated in figures 7.11, 7.12, 7.13, 7.14, and 7.15. The objective of this

instrumentation configuration was to acquire strains on ID segments E and F, while also acquiring accelerations from some of the girders and acoustic emissions on the intermediate diaphragm. The loading tests performed are listed in table 7.1. After the first set of tests was completed, the strain gauges were mounted to the girders in the second set of tests, and the deflection transducers and accelerometers were installed on each of girders (G1 to G7), and the truck loadings were performed. Finally, in the third set of tests, the strain gauges were relocated and mounted to ID segments C and D. Deflections and accelerations were again acquired from all girders, while the acoustic emissions sensors were installed at the bottom of G4 and on ID segment D, and the loading tests were performed.

7.5.1 Loading Description for Cases with Strain Gauges on ID Segments E and F

In this loading test set, four loading tests were performed, of which three were static and one was dynamic (figure 7.8). The first static loading test was performed with Truck 1 on the shoulder. The second one was done with Truck 1 on Lane 1, while the third static test had Truck 2 on the shoulder and Truck 1 on Lane 1. These positions were selected with the objective to cause maximum load effects on the interior girder G6 and exterior girder G7, as well as in ID segments E and F. In all static tests, the trucks were moving side-by-side at a crawling speed of about 5 mph without stopping (SR tests) or stopping with the middle axle at the mid-span (SS tests). Trucks 1 and 2 were then driven at 40 mph on Lane 1. Strains on ID segments E and F were acquired, as well as deflections, accelerations, and acoustic emissions. Each test was repeated in order to provide verification and confirmation of results.

7.5.2 Loading Description for Cases with Strain Gauges on Girders

Seven tests were performed in this loading test set (figure 7.9). These loading tests are three static with one truck on the shoulder, on Lane 1 and on Lane 2; one static with Truck 1 on Lane 1 and Truck 2 on the shoulder; and another static with Truck 1 on Lane 1 and Truck 2 on Lane 2.

These two tests were intended to produce maximum effects on girders G4 and G7. Two dynamic tests were performed with Truck 1 riding on Lane 1 and Lane 2 at a speed of about 40 mph. Each test was repeated in order to provide verification and confirmation of results.

7.5.3 Loading Description for Cases with Strain Gauges on ID Segments C and D

In this loading test set, five loading tests were performed, of which three were static and two were dynamic (figure 7.10). The first static loading test was performed with Truck 1 on Lane 1, the second one with Truck 1 on Lane 2, while the third static test had Truck 1 on Lane 1 and Truck 2 on Lane 2. These positions were selected to cause maximum effects on the interior girder G4 and ID segments C and D. In all static tests, the testing trucks were driven side-by-side at a crawling speed of about 5 mph without stopping (SR tests) or stopping with the middle axle at the mid-span (SS tests). Truck 1 was then driven at 40 mph on Lanes 1 and 2. Strains on ID segments C and D were acquired as well as deflections, accelerations, and acoustic emissions. Each test was repeated in order to provide verification and confirmation of results.

Table 7.1
Loading tests performed

Test Name	**Test Type**	**Loading Position**	**Members of Interest**
SR_T1Sh_P1_ID_EF	Static Rolling	Truck 1on Shoulder	ID Segments E and F
SS_T1Sh_P1_ID_EF	Static Stopping	Truck 1on Shoulder	ID Segments E and F
SR_T1Sh_P2_ID_EF	Static Rolling	Truck 1 on Shoulder	ID Segments E and F
SS_T1Sh_P2_ID_EF	Static Stopping	Truck 1 on Shoulder	ID Segments E and F
SR_T1L1_P1_ID_EF	Static Rolling	Truck 1 on Lane 1	ID Segments E and F

(Table Continued)

SS_T1L1_P1_ID_EF	Static Stopping	Truck 1 on Lane 1	ID Segments E and F
SR_T1L1_P2_ID_EF	Static Rolling	Truck 1 on Lane 1	ID Segments E and F
SS_T1L1_P2_ID_EF	Static Stopping	Truck 1 on Lane 1	ID Segments E and F
SR_T1L1_T2Sh_P1_ID_EF	Static Rolling	Truck 1 on Lane 1 and Truck 2 on Shoulder	ID Segments E and F
SS_T1L1_T2Sh_P1_ID_EF	Static Stopping	Truck 1 on Lane 1 and Truck 2 on Shoulder	ID Segments E and F
SR_T1L1_T2Sh_P2_ID_EF	Static Rolling	Truck 1 on Lane 1 and Truck 2 on Shoulder	ID Segments E and F
D40_T1L1_T2L2_P1_ID_EF	Dynamic at 40 MPH	Truck 1 on Lane 1 and Truck 2 on Lane 2	ID Segments E and F
D40_T1L1_T2L2_P2_ID_EF	Dynamic at 40 MPH	Truck 1 on Lane 1 and Truck 2 on Lane 2	ID Segments E and F
SR_T1L1_P1_GIRDERS	Static Rolling	Truck 1 on Lane 1	Girders
SS_T1L1_P1_GIRDERS	Static Stopping	Truck 1 on Lane 1	Girders
SR_T1L1_P2_GIRDERS	Static Rolling	Truck 1 on Lane 1	Girders
SS_T1L1_P2_GIRDERS	Static Stopping	Truck 1 on Lane 1	Girders
SR_T1Sh_P1_GIRDERS	Static Rolling	Truck 1 on Shoulder	Girders
SS_T1Sh_P1_GIRDERS	Static Stopping	Truck 1 on Shoulder	Girders
SR_T1Sh_P2_GIRDERS	Static Rolling	Truck 1 on Shoulder	Girders
SS_T1Sh_P2_GIRDERS	Static Stopping	Truck 1 on Shoulder	Girders
SR_T2L1_P1_GIRDERS	Static Rolling	Truck 2 on Lane 1	Girders

(Table Continued)

SR_T2Sh_P1_GIRDERS	Static Rolling	Truck 2 on Shoulder	Girders
SS_T2Sh_P1_GIRDERS	Static Stopping	Truck 2 on Shoulder	Girders
SR_T1L1_T2Sh_P1_GIRDERS	Static Rolling	Truck 1 on Lane 1 and Truck 2 on Shoulder	Girders
SS_T1L1_T2Sh_P1_GIRDERS	Static Stopping	Truck 1 on Lane 1 and Truck 2 on Shoulder	Girders
D40_T1L1_GIRDERS	Dynamic at 40 MPH	Truck 1 on Lane 1	Girders
D30_T1L1_GIRDERS	Dynamic at 30 MPH	Truck 1 on Lane 1	Girders
D30_T1L1_B1_GIRDERS	Dynamic at 30 MPH	Truck 1 on Lane 1	Girders
D40_T1L1_B1_GIRDERS	Dynamic at 40 MPH	Truck 1 on Lane 1	Girders
D30_T1L1_B2_GIRDERS	Dynamic at 30 MPH	Truck 1 on Lane 1	Girders
D40_T1L1_B2_GIRDERS	Dynamic at 40 MPH	Truck 1 on Lane 1	Girders
D30_T1L1_B3_GIRDERS	Dynamic at 30 MPH	Truck 1 on Lane 1	Girders
D40_T1L1_B3_GIRDERS	Dynamic at 40 MPH	Truck 1 on Lane 1	Girders
SR_T1L2_P1_GIRDERS	Static Rolling	Truck 1 on Lane 2	Girders
SS_T1L2_P1_GIRDERS	Static Stopping	Truck 1 on Lane 2	Girders
SR_T1L2_P2_GIRDERS	Static Rolling	Truck 1 on Lane 2	Girders
SS_T1L2_P2_GIRDERS	Static Stopping	Truck 1 on Lane 2	Girders
D38.5_T1L2_GIRDERS	Dynamic at 38.5 MPH	Truck 1 on Lane 2	Girders
D38.5_T1L2_B1_GIRDERS	Dynamic at 38.5 MPH	Truck 1 on Lane 2	Girders

(Table Continued)

D38.5_T1L2_B3_GIRDERS	Dynamic at 38.5 MPH	Truck 1 on Lane 2	Girders
D38.5_T1L2_B2_GIRDERS	Dynamic at 38.5 MPH	Truck 1 on Lane 2	Girders
D40_T1L1_B3_GIRDERS	Dynamic at 40 MPH	Truck 1 on Lane 1	Girders
D43_T1L1_B3inv_GIRDERS	Dynamic at 43 MPH	Truck 1 on Lane 1	Girders
SR_T1L1_T2L2_P1_GIRDERS	Static Rolling	Truck 1 on Lane 1 and Truck 2 on Lane 2	Girders
SR_T1L1_T2L2_P2_GIRDERS	Static Rolling	Truck 1 on Lane 1 and Truck 2 on Lane 2	Girders
SR_T1L1_P1_ID_CD	Static Rolling	Truck 1 on Lane 1	ID Segments C and D
SS_T1L1_P1_ID_CD	Static Stopping	Truck 1 on Lane 1	ID Segments C and D
SR_T1L1_P2_ID_CD	Static Rolling	Truck 1 on Lane 1	ID Segments C and D
SS_T1L1_P2_ID_CD	Static Stopping	Truck 1 on Lane 1	ID Segments C and D
SR_T1L1_T2L2_P1_ID_CD	Static Rolling	Truck 1 on Lane 1	ID Segments C and D
SS_T1L1_T2L2_P1_ID_CD	Static Stopping	Truck 1 on Lane 1	ID Segments C and D
SR_T1L1_T2L2_P2_ID_CD	Static Rolling	Truck 1 on Lane 1	ID Segments C and D
SS_T1L1_T2L2_P2_ID_CD	Static Stopping	Truck 1 on Lane 1	ID Segments C and D
SR_T1L2_P1_ID_CD	Static Rolling	Truck 1 on Lane 2	ID Segments C and D
SR_T1L2_P2_ID_CD	Static Stopping	Truck 1 on Lane 2	ID Segments C and D

(Table Continued)

SS_T1L2_P1_ID_CD	Static Stopping	Truck 1 on Lane 2	ID Segments C and D
SS_T1L2_P2_ID_CD	Static Stopping	Truck 1 on Lane 2	ID Segments C and D
D40_T1L2_P1_ID_CD	Dynamic at 40 MPH	Truck 1 on Lane 2	ID Segments C and D
D40_T1L2_P2_ID_CD	Dynamic at 40 MPH	Truck 1 on Lane 2	ID Segments C and D
D40_T1L1_P1_ID_CD	Dynamic at 40 MPH	Truck 1 on Lane 1	ID Segments C and D
D40_T1L1_P2_ID_CD	Dynamic at 40 MPH	Truck 1 on Lane 1	ID Segments C and D

7.6 Instrumentation Plan

Strains and deflections were continuously acquired for the entire bridge test in all loading paths. The instrumentation positions of the strain gauges, acoustic emissions sensors, cable extension transducers, and accelerometers on the girders and ID segments are shown below in figures 7.11, 7.12, 7.13, 7.14, and 7.15.

7.6.1 Instrumentation for Cases with Strain Gauges on ID Segments E and F

In this test set, the acquisition of data was concentrated on ID segments E and F. The numbered strain gauges were placed on the sides of the most stressed ID segments, as illustrated in figure 7.11. Accelerometers were place at the bottom of girder G3, G4, G5, G6, and G7. Due to the short length of the inspection truck's arm, G1 and G2 were not reached on the first day of tests for accelerometer mounting, and cable extension transducers were not used on any girder. Acoustic emissions sensors were mounted to ID segments E and F on both sides of girder G6 (figure 7.12).

7.6.2 Instrumentation for Loading Cases with Strain Gauges on Girders

In this test set, the acquisition of data was concentrated on the girders (figure 7.13). Strain gauges, accelerometers, and cable extension transducers were placed 1 ft. way from the mid-span on all seven girders to avoid stress concentration due to closeness to the diaphragm. The composite

action between girders and the deck was investigated through placing extra strain gauges on G4 and next to it on the deck, as shown in figure 7.14. The location of acoustic emission sensors are shown in figure 7.15.

7.7 Instrumentation for Cases with Strain Gauges on ID Segments C and D

For this set of tests, the strain gauges were again relocated in order to acquire data from the maximum effects on the ID segments C and D. They were placed on the ID with those two segments on both sides of girder G4, as shown in figure 7.16. Accelerometers and cable extension transducers were kept attached to the bottom of the girders (figure 7.13) and the acoustic emission sensors were located at the same position as in the previous set of tests (figure 7.14).

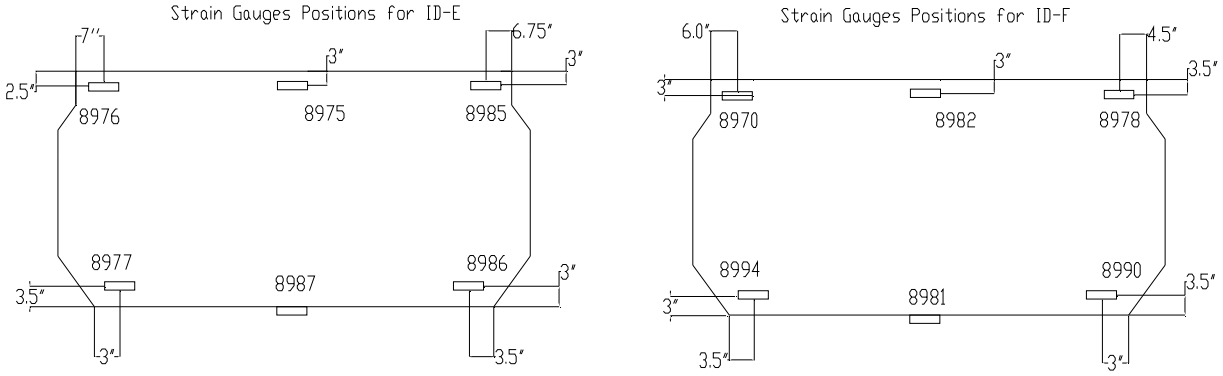

Figure 7.11
Strain gauges positions for loading cases ID_EF

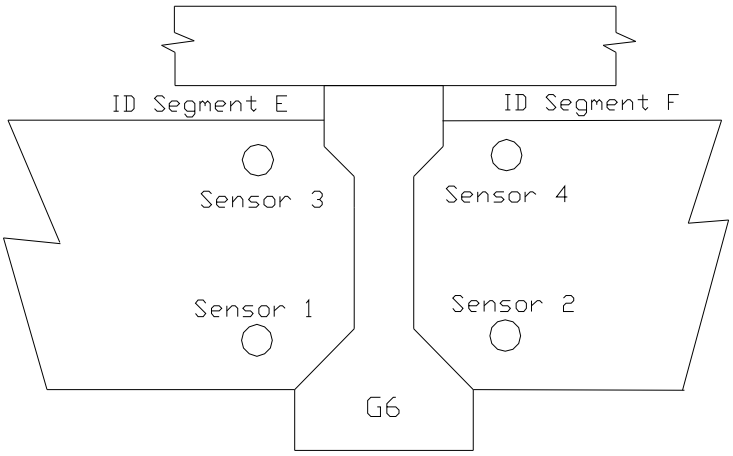

Figure 7.12
Acoustic emissions sensors positions for loading cases ID_EF

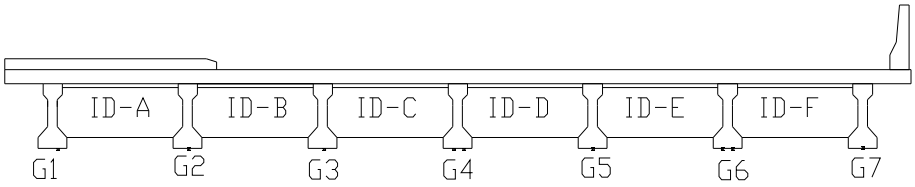

STRAIN GAGE #	8990	8981	8970	8983,8976	8999	8994,8991	8978
ACCELEROMETER #	7	3	6	5	1	4	2
LVDT NAME	A1	A2	A3	A4	B1	B4	B3

Figure 7.13
Instrumentation details for loading cases of girders

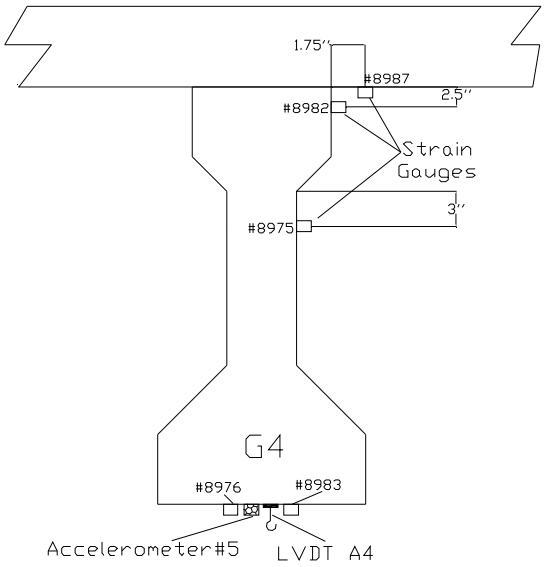

Figure 7.14
Instrumentation details for girder 4

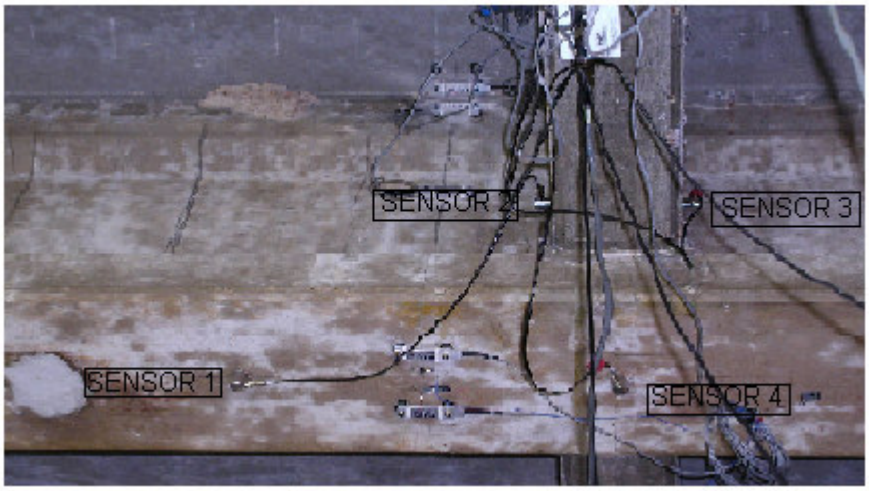

Figure 7.15
Acoustic emissions sensors positions for loading cases of girders and ID_EF

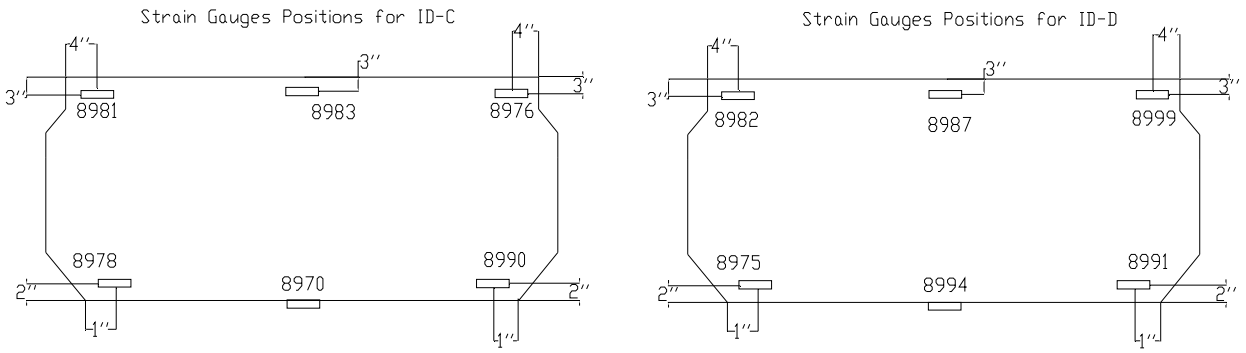

Figure 7.16
Instrumentation details for loading cases of ID_CD

CHAPTER 8. LOAD TESTS AND FINITE ELEMENT ANALYSIS

8.1 Introduction

Load testing is used to evaluate the response of bridges to predetermine loads and to verify their performance in relation to analytical response predictions. There are basically two types of load tests: diagnostic tests and proof tests. Diagnostic tests are used to evaluate certain responses of bridges and to validate analytical or mathematical models. Proof tests are performed to determine the maximum safe load carrying capacity of bridges within the linear-elastic range.

Load testing can be classified as static and dynamic. While static load tests are performed to eliminate the effect of any vibrations, dynamic tests can be used to measure modes of vibration, frequencies and dynamic load allowance, among others.

Static and dynamic diagnostic load tests were performed on the studied bridge, as described in chapter 7. These tests were performed with multiple objectives; the ones relevant to this study are: to evaluate intermediate diaphragms effectiveness and to determine live load distribution and dynamic load allowance. The acquired data analyzed for these purposes were limited to strains and deflections.

8.2 Bridge Loading and Load Distribution Factors

Multiple lane loading configurations were applied in this study in order to consider different scenarios, as described in Chapter 7. The finite element model was loaded in a similar way as the actual bridge, taking into account the same truck axle spacing and loading as measured in the field.

Load distribution factors (LDF) are essential for rational design and rating of bridges. From Ghosn et al. (1986), LDF for each girder is assumed to be equal to the ratio of its strain to the sum of strains of all girders. The weighed strains method was used by Stallings and Yoo (1993) to take into account the different section modulus of girders. This same weighed method was used for strains and deflections in order to calculate LDFs based on the predicted FE results.

The equations below were used to calculate the LDFs (lanes/girder) based on strains and deflections:

a. AASHTO Standard (2002): $LDF = \frac{S(ft)}{D} * 0.5$, where D is 5.5 for interior and exterior prestressed concrete girders;

b. AASHTO LRFD (2004): $LDF = .075 + \left(\frac{S}{9.5}\right)^{0.6}\left(\frac{S}{L}\right)^{0.2}\left(\frac{K_g}{12.0Lt_s^3}\right)^{0.1}$ for interior girders, and multiplied by $e = 0.77 + \frac{d_e}{2800}$ for exterior ones;

c. Finite Element: $LDF = \frac{M_i}{(\sum_{i=1}^{k} M_i)/n} = \frac{nE_iS_i\varepsilon_i}{\sum_{i=1}^{k} E_iS_i\varepsilon_i} = \frac{n\cancel{E_iS_i}\varepsilon_i}{\cancel{E_iS_i}\sum_{i=1}^{k}\varepsilon_i} = \frac{n\varepsilon_i}{\sum_{i=1}^{k}\varepsilon_i}$

where k is the total number of girders, i is the girder for which the load distribution factor is calculated, and n is the number of transversely positioned HS20 trucks loading the bridge, which is 2 in this study. This same procedure was followed for the LDF calculation using deflections.

8.3 Dynamic Allowance Factor (IM)

Bridge vibrations due to moving loads have gained importance due to the accelerated deterioration they can cause in bridge structures if not within acceptable ranges. In order to calculate the impact factor (IM) for this bridge, static and dynamic measurements for strains and deflections were correlated using the equation IM(%) = (Rd/Rs – 1) x 100, in which Rd and Rs are the maximum dynamic and static responses of the bridge, respectively. These results were then compared to the AASHTO Standard and LRFD.

8.4 Actual Bridge Concrete Strength

Non-destructive methods to determine surface hardness are well established and relatively inexpensive; however, they have a limited application in assessing distressed structures (Transue et

al., 1999). ASTM C 805-85 presents the methodology to the application of the rebound hammer method. This method is limited when used in massive structures, although useful to determine the concrete strength near its surface.

For the tested bridge, the concrete strength was verified using a rebound hammer model W-M-250. In this application, readings are based on the rebound impact of a hammer on a piston which rests in contact with the surface of the member whose strength is to be determined. Readings were taken to determine the strength of all girders, deck, end diaphragm and railing.

Tested surfaces were first sounded using a regular hammer to ensure that no concrete spalling or other defects were taking place, thus avoid incorrect readings. Tested spots were smoothed, whenever needed, using a hand-held Makita grinder in order to ensure proper contact with the rebound hammer. Sixteen points in a 4" x 4" grid were tested for each location where the concrete strength was to be determined; these points were spaced 1 inch apart. Of these sixteen points tested, readings further than 3.5 points (no unit) from the overall average were disregarded. A new average of the ten best readings (bold face numbers) was then taken and converted into concrete strength using a calibrated figure similar to Figure 8.1. These test readings are presented below in tables 8.1 through 8.3.

In table 8.1, rebound hammer test readings obtained from the web of all seven prestressed concrete girders are presented. These readings consistently resulted in concrete strengths above 8,500 psi (which is the upper limit of the rebound hammer used) upon conversion ($\alpha = 0°$), except for girder #7, whose measured strength was 7,750 psi. According to records available, the design strength for the girders was 6,000 psi. Test results indicate that the current strength is over 40% higher than the design one. This increased strength could be the result of two factors: first, the natural strengthening of the concrete due to hardening; second, the initial concrete strength most likely was above the design one. Laboratory records indicating the actual concrete strength when it

was poured were not available. If we estimate that the original concrete strength was about 6,500 psi, which is a reasonable assumption, the total strength increase is a little over 30%, which justifies the concrete strength assumed in the analytical finite element model. This kind of concrete strength increase is also indicated by Calcada et Al. (2005).

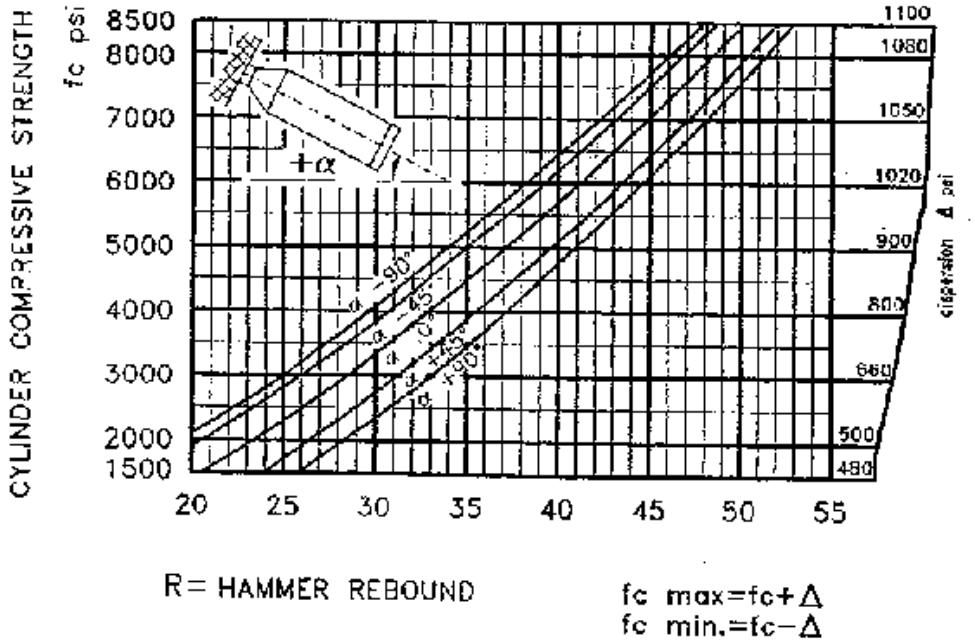

Figure 8.1
Rebound hammer conversion curves example
(Note: not the same as the one used)

The readings obtained from the deck are presented in table 8.2. These readings produced concrete strengths of 5,400 psi and 6,000 psi ($\alpha = +90°$) at the two spots tested. The design concrete strength in this case was 3,500 psi and it is safe to assume that concrete strength equal or higher than 4,000 psi could have been used; however, there is no recorded data to back up this assumption. This would result in an increase of approximately 35% to 50% in relation to the actual concrete strength.

Table 8.3 shows the readings obtained from the end diaphragm and the railing. These readings resulted in concrete strengths close to 6,000 psi ($\alpha = 0°$). The same arguments discussed above are applicable here as well, resulting in a concrete strength increase of about 50%.

In addition to tests on the bridge itself, a concrete beam and three concrete cylinders from the same batch were tested as well in the laboratory. These results are presented in tables 8.4 and 8.5. The rebound hammer average strength for the three cylinders was about 5,080 psi, which is about 50% higher than the design concrete strength of 3,500 psi. As for the beam strength, readings were taken on one side and at the end. The strength at the side was 5,000 psi and 6,250 psi at the end, indicating that the member thickness at the location tested has a significant influence on the result.

Compressive tests were then performed in order to confirm that strengths measured with the rebound hammer were acceptable. The three cylinders tested were cured in accordance with ASTM C192 and tested with a Forney LT-8061-FTS/M compressive test machine. Ultimate concrete strengths for cylinders 1, 2 and 3 were 7,992 psi, 8,250 psi, and 8,447 psi, respectively. The average ultimate strength was 8,230 psi; standard deviation and coefficient of variation were 228.18 psi and 2.77, respectively. These tests indicate that over a short period of 24 months the concrete hardened by about 135%. These results showed that rebound hammer readings were lower than those from compressive tests, possibly due to effect of small dimensions of cylinders and beam tested.

Overall, these rebound hammer test readings qualitatively indicate that the concrete strength increase of 30% used in the finite element model is reasonable, maybe even conservative. This assumption was also confirmed through the comparison of results from static and dynamic load tests to FE model results, as described later in this chapter.

8.5 Maximum Allowable Vehicle Loading

Prior to load test the selected bridge, analyses were performed for legal weights according to "Louisiana Regulations: Trucks, Vehicles and Loads" (2000). These regulations limit the legal license weights on state roads. The truck model chosen for the tests is classified as Type 2, which

can carry a maximum legal weigh of 49,000 lb on non-interstate highways.

Two lanes were simultaneously loaded with 49,000 lb trucks and two axle loading distribution: 1:2:2 and 1:4:4. The axle loading ratio is the fraction of the load taken by each of the three axles; in the first case, the front axle carried 9,800 lb, while the back axles carried 19.600 lb each. In the second case, the front axle carried 5,444 lb and the back axles 21,778 lb each.

Table 8.1
Rebound hammer readings for girders concrete strength

G1 (>8,500 psi)				
	1	2	3	4
A	**56.5**	**58.5**	**58.5**	56.5
B	**57.5**	64.5	55.5	56
C	**57.5**	**59.5**	60.5	56.5
D	**57**	**57**	**58.5**	**59**
AVERAGE =				58.06
AVERAGE OF 10 BEST READINGS =				57.95

G2 (>8,500 psi)				
	1	2	3	4
A	**55**	**56**	60.5	**54.5**
B	**57**	**55**	52	60
C	**56**	58	53	**54.5**
D	**54**	53.5	**58**	**55**
AVERAGE =				55.75
AVERAGE OF 10 BEST READINGS =				55.50

G3 (>8,500 psi)				
	1	2	3	4
A	**57.5**	**59.5**	51	**55**
B	**58**	**57.5**	59.5	59.5
C	**56**	**56.5**	61.5	**59**
D	**57**	61	41	**58**
AVERAGE =				56.72
AVERAGE OF 10 BEST READINGS =				57.40

G4 (>8,500 psi)				
	1	2	3	4
A	53	61	**59**	60
B	**59**	**57.5**	**57.5**	**59.5**
C	**59**	61	56.5	**58.5**
D	**59**	56.5	**58**	**59.5**
AVERAGE =				58.41
AVERAGE OF 10 BEST READINGS =				58.65

G5 (>8,500 psi)				
	1	2	3	4
A	57	**58.5**	**58.5**	56
B	57	**59**	**57**	64
C	**58**	**58.5**	**58**	**58**
D	**57.5**	**58**	60.5	60.5
AVERAGE =				58.50
AVERAGE OF 10 BEST READINGS =				58.10

G6 (>8,500 psi)				
	1	2	3	4
A	56	**59**	**59**	**59**
B	**59**	**58**	**59**	**58**
C	57	**59**	**59**	64
D	**61**	68	62	56
AVERAGE =				59.56
AVERAGE OF 10 BEST READINGS =				59.00

G7 (7,750 psi)				
	1	2	3	4
A	**53**	**53**	**53**	56
B	49	55	**52**	**55**
C	59	50	**55**	**52**
D	48	**52**	**52**	**52**
AVERAGE =				52.88
AVERAGE OF 10 BEST READINGS =				52.90

Figure 8.2 shows the deflections on all girders due to the maximum legal loading for both loading configurations, while figure 8.3 presents their respective live load distribution. The results of these finite element analyses were used to help determine the load level that could not be a threat to the structural integrity of the bridge being tested. This evaluation determined that the load level obtained from the chosen loading vehicles would not jeopardize the bridge structure.

Table 8.2
Rebound hammer readings for deck concrete strength

BETWEEN G1 AND G2 (5,400 psi)				
	1	2	3	4
A	36.5	**48.5**	**46**	**45**
B	**45**	**45.5**	**45.5**	43
C	43	**46.5**	**46.5**	53.5
D	**45.5**	50	50	**45**
AVERAGE =				45.94
AVERAGE OF 10 BEST READINGS =				45.90

BETWEEN G6 AND G7 (6,000 psi)				
	1	2	3	4
A	**48.5**	45.5	**46.5**	55
B	53.5	45	**53**	55.5
C	**46.5**	54.5	**46.5**	**52.5**
D	**47**	**48**	**48.5**	**46.5**
AVERAGE =				49.53
AVERAGE OF 10 BEST READINGS =				48.35

Table 8.3
Rebound hammer readings for end diaphragm and railing concrete strength

BETWEEN G6 AND G7 (6,000 psi)				
	1	2	3	4
A	27.5	54	**47**	**48**
B	51.5	52	34	**42.5**
C	53.5	**44**	**47.5**	**43**
D	**43**	**42.5**	**48.5**	**45**
AVERAGE =				45.22
AVERAGE OF 10 BEST READINGS =				45.10

RAILING (5,900 psi)				
	1	2	3	4
A	**46.5**	**43.5**	54.5	**45**
B	**46**	**46**	**45**	48.5
C	**44.5**	40.5	**44.5**	**42**
D	39.5	39	39	40.5
AVERAGE =				44.03
AVERAGE OF 10 BEST READINGS =				44.78

8.6 Compilation of Static Results

Strains and deflections results were obtained from static and dynamic experimental loading tests, using the test trucks as described in Chapter 7. These results were compared to the ones predicted by a finite element model of the bridge. Load distribution factors and dynamic allowance factors were then calculated as described above and compared with those values specified in AASHTO Standard (2002) and AASHTO LRFD (2004).

The finite element model of the tested bridge was initially analyzed with and without

intermediate diaphragms for loading cases T1L1_T2Sh and T1L1_T2L2. Concrete strengths used were the same as in the original design, which are 6,000 psi for prestressed concrete girders, and 3,500 psi for the deck, diaphragms and railings. This case is defined as FE_Design. It was noticed for both loading cases that strains and deflections predicted were consistently higher than the measured ones, even for the FE model without the intermediate diaphragm. These results indicate that the actual bridge is stiffer than its FE model, as shown in figures 8.4 and 8.5. Load distribution factors were calculated for measured and predicted strains and deflections and then compared to the AASHTO codes values. Figure 8.6 shows that AASHTO load distribution values are higher than the predicted and measured ones.

Table 8.4

Rebound hammer readings for concrete beam

BEAM SIDE (5,000 psi)				
	1	2	3	4
A	37	37.5	46.5	45
B	**37.5**	35	**40**	**41**
C	44.5	**40**	**40.5**	**40.5**
D	**40.5**	**40.5**	**39.5**	**40.5**
AVERAGE =				40.375
AVERAGE OF 10 BEST READINGS =				40.05

BEAM END (6,250 psi)				
	1	2	3	4
A	**45**	**45**	**47.5**	**46**
B	44	**45**	49	**46**
C	**45**	48	44	**46.5**
D	44	**45.5**	**46**	47.5
AVERAGE =				45.875
AVERAGE OF 10 BEST READINGS =				46.05

After processing finite element results for design concrete strength, the model was further refined in order to correct the bridge stiffness. In general, the measured results (strain and deflections) were less than finite element predictions and AASHTO code specifications (Standard and LRFD) due to field uncertainties for the bridge. One of the reasons for the difference between predicted and measured results is the actual concrete strength, which is currently higher than that specified in the project plans because of concrete hardening with time, as demonstrated earlier. Besides, concrete strength during pouring in most cases is already higher than the specified design strength. Real support conditions are also a factor. The anchor bolts may provide some constraints to the bridge that renders the pin-roller type of beam model inaccurate.

Table 8.5
Rebound hammer readings for cylinders

CYLINDER 1 (5,100 psi)				
	1	2	3	4
A	**37.5**	**39.5**	**39.5**	**38.5**
B	35	**39**	**40**	40
C	42	34	**36**	35
D	34	**37**	**38**	**36.5**
			AVERAGE =	37.5938
			AVERAGE OF 10 BEST READINGS =	38.15

CYLINDER 2 (5,000 psi)				
	1	2	3	4
A	35	33.5	**38**	**38.5**
B	**39**	**37.5**	**37**	41.5
C	**36.5**	**37.5**	**36.5**	**39**
D	40.5	**39.5**	40	34
			AVERAGE =	37.7188
			AVERAGE OF 10 BEST READINGS =	37.9

CYLINDER 3 (5,150 psi)				
	1	2	3	4
A	**39**	40	41	35.5
B	33.5	40	**40**	**40**
C	**37.5**	**37.5**	**36.5**	**36.5**
D	34.5	**39**	**40**	**38.5**
			AVERAGE =	38.0625
			AVERAGE OF 10 BEST READINGS =	38.45

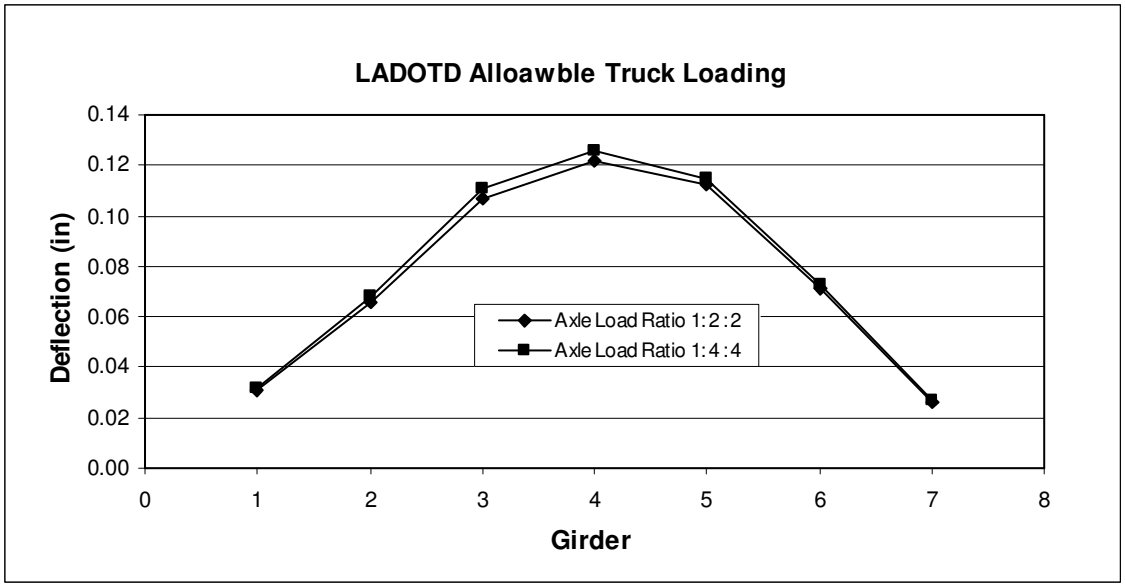

Figure 8.2
Deflections caused by the maximum allowable truck loading

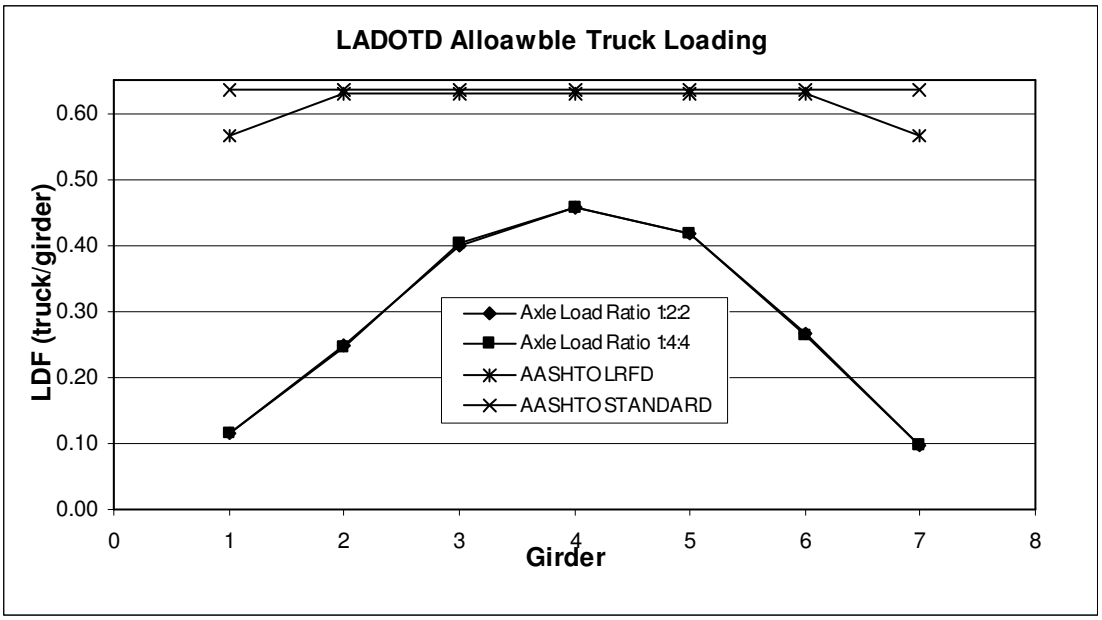

Figure 8.3
LDF Caused by the maximum allowable truck loading

It is well known that the connection between diaphragm and girders may not be fully rigid, although the real stiffness contribution of intermediate diaphragms (ID) has not been accurately defined. The intense vibration caused by heavy trucks at high speeds may result in cracks at the cold joint in the diaphragm-girder interface, thus influencing ID effectiveness. Some studies show that the actual ID stiffness contribution is about 30% of its whole section stiffness (Kostem et al. 1977, Cai and Shahawy, 2004).

Based on above arguments, two more cases were investigated. In the first one, the ID concrete elastic modulus was reduced to 30% of its design value and the other members were kept the same as their original value. This case is defined as FE_30%ID. In the second one, the ID concrete elastic modulus was reduced to 30% of its design value, while the concrete strength of all other members was increased by 30%. This case is defined as FE_30%ID_130%All.

After adjusting the finite element model to conform to existing research regarding concrete stiffness, the model was once again loaded for cases T1L1_T2Sh and T1L1_T2L2. Strain results show that the reduction of ID stiffness by itself produces results closer in pattern to the tests,

especially for exterior girders. The same improvement was observed for deflections. The finite element model results were further improved when the concrete strength for all other members was increased by 30%. Although this was evident for strain results, deflections were slightly lesser than the tests for the most stressed girders in both loading cases. Results for both loading cases are presented in figures 8.7 and 8.8. Load distribution factors were calculated for these two loading cases with the same strength refinement were compared to the experimental loading test and then to the bridge model with concrete design strength and to the AASHTO codes values. Best results were accomplished when the overall concrete strength was increased by 30% with reduced ID stiffness (Case FE_30%ID_130%All). This was clearly observed for deflection, in which loading test results were approached for interior and exterior girder. These values are shown in figures 8.9 and 8.10.

Additional loading tests were performed with one loaded lane only for loading cases T1Sh, T1L1 and T1L2. The respective results are presented in figures 8.11, 8.12, 8.13, 8.14 and 8.15.

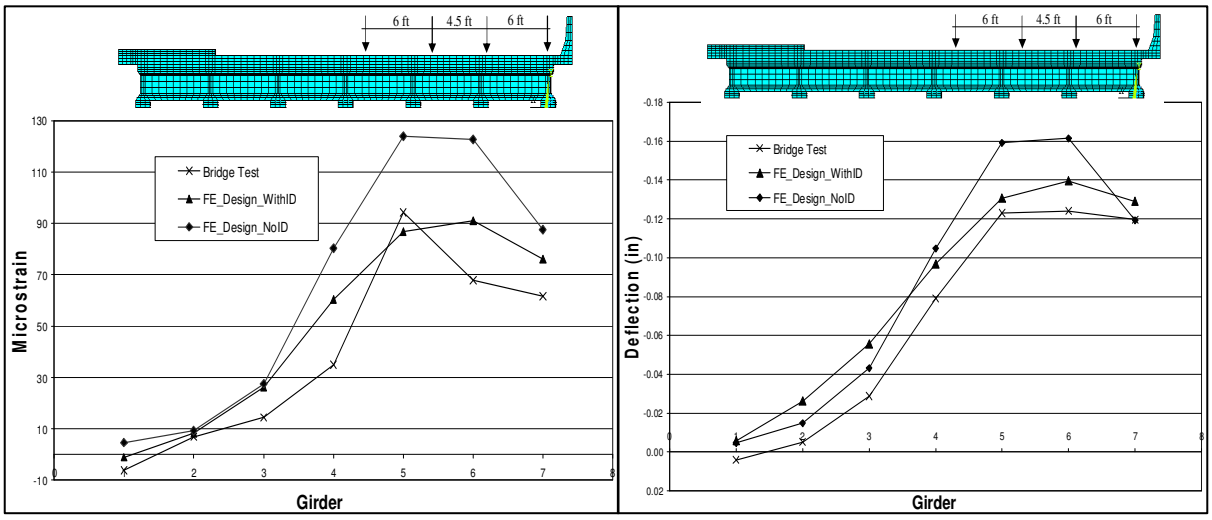

Figure 8.4
Strains and deflections comparisons for case T1L1_T2Sh
(bridge test and FE with design concrete stiffness)

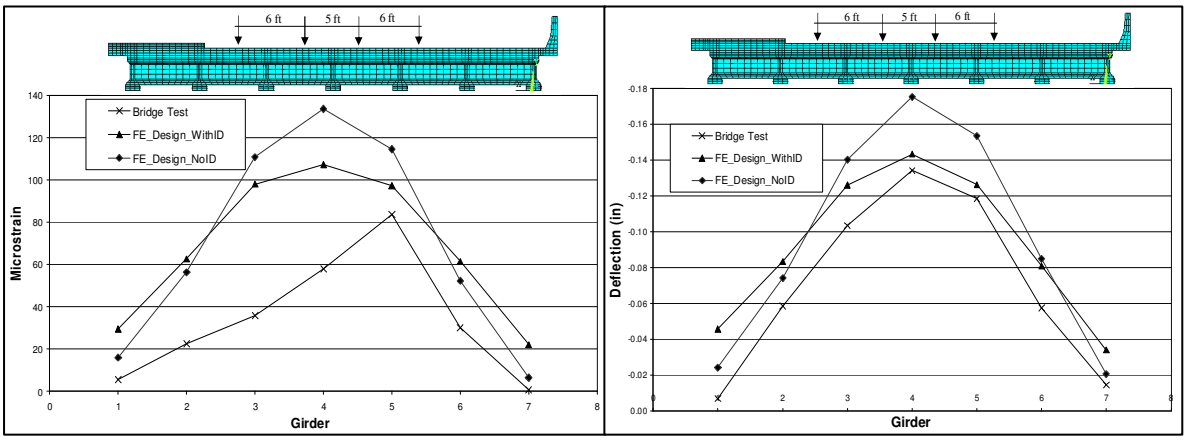

Figure 8.5
Strains and deflections comparisons for case T1L1_T2L2
(bridge test and FE with design concrete stiffness)

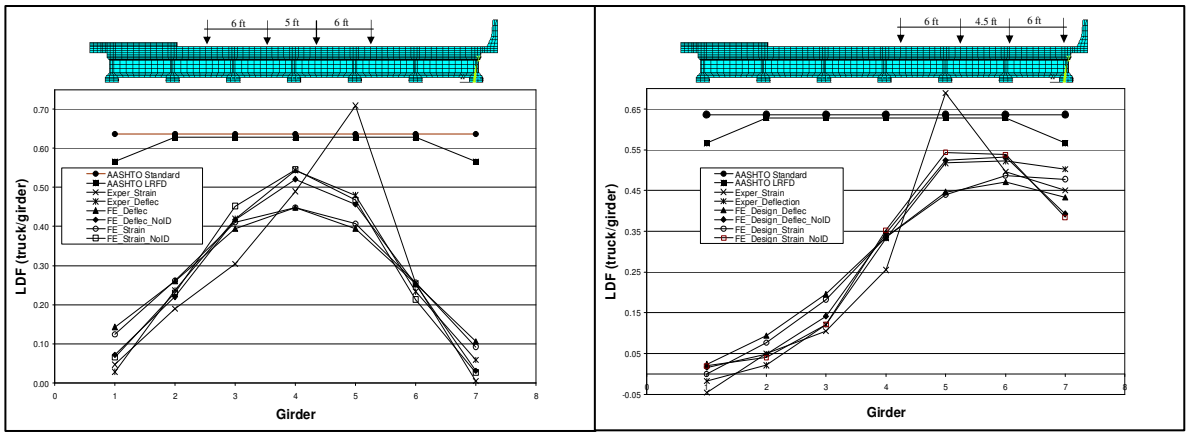

Figure 8.6
LDF comparisons for strains and deflections for both cases above
(bridge test, FE with design concrete stiffness and AASHTO)

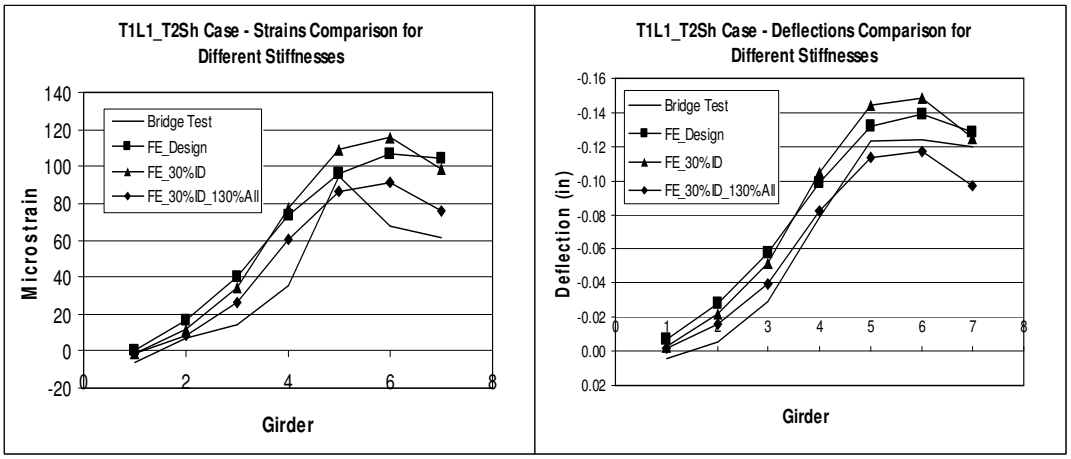

Figure 8.7
Strains and deflections comparisons for case T1L1_T2Sh with different concrete stiffnesses

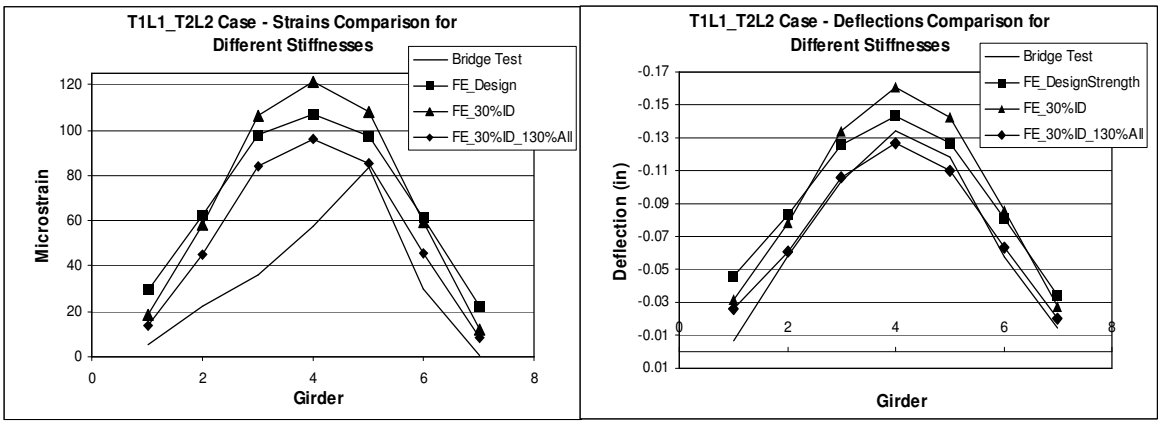

Figure 8.8
Strains and deflections comparisons for case T1L1_T2L2
with different concrete stiffnesses

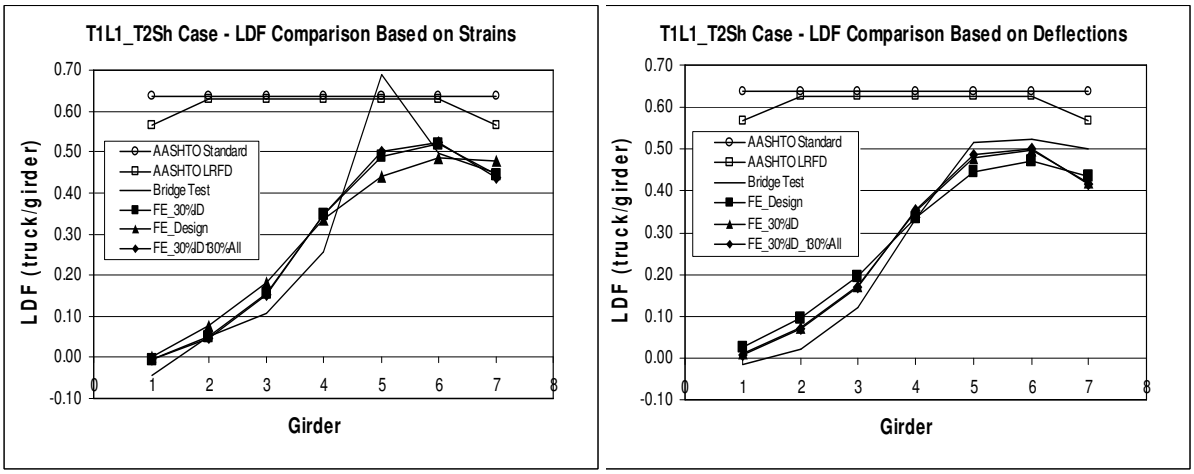

Figure 8.9
LDF comparison for case T1L1_T2Sh with different concrete stiffnesses

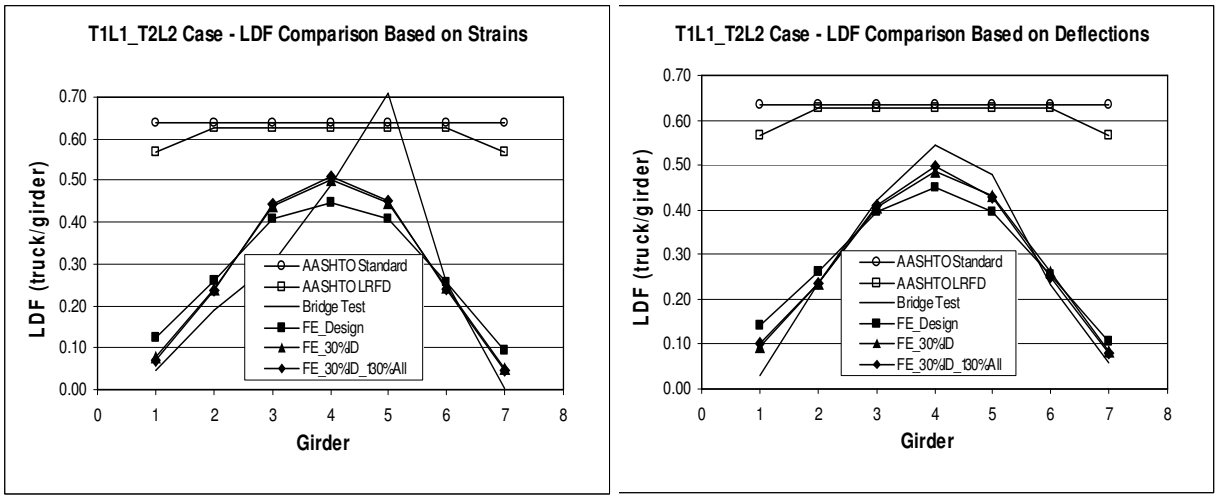

Figure 8.10
LDF comparison for case T1L1_T2L2 with different concrete stiffnesses

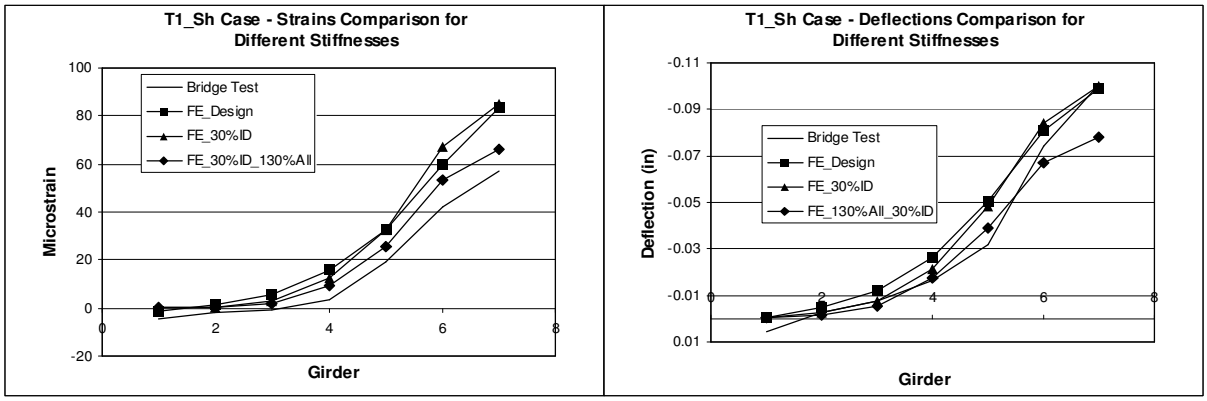

Figure 8.11
Strains and deflections comparisons for case T1Sh with different concrete stiffnesses

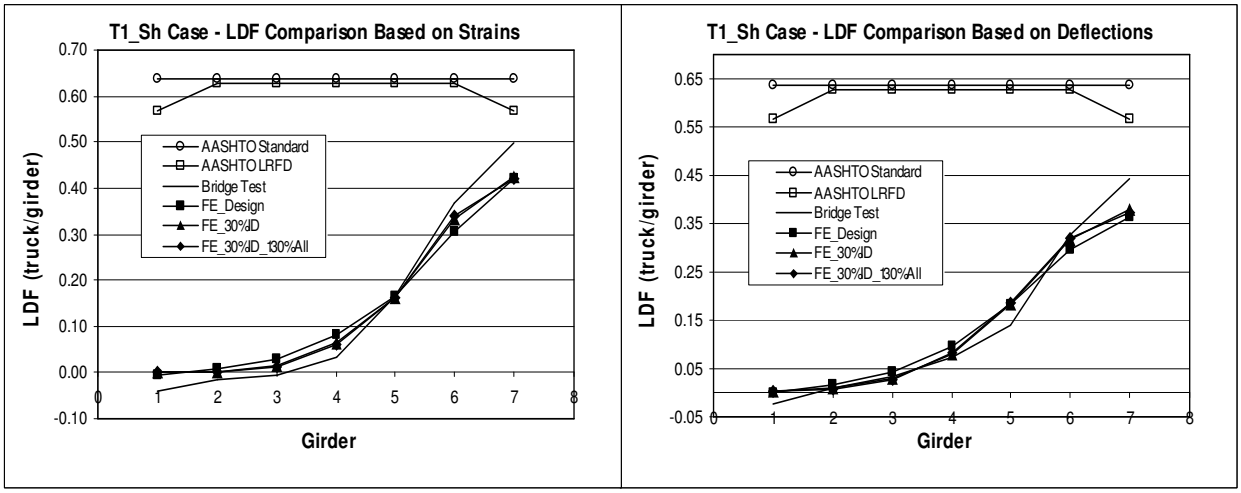

Figure 8.12
LDF comparison for case T1Sh with different concrete stiffnesses

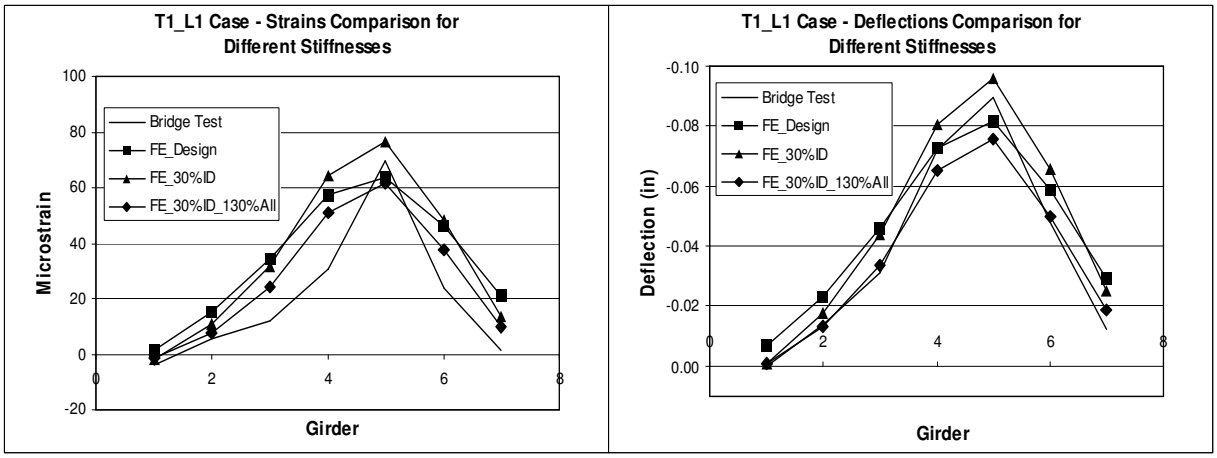

Figure 8.13
Strains and deflections comparisons for case T1L1 with different concrete stiffnesses

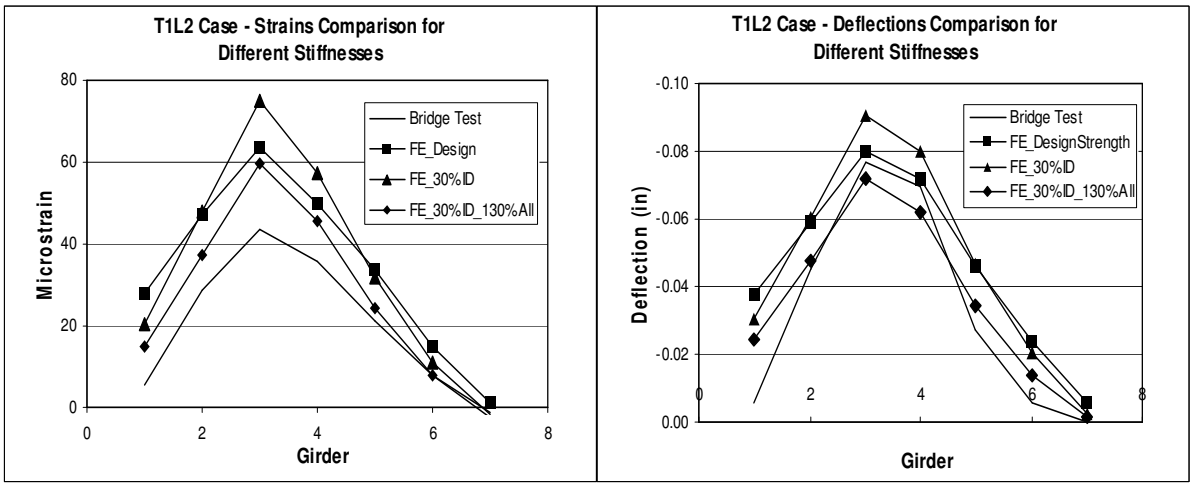

Figure 8.14
Strains and deflections comparisons for case T1L2 with different concrete stiffnesses

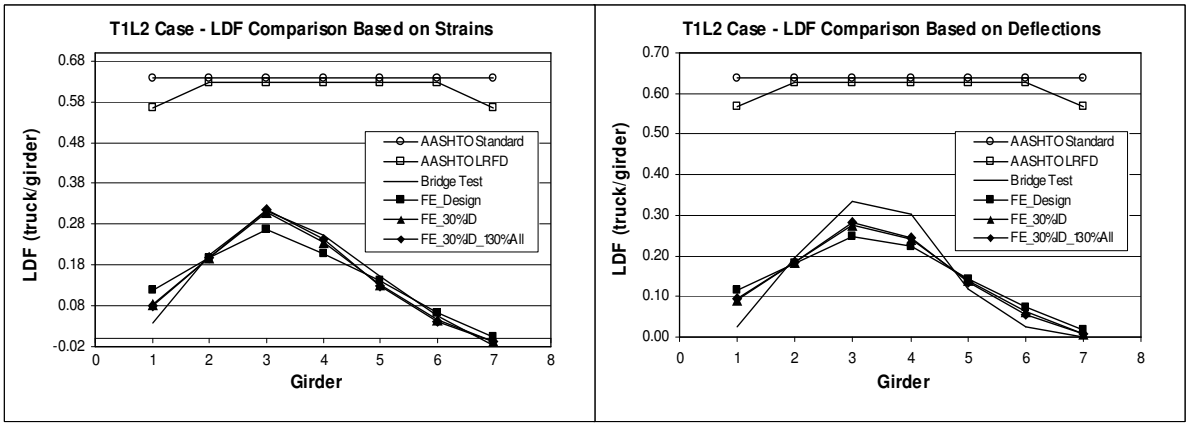

Figure 8.15
LDF comparison for case T1L2 with different concrete stiffnesses

8.7 Compilation of Dynamic Results

The dynamic response of the bridge due to moving trucks was investigated. The results depicted herein were obtained from multiple truck passes at various speeds. Strains and deflections were obtained from truck 1 passing on lane 1 (T1L1) at 30 and 40 MPH and passing on lane 2 (T1L2) at 38.5 MPH. Multiple passes took place in order to study the effect of approach slab joint unevenness on the load distribution and impact factor (IM). In addition to static and dynamic loadings of the bridge in its current condition, additional pavement unevenness was simulated by wood boards of different thicknesses; board thicknesses of 0.5", 1" and 1.5" were used and

indicated as boards B1, B2 and B3, respectively.

Tables 8.6, 8.7 and 8.8 summarize load distribution results for girders G4, G5 and G6 when lane 1 is loaded and girders G2, G3 and G4 when lane 2 is loaded. These girders show more significant results due to the amount of load they support, while the ones not shown indicate excessive and unreliable values due to signal noise in the strain and deflection readings. The non-controlling girders were not the focus of our concern. Results based on strains and deflections were tabulated for speeds 30 MPH and 40 MPH for lane 1 and 38.5 MPH for lane 2 for the board thicknesses indicated above and then compared to their respective static readings, as well as dynamic without any board.

Girder G5 took the greatest amount of load when lane 1 was loaded. This value was 50.2% and 33.4% of the static truck loading based on strains and deflections, respectively. At 30 MPH, when no board was used, the amount of loaded taken by G5 was reduced to 45.5% and increased to 35.2% based on strains and deflections, respectively (table 8.6). The unevenness was then increased by using boards B1, B2 and B3, as described earlier. As a result, the strain based load distribution percentage decreased to 47%, 46.1% and 40.2%, while equivalent deflection based results were 35.5%, 34.2%, and 33.4%. It was noticed that the load distribution appears to have an inverse relation to the increase on pavement unevenness, as the strain based dynamic to static ratio decreased from 91% (when no board was used) to 80% (for B3). The same ratio based on deflections decreased from 105% to 100%. This trend was observed for girders G4 and G5 as well. In G4, the dynamic to static ratio decreased from 98% to 86% based on strains and from 105% to 95% based on deflections. These values were 97% to 89% and 99% to 97% for G6 based on strains and deflections, respectively. Therefore, the dynamic effect helps distribute loads more uniformly among the girders.

Girders G2, G3 and G4 took most of the static truck loading when lane 2 was loaded, as

shown in table 8.7. Girder G3 took 31.1% (in terms of strain) and 33.3% (in terms of deflection) of the truck load when the bridge was statically loaded. At 38.5 MPH, when no board was used, G3 took 28.6% of the truck load based on strains and 33.9% based on deflections (table 8.7). This value decreased consistently with the increase in pavement unevenness. Load distribution results for B3 were as low as 23.9% for strains and 26.3% for deflections. As for the dynamic to static ratio, it decreased from 92% to 77% based on strains and 102% to 79% based on deflections. Again, girders G2 and G4 presented the same trend, resulting in a more even load distribution as the pavement unevenness increases. Based on strains, the dynamic to static ratio decreased from 116% to 89% (for G2) and from 89% to 72% (for G4); based on deflections, these results reduced from 110% to 84% (for G2) and 88% to 75% (for G4).

Lane 1 was once again loaded dynamically, this time at 40 MPH. In this case, G5 took 45.5% of the loading based on strains and 35.2% based on deflections when no board was used; this value consistently decreased as the board thickness was increased. For B3, G5 took 39.8% based on strains and 30.2% based on deflections. The dynamic to static readings ratio decreased from 91% to 79% based on strains and 105% to 90% based on deflections. This ratio decreased for G4 and G6 based on strains; for deflections, the dynamic to static ratio decreased for G4 and remained the same for G6, as show in table 8.8.

Overall, the maximum load taken by any girder was less the load distribution factor (LDF) calculated using AASHTO Standard and LRFD. According to AASHTO Standard, the most loaded girder takes 63.6% of the loading, while AASHTO LRFD equation produces 62.8% for interior girders and 56.6% for exterior ones.

The effect of pavement unevenness on the dynamic allowance (IM) factor was also evaluated and presented in tables 8.9, 8.10 and 8.11. At 30 MPH with lane 1 loaded, the IM factor was similar for G4, G5 and G6. G5, the most loaded girder, had a virtually non-existing IM change

due to increase in pavement unevenness based on strains; based on deflections, from no wood board to B3 its IM change was 20%, i.e., from 0.96 to 1.16 (table 8.9). Similarly, the strain based IM change was very small for G4 and G6; however, the deflection based values were 14% (from 0.96 to 1.10) and 22% (from 0.90 to 1.12), respectively.

At 38 MPH with the truck passing on lane 2, IM values were significant based on strain and deflections for G2, G3 and G4 (table 8.10). From no wood board to B3, the strain based value increase for IM was 30% in G3, i.e. from 0.93 to 1.23, while its respective deflection based value was 35% (from 1.09 to 1.44) . For G2, the IM increase based on strains was 25% (from 1.17 to 1.42), while it was 35% based on deflections (from 1.18 to 1.53). The IM value increase for G4 based on strains and deflections were 25% (from 0.90 to 1.15) and 43% (from 0.94 to 1.37), respectively.

Lane 1 was again dynamically loaded, this time at 40 MPH. The IM value increase from the no board condition (actual unevenness of the bridge) to board B3 was 28% (from 1.03 to 1.31) when based on strains for G5, while it was 38% (from 1.05 to 1.43) when based on deflections (table 8.11). G4 had an IM value increase of 9% (from 1.11 to 1.20) based on strains and 34% (from 1.00 to 1.34) when based on deflections. As for G6, the increase in IM value was 46% (from 1.10 to 1.56) when based on strains and 61% (from 1.04 to 1.65) when based on deflections.

For this bridge, IM values were well within AASHTO Standard (28%) and AASHTO LRFD (33%) values for all unevenness cases considered at 30 MPH. However, as the speed was increased to 38.5 MPH and 40 MPH, IM values were considerably higher for board B3 condition, in which the pavement had a 1.5" "bump" at its approach. This is a common condition on older bridges, in which differential settlement under the approach slab causes such pavement unevenness. Since IM results were much higher than the currently recommended design values, more bridges should be investigated in order to quantify the actual IM values based on pavement unevenness.

A summary of the strains and deflections collected during the load dynamic tests is presented in figure 8.16, with respective load distribution and dynamic allowance curves shown in figures 8.17 and 8.18. Time dependent curves for strains and deflections for the girders summarized in the tables are also presented in figures 8.19 and 8.20.

Table 8.6
Load distribution for dynamic load tests at 30 MPH

LDF Comparison at 30 MPH						
	Strain Based (trucks/girder)			Deflection Based (trucks/girder)		
Girder	Max. Static	Max. Dynamic (No Board, B1, B2, B3)	Dyn/Stat	Max. Static	Max. Dynamic (No Board, B1, B2, B3)	Dyn/Stat
G4	0.220	0.215	0.98	0.271	0.285	1.05
		0.221	1.01		0.261	0.96
		0.211	0.96		0.271	1.00
		0.190	0.86		0.256	0.95
G5	0.502	0.455	0.91	0.334	0.352	1.05
		0.470	0.94		0.355	1.06
		0.461	0.92		0.342	1.02
		0.402	0.80		0.334	1.00
G6	0.170	0.164	0.97	0.180	0.178	0.99
		0.161	0.95		0.194	1.08
		0.158	0.93		0.178	0.99
		0.151	0.89		0.174	0.97

Table 8.7
Load distribution for dynamic load tests at 38.5 MPH

LDF Comparison at 38.5 MPH						
	Strain Based (trucks/girder)			Deflection Based (trucks/girder)		
Girder	Max. Static	Max. Dynamic (No Board, B1, B2, B3)	Dyn/Stat	Max. Static	Max. Dynamic (No Board, B1, B2, B3)	Dyn/Stat
G2	0.205	0.237	1.16	0.196	0.215	1.10
		0.214	1.04		0.216	1.10
		0.220	1.07		0.203	1.03
		0.183	0.89		0.165	0.84
G3	0.311	0.286	0.92	0.333	0.339	1.02
		0.275	0.88		0.328	0.99
		0.261	0.84		0.315	0.95
		0.239	0.77		0.263	0.79
G4	0.254	0.225	0.89	0.302	0.264	0.88
		0.223	0.88		0.257	0.85
		0.212	0.83		0.236	0.78
		0.183	0.72		0.227	0.75

Table 8.8
Load distribution for dynamic load tests at 40 MPH

LDF Comparison at 40 MPH						
	Strain Based (trucks/girder)			Deflection Based (trucks/girder)		
Girder	Max. Static	Max. Dynamic (No Board, B1, B2, B3)	Dyn/Stat	Max. Static	Max. Dynamic (No Board, B1, B2, B3)	Dyn/Stat
G4	0.220	0.215	0.98	0.271	0.272	1.00
		0.216	0.98		0.270	1.00
		0.211	0.96		0.267	0.99
		0.160	0.73		0.229	0.85
G5	0.502	0.455	0.91	0.334	0.352	1.05
		0.437	0.87		0.337	1.01
		0.464	0.92		0.330	0.99
		0.398	0.79		0.302	0.90
G6	0.170	0.164	0.97	0.180	0.188	1.04
		0.162	0.95		0.186	1.04
		0.166	0.98		0.187	1.04
		0.160	0.95		0.187	1.04
AASHTO Standard		0.636 (int. and ext. girders)				
AASHTO LRFD		0.628 (int. girders) and 0.566 (ext. girders)				

Table 8.9
Dynamic allowance factors for dynamic load tests at 30 MPH

Dynamic Allowance (IM) Comparison at 30 MPH						
	Strain Based			Deflection Based		
Girder	Max. Static (με)	Max. Dynamic (No Board, B1, B2, B3)	Dyn/Stat	Max. Static (in)	Max. Dynamic (No Board, B1, B2, B3)	Dyn/Stat
G4	31	34	1.11	-0.07	-0.07	0.96
		33	1.08		-0.07	0.91
		32	1.05		-0.07	1.01
		34	1.11		-0.08	1.10
G5	70	72	1.03	-0.09	-0.09	0.96
		70	1.01		-0.09	1.01
		70	1.01		-0.09	1.03
		72	1.03		-0.10	1.16
G6	24	26	1.10	-0.05	-0.04	0.90
		24	1.02		-0.05	1.02
		24	1.02		-0.05	1.00
		27	1.15		-0.05	1.12

Table 8.10
Dynamic allowance factors for dynamic load tests at 38.5 MPH

Dynamic Allowance (IM) Comparison at 38.5 MPH						
	Strain Based			Deflection Based		
Girder	Max. Static (με)	Max. Dynamic (No Board, B1, B2, B3)	Dyn/Stat	Max. Static (in)	Max. Dynamic (No Board, B1, B2, B3)	Dyn/Stat
G2	29	33	1.17	-0.05	-0.05	1.18
		32	1.13		-0.06	1.26
		37	1.28		-0.06	1.36
		41	1.42		-0.07	1.53
G3	43	40	0.93	-0.08	-0.08	1.09
		42	0.96		-0.09	1.13
		43	1.00		-0.10	1.25
		53	1.23		-0.11	1.44
G4	36	32	0.90	-0.07	-0.07	0.94
		34	0.95		-0.07	0.98
		35	0.99		-0.07	1.03
		41	1.15		-0.10	1.37

Table 8.11
Dynamic allowance factors for dynamic load tests at 40 MPH

Dynamic Allowance (IM) Comparison at 40 MPH						
	Strain Based			Deflection Based		
Girder	Max. Static (με)	Max. Dynamic (No Board, B1, B2, B3)	Dyn/Stat	Max. Static (in)	Max. Dynamic (No Board, B1, B2, B3)	Dyn/Stat
G4	31	34	1.11	-0.07	-0.07	1.00
		34	1.13		-0.08	1.05
		32	1.05		-0.08	1.15
		37	1.20		-0.10	1.34
G5	70	72	1.03	-0.09	-0.09	1.05
		69	1.00		-0.09	1.06
		71	1.01		-0.10	1.15
		91	1.31		-0.13	1.43
G6	24	26	1.10	-0.05	-0.05	1.04
		26	1.09		-0.05	1.09
		25	1.08		-0.06	1.21
		37	1.56		-0.08	1.65
AASHTO Standard		0.28				
AASHTO LRFD		0.33				

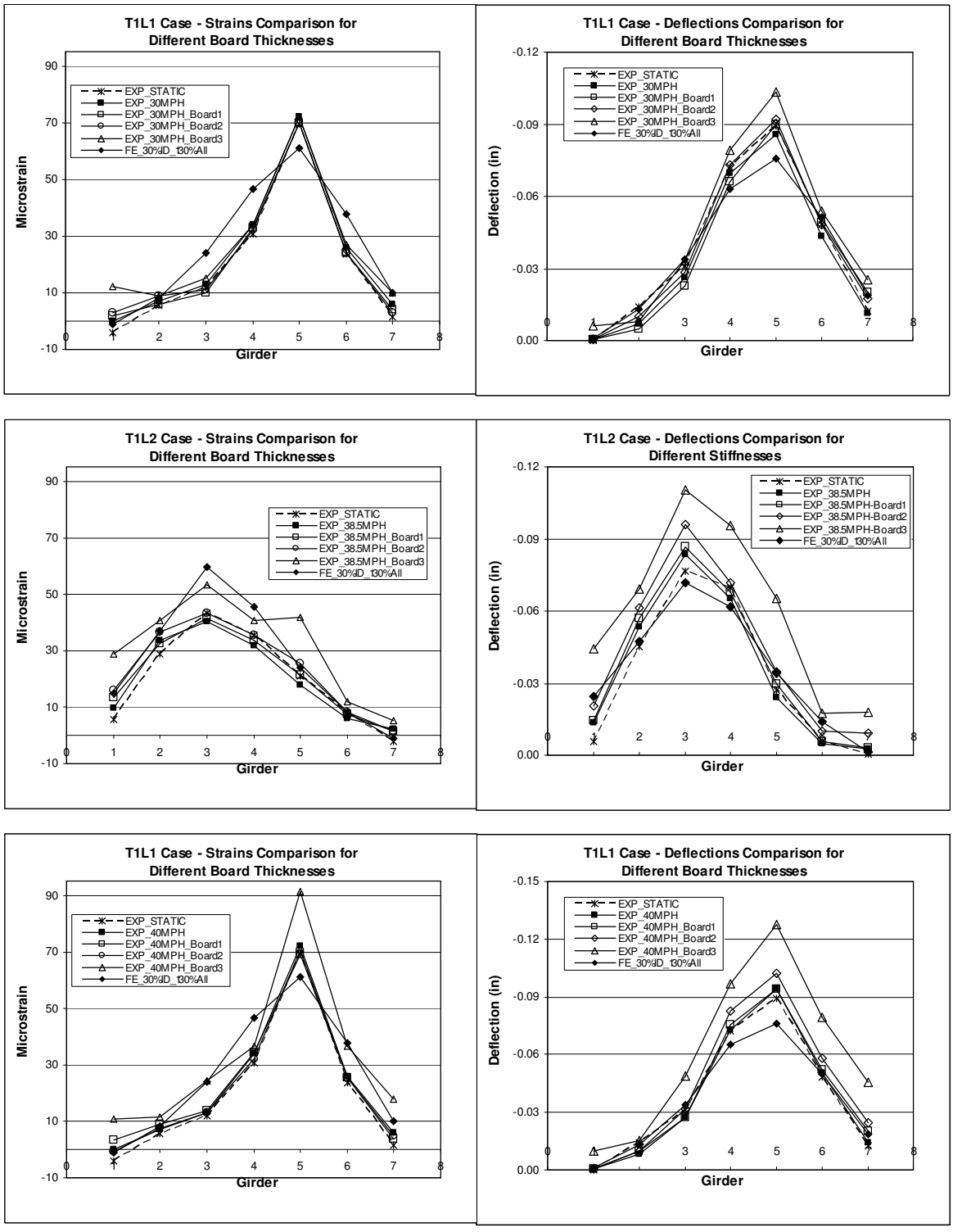

Figure 8.16
Summary of trains and deflections comparisons for different loading cases, board thicknesses and speeds

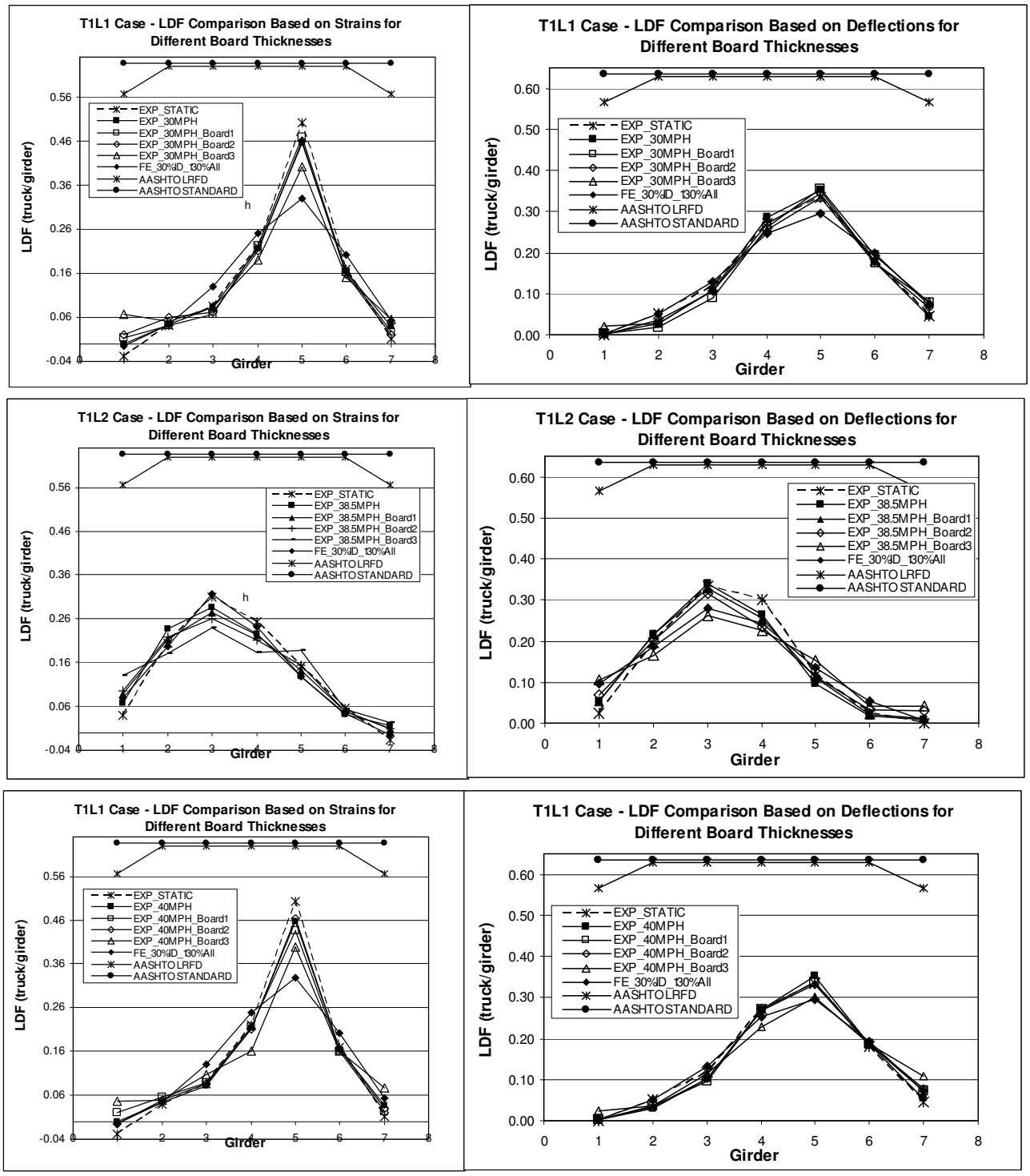

Figure 8.17
Summary of load distributions comparisons for different
loading cases, board thicknesses and speeds

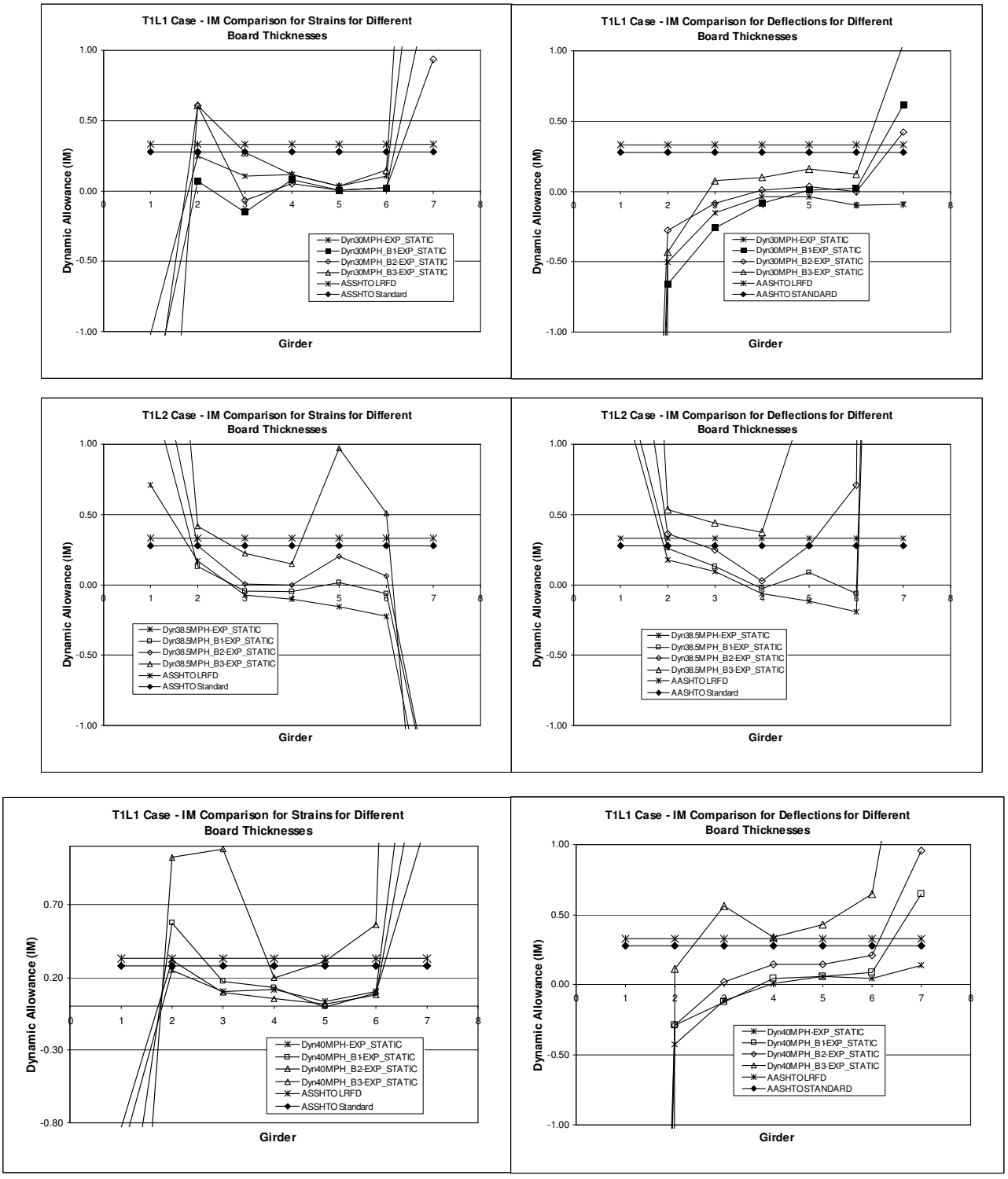

Figure 8.18
Summay of dynamic allowance comparisons for different
loading cases, board thicknesses and speeds

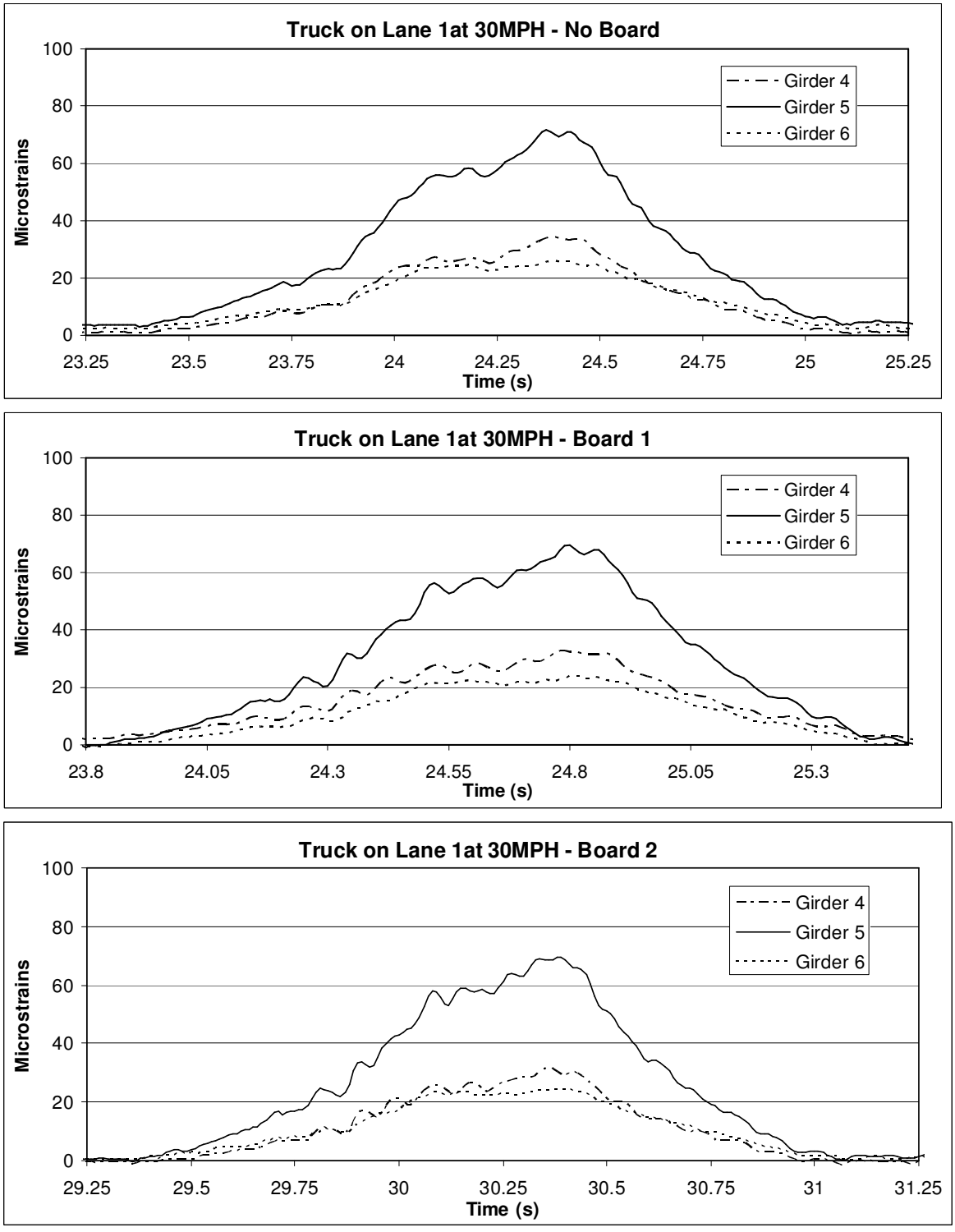

Figure 8.19
Microstrains due to dynamic loading tests for the three most affected girders for different loading cases, board thicknesses and speeds

(Fig. Continued)

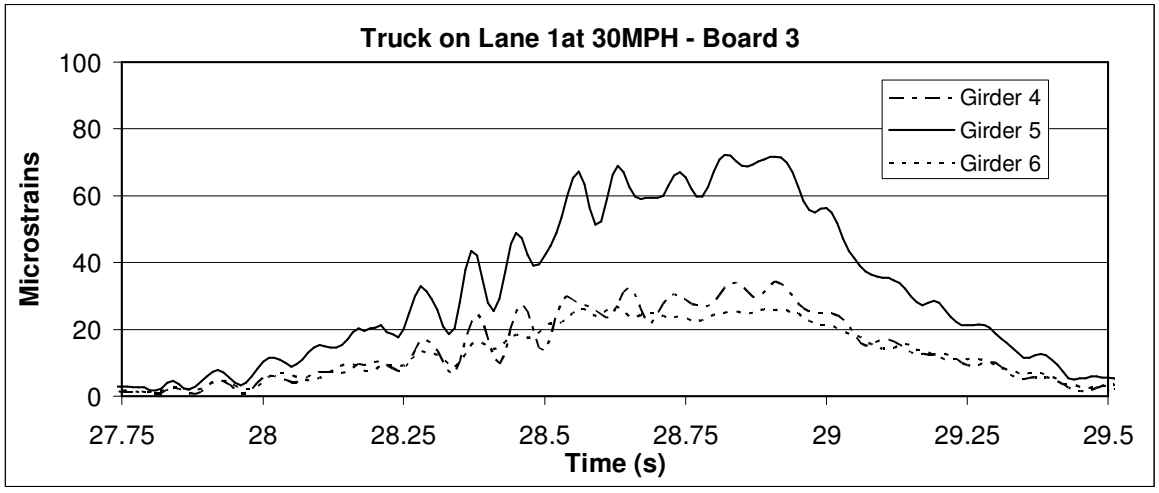

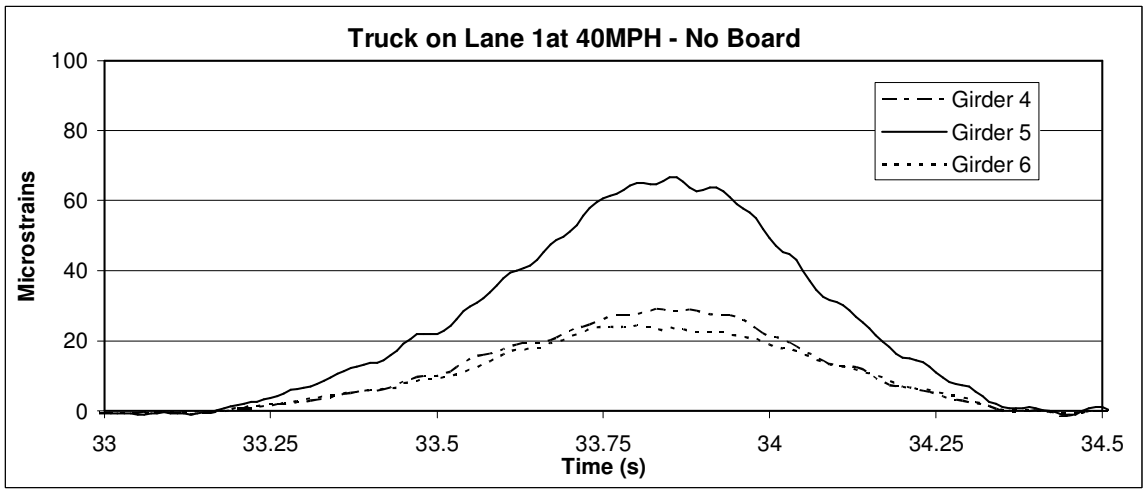

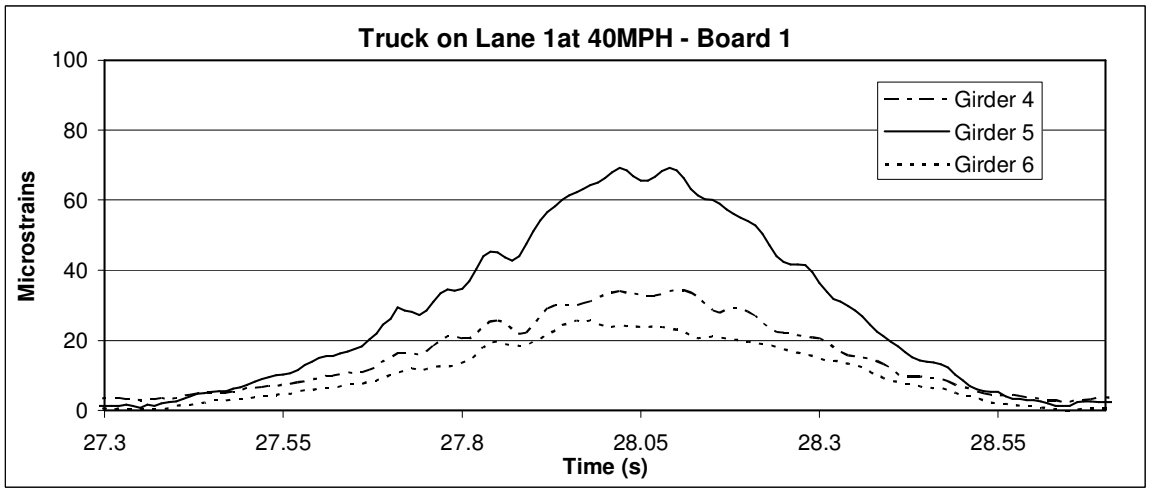

(Fig. Continued)

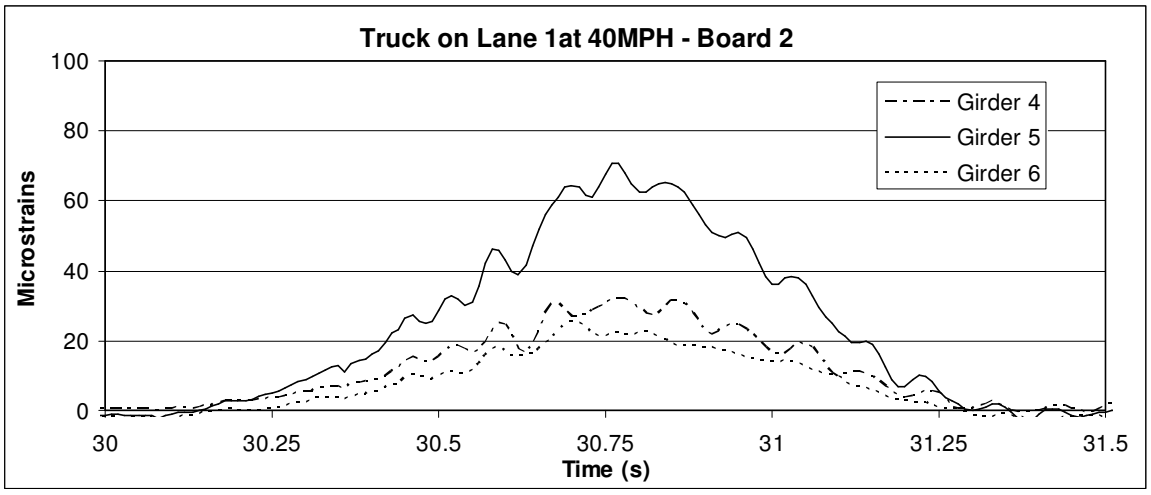

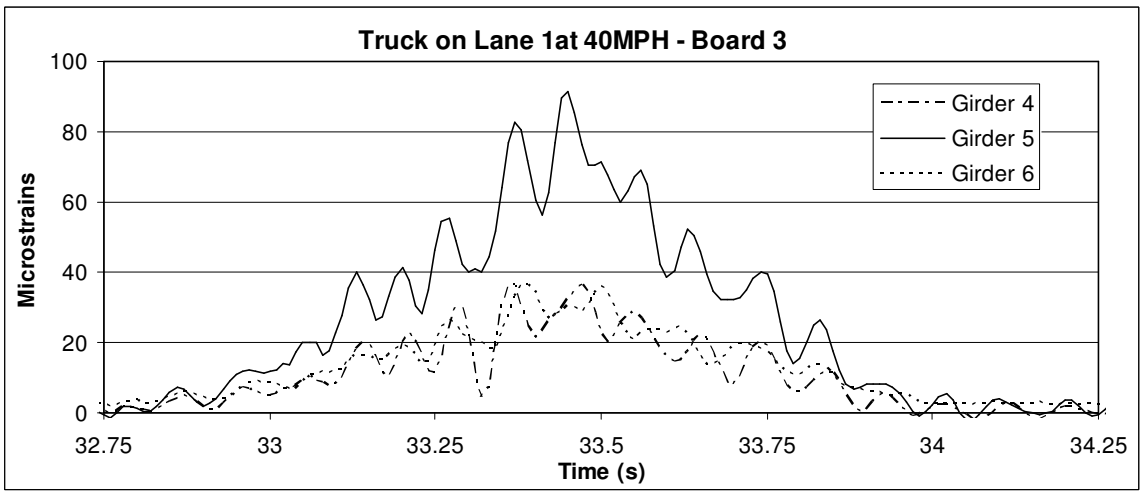

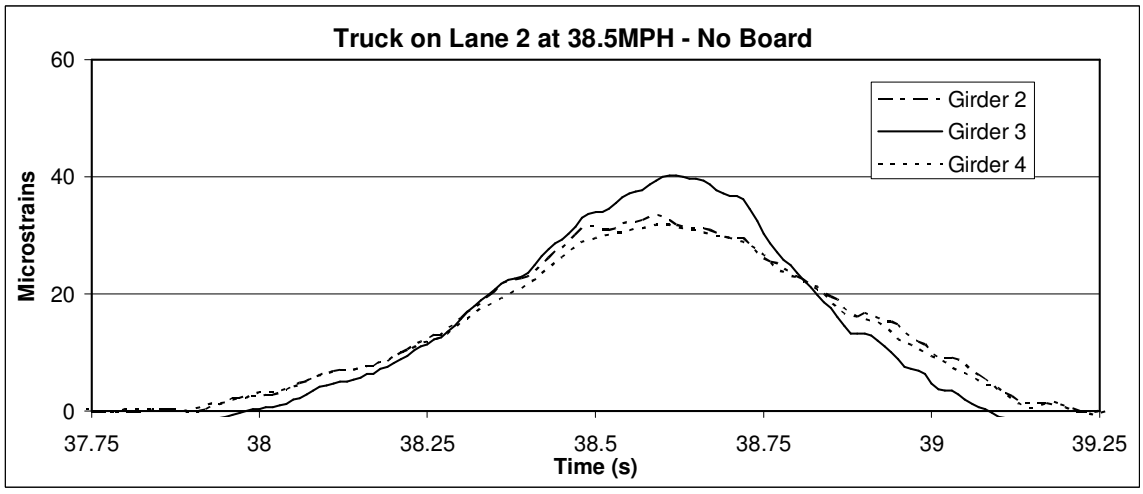

(Fig. Continued)

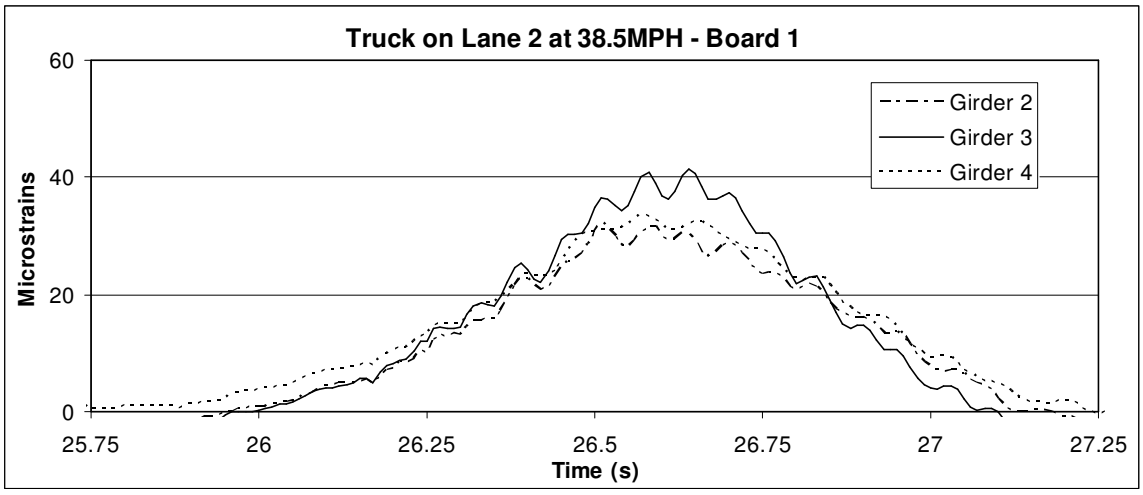
Truck on Lane 2 at 38.5MPH - Board 1
Microstrains
Time (s)
Girder 2
Girder 3
Girder 4
0
20
40
60
25.75
26
26.25
26.5
26.75
27
27.25

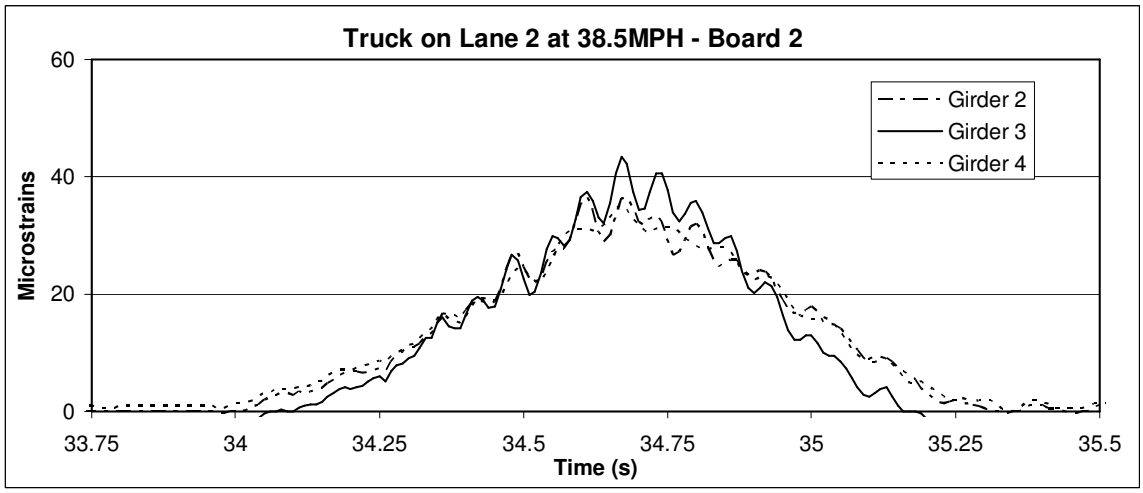
Truck on Lane 2 at 38.5MPH - Board 2
Microstrains
Time (s)
Girder 2
Girder 3
Girder 4
0
20
40
60
33.75
34
34.25
34.5
34.75
35
35.25
35.5

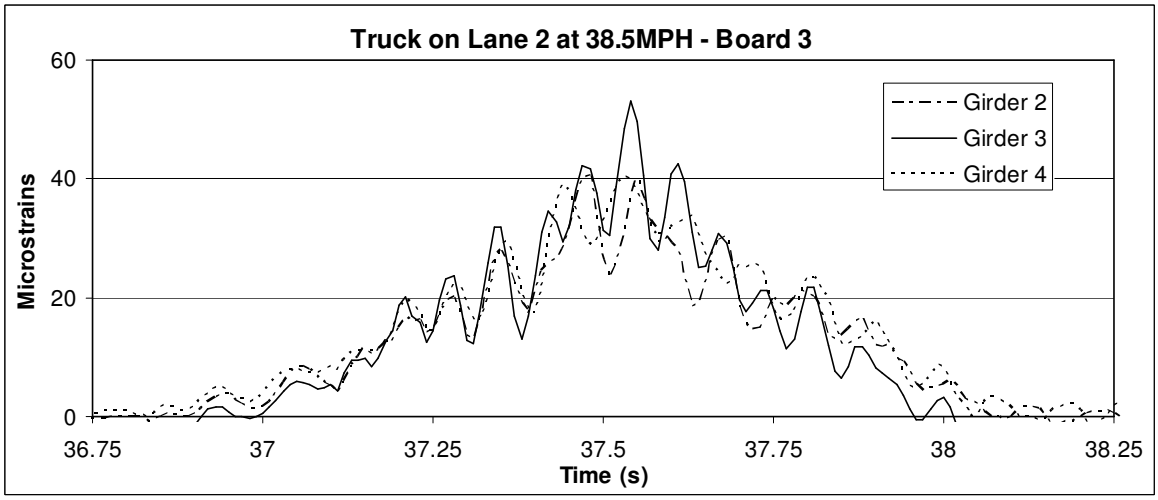
Truck on Lane 2 at 38.5MPH - Board 3
Microstrains
Time (s)
Girder 2
Girder 3
Girder 4
0
20
40
60
36.75
37
37.25
37.5
37.75
38
38.25

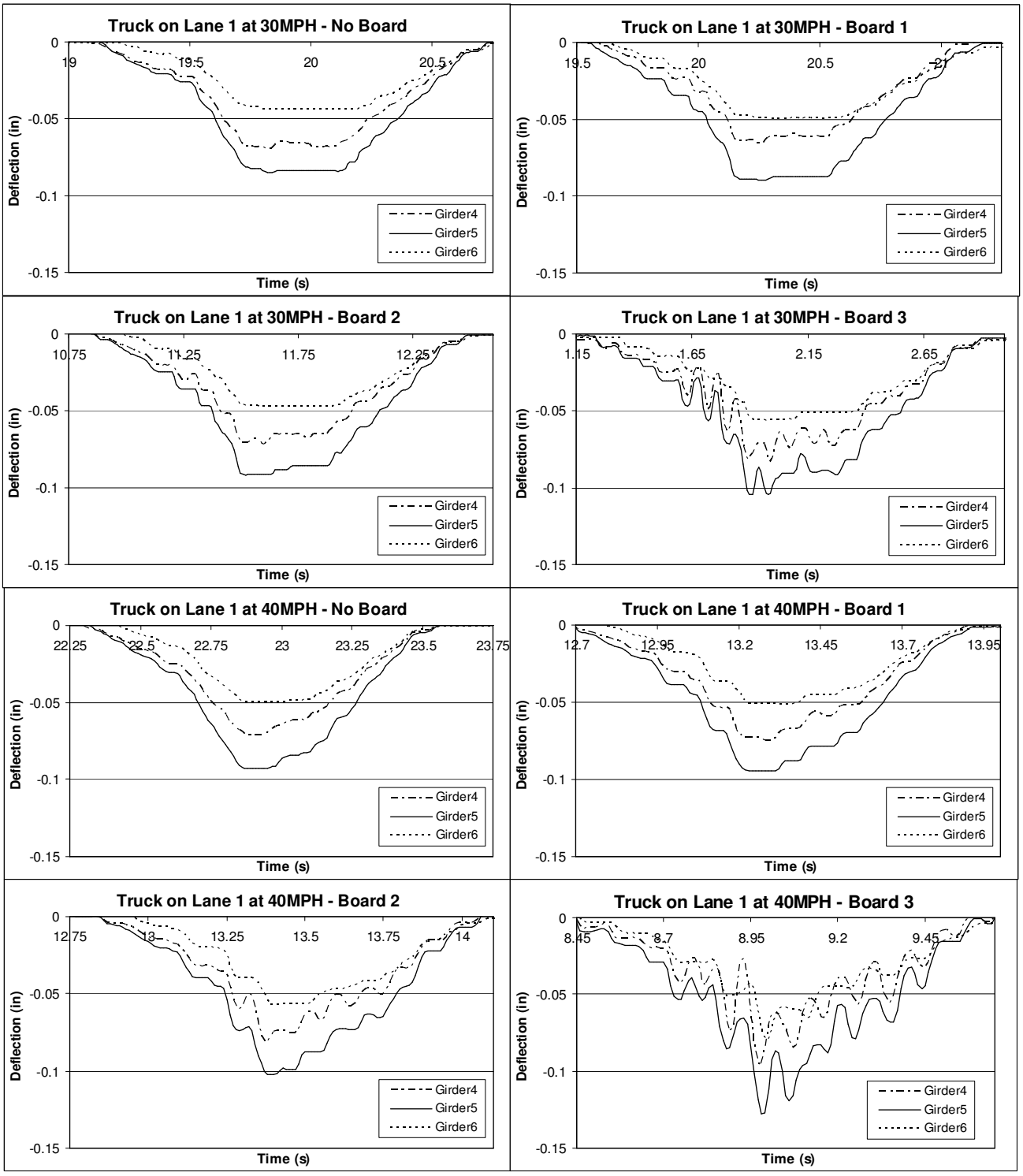

Figure 8.20
Deflections due to dynamic loading tests for the three most affected girders for different loading cases, board thicknesses and speeds

(Fig. Continued)

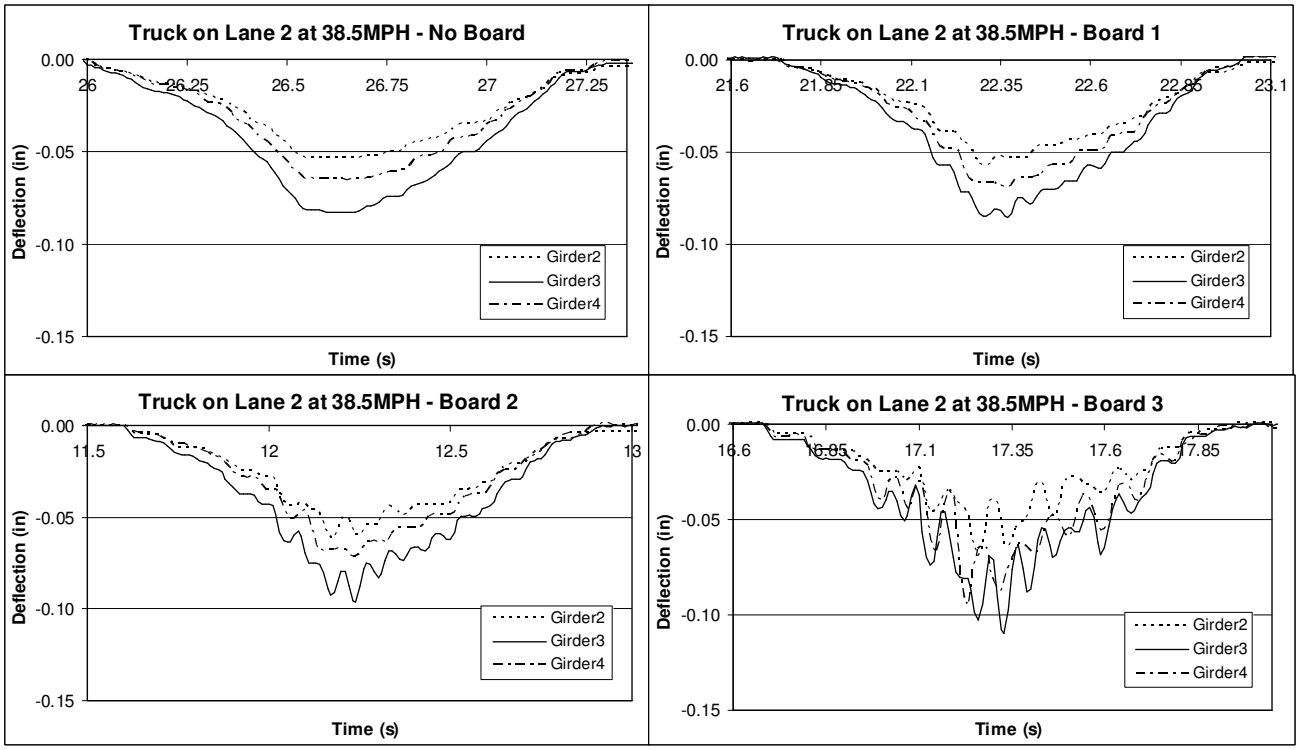
Truck on Lane 2 at 38.5MPH - No Board
Deflection (in)
0.00
-0.05
-0.10
-0.15
26
26.25
26.5
26.75
27
27.25
Time (s)
Girder2
Girder3
Girder4
Truck on Lane 2 at 38.5MPH - Board 1
Deflection (in)
0.00
-0.05
-0.10
-0.15
21.6
21.85
22.1
22.35
22.6
22.85
23.1
Time (s)
Girder2
Girder3
Girder4
Truck on Lane 2 at 38.5MPH - Board 2
Deflection (in)
0.00
-0.05
-0.10
-0.15
11.5
12
12.5
13
Time (s)
Girder2
Girder3
Girder4
Truck on Lane 2 at 38.5MPH - Board 3
Deflection (in)
0.00
-0.05
-0.10
-0.15
16.6
16.85
17.1
17.35
17.6
17.85
Time (s)
Girder2
Girder3
Girder4

CHAPTER 9. NONLINEAR ANALYSIS OF PRESTRESSED CONCRETE BRIDGES

9.1 Introduction

Live loads have been a focal concern in bridge design for a long time, with their regulation appearing in the form of empirical distribution factors in the first edition of the AASHTO code in 1931 (Senders, 1984). They play a key role in the structural degradation of bridges as crack initiators and propagators. Although significant progress has been made since then, much is yet to be accomplished in this area. A large sum of money is spent annually due to the high number of deficient bridges which are recommended to weight-limiting posting, rehabilitation or decommissioning and replacement. The knowledge of how live loads are distributed beyond the elastic range will increase engineers' ability to evaluate the condition of both existing and new bridges using predictive analysis.

As the most important nodes in the terrestrial transportation network, bridges are the main way to overcome natural obstacles such as rivers and canyons. They are extremely important to alleviate traffic flux in heavily populated areas in the form of overpasses. Their absence would cause severe delays in the flow of passengers and goods, causing unaccountable losses.

Studies (TRIP, 2002 and ASCE Report Card, 2005) indicate that the average age of bridges has reached over 40 years. About 27 percent of the 590,750 bridges in the country are classified as structurally deficient or functionally obsolete. Moreover, it is estimated that 9.4 billion dollars per year for 20 years will be needed to eliminate these structural deficiencies which restrict road capacities and/or speed limits. The overall condition of bridges in the nation was rated as C by the ASCE Report Card (2005).

These high numbers show the need to develop accurate predictive analysis methods for live load distribution. These methods will enable engineers to design bridge systems which will perform as expected at minimum maintenance costs by withstanding deterioration in a more effective way.

Nonlinear live load distribution analyses up to ultimate strength are tools needed to assure that these predictive methods are structurally sound.

Load distribution factors (LDFs) calculated according to AASHTO LRFD (2004) yield linear results, which, theoretically, correspond to service loadings. Load distribution is determined by distribution factors which were reported to be within 5% of the distribution factors calculated with detailed finite element models (Zokaie, 1991). Zokaie's study is the basis for LDF regulations in the current AASHTO LRFD code (2004). These distribution factors are based on linear analysis of simply supported bridges using HS20 trucks.

Bridge performance at the ultimate stage has not been extensively studied and may be significantly different from that in the service stage. To narrow the gap between service and ultimate analyses, main objectives of this study were to:

a. demonstrate how the load distribution affects the behavior of each girder as the live load is increased up to the bridge's ultimate capacity;
b. understand bridge systems' performance in inelastic stages;
c. predict the bridge's ultimate capacity; and
d. discuss effective flange width at inelastic stages

This information will help engineers evaluate bridge capacity more accurately, thus avoiding unnecessary and costly bridge postings as well as identifying unsafe bridges from the transportation network. Particularly, a nonlinear analysis would help researchers understand the real capacity of the prestressed bridges, especially if the IDs are eliminated. Comparisons of load distributions were performed using the strains, deflections, and section moments obtained using a full 3D finite element analysis of the tested bridge.

9.2 Nonlinear Bridge Modeling

Finite element modeling of concrete is difficult because of its non-homogeneous and

anisotropic properties. According to Nilson (1968), early simulations were widely based on predefined cracking patterns, which were very limited due to the need for frequent adjustments to the input files. Isoparametric formulations were later introduced to represent cracking in concrete. The first method to use these formulations was the smeared cracking, which considers cracked concrete an orthotropic material (Rashid, 1968). According to this approach, cracking takes place whenever the principal stress in any direction exceeds the ultimate tensile stress. The elastic modulus is then assumed to be zero in the direction perpendicular to the crack (Suidan and Schnobrich, 1973).

Once the modeling techniques applied in this study were verified through a simple span girder, as previously described in chapter 5, a 3D full finite element analytical model of the entire bridge tested (Bridge 1) was developed and run using ANSYS 9.0. The deck, diaphragms, and edge stiffeners were modeled as nonlinear SOLID65 elements near the mid-span and as linear with SOLID45 elements at the ends; both types had fc' = 3.5 ksi. The strands were modeled as LINK8 elements with 270 ksi strength, while the prestressed girders were modeled as linear toward the supports and nonlinear near the mid-span. Similarly, their linear portion was modeled using SOLID45 and the nonlinear using SOLID65; a concrete strength of 6 ksi was considered for all girders.

Two bridge configurations of Bridge 1 were analyzed, as shown in figure 9.1. In the first configuration, only the girders and the deck were modeled; it contains 51,263 solid elements. In the second configuration, the whole bridge was modeled, except its ID. The ID was not considered in this study to be consistent with the models used to develop the AASHTO LRFD (2004) load distribution factors and also to demonstrate the bridge's capacity without IDs. This model contained 62,360 solid elements. Both configurations contained 2,493 link elements.

A second bridge (Bridge 2) was modeled and loaded from service to ultimate capacity for

the effective flange width evaluation and ultimate load rating calculation; loading case RDL was the only l used in Bridge 2, which is a 105 feet long, prestressed concrete slab-on-girder bridge with seven AASHTO Type IV girders spaced 72 inches on center.

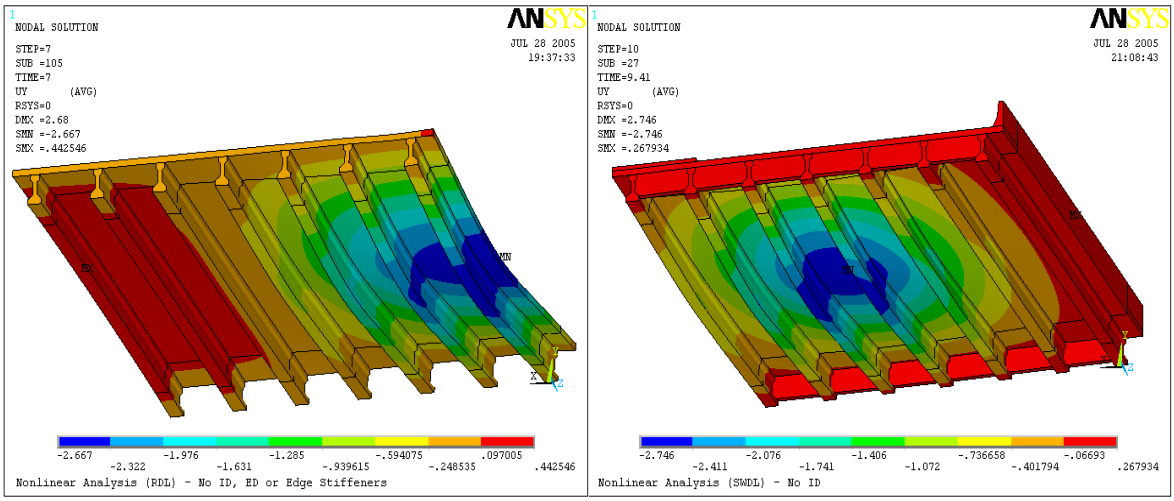

Figure 9.1
Bridge configurations studied

9.3 Bridge Loading and Live Load Distribution

To cover different scenarios, three loading cases were considered in this study. In each of them, two lanes were loaded with HS20 trucks positioned transversely as described in figure 9.2. These three positions represent the two worst cases towards the exterior girders (RDL and SWDL) and the traffic lanes (TL). In this study, all HS20 tucks were positioned with their middle axle at the midspan. The finite element model was loaded up to failure for the three loading cases shown in figure 9.2; respective results are presented later in this chapter.

The equations used to calculate the LDFs (lanes/girder) are the same used in chapter 8, which are the following:

a. AASHTO Standard (2002): $LDF = \frac{S(ft)}{D} * 0.5$, where D is 5.5 for interior and exterior prestressed concrete girders;

b. AASHTO LRFD (2004): $LDF = .075 + \left(\frac{S}{9.5}\right)^{0.6}\left(\frac{S}{L}\right)^{0.2}\left(\frac{K_g}{12.0Lt_s^3}\right)^{0.1}$ for interior girders

and that value multiplied by $e = 0.77 + \frac{d_e}{2800}$ for exterior ones;

c. Finite Element: $LDF = \frac{M_i}{(\sum_{i=1}^{k} M_i)/n} = \frac{nE_iS_i\varepsilon_i}{\sum_{i=1}^{k} E_iS_i\varepsilon_i} = \frac{\cancel{nE_iS_i}\varepsilon_i}{\cancel{E_iS_i}\sum_{i=1}^{k}\varepsilon_i} = \frac{n\varepsilon_i}{\sum_{i=1}^{k}\varepsilon_i}$

where k is the total number of girders, i is the girder for which the load distribution factor is calculated, and n is the number of transversely positioned HS20 trucks loading the bridge, which is 2 in this study. This same procedure was followed for the LDF calculation using deflections.

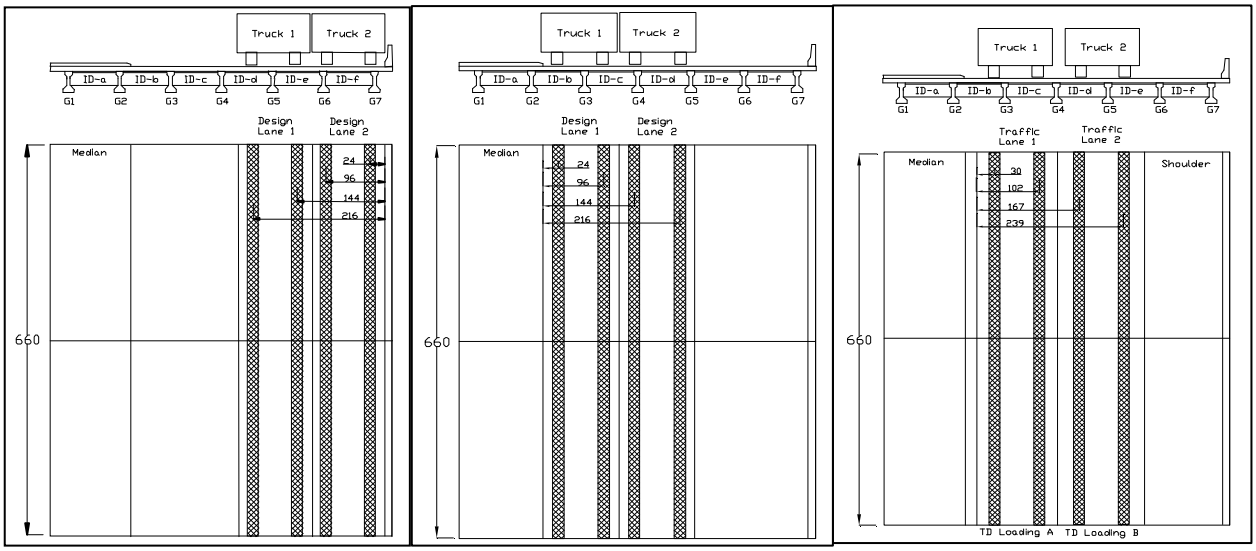

RDL
(Railing Design Lanes)

SWDL
(Sidewalk Design Lanes)

TL
(Traffic Lanes)

Figure 9.2
Loading cases studied

9.4 Finite Element Model Results

Figures 9.3, 9.4, and 9.5 show some of the calculated load distribution for the three loading scenarios in the two bridge configurations using the three LDF calculation methods discussed earlier. FE results were obtained based on strains, deflections, and section moments at the midspan. The respective equations are shown above. In these figures, Moment_1Truck_TL represents the

service loading level. The legend means that LDFs were calculated using section moments and that both traffic lanes were loaded with one truck per lane for the TL loading case; this description method applies to all legends.

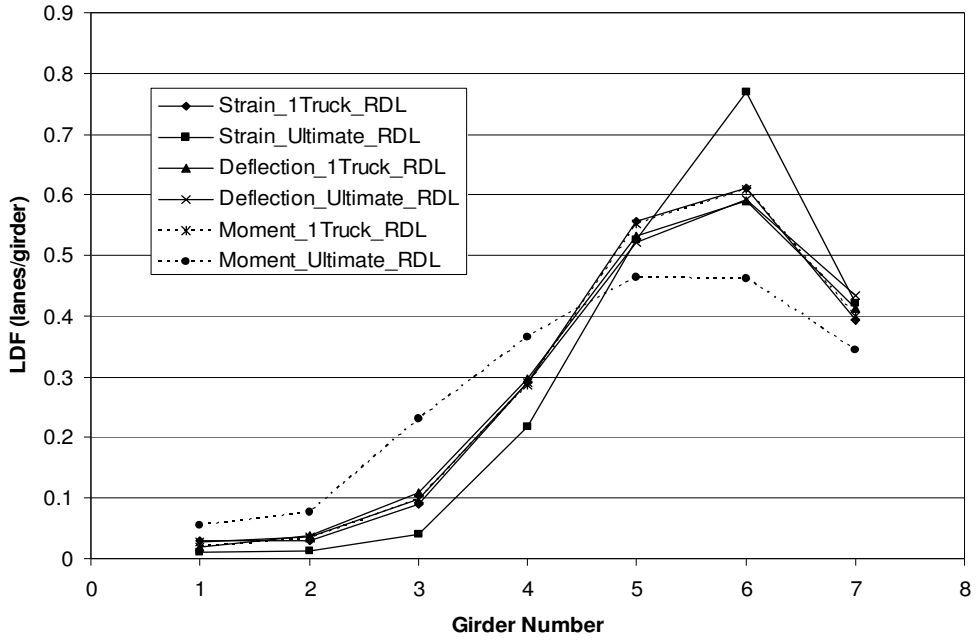

Figure 9.3
RDL loading - without ID

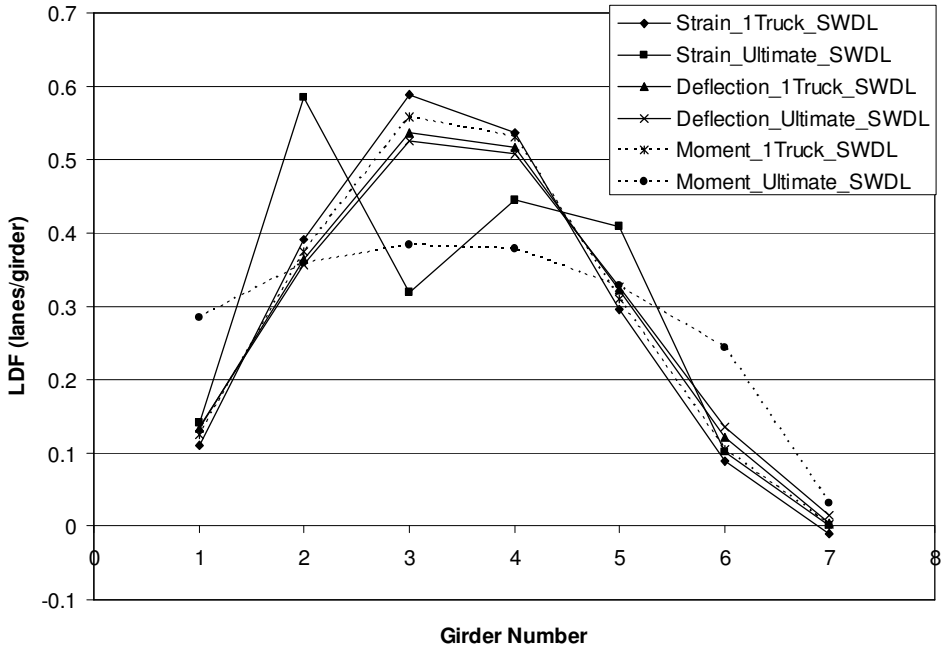

Figure 9.4
SWDL loading - without diaphragms and without edge stiffeners

According to the results obtained, it was verified that the use of strains to calculate LDFs is acceptable in the elastic range (_1Truck cases), as expected. Thus, LDF values calculated resulted consistently in numbers of the same order as those obtained using deflections and moments. However, using strains to calculate LDFs at ultimate stages (_Ultimate cases) led to unpredictability. This is explained by large strains that develop at crack locations at the bottom of the girders. Therefore, the use of strains to obtain LDFs should be limited to linear ranges in both experimental and computational analyses, since strains are not reliable after cracking.

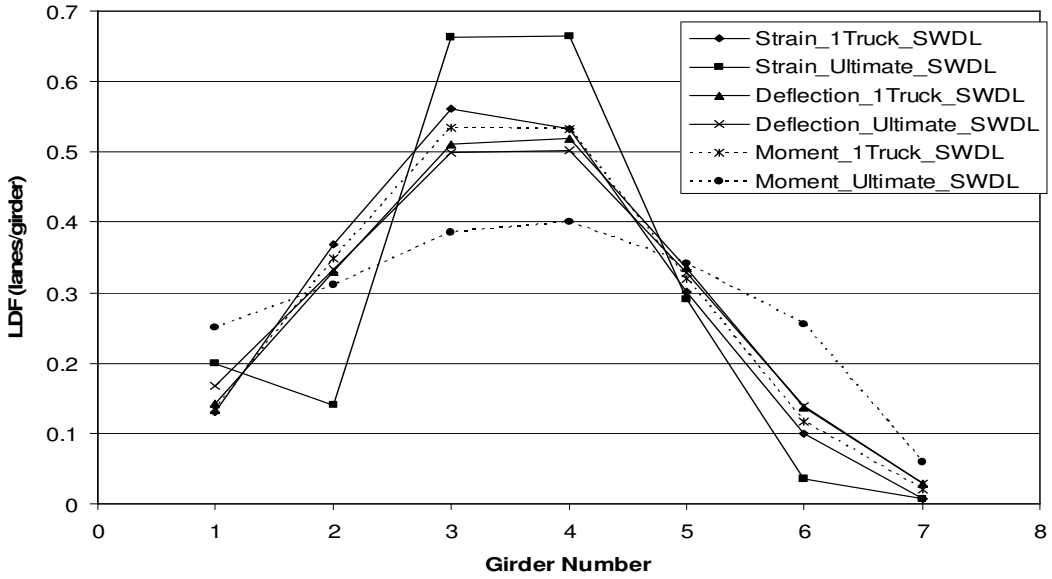

Figure 9.5
SWDL loading - without ID

Similarly, the use of deflections to calculate LDFs was consistently acceptable in the linear range (figures 9.3, 9.4, and 9.5). Although the results generated from deflections were consistent for all loading cases at ultimate stages, they were misleading. They remained somewhat similar to the results in the linear range which means that the use of deflections to predict live load distribution at failure resulted in incorrect values for the bridge studied. If this is confirmed after further investigation, the use of deflections should also be limited to linear ranges.

The theoretical ultimate LDF value was calculated by dividing the number of lanes loaded

by the number of girders, assuming that all girders take the same amount of load at the ultimate stage due to ideal load redistribution. In this study, this value was 0.286, which means that the live load taken by each girder should converge to this value under ideal circumstances. This redistribution trend was observed in all loading cases studied (figures 9.3, 9.4, and 9.5) when the load distribution was calculated using the section moments. This trend is clearly illustrated in figure 9.6 for the case without ID, but with edge stiffeners. This figure also shows that the calculated LDF is lower than those calculated using AASHTO LRFD (2004) and AASHTO Standard (2002) equations. The amount of live load taken by each girder consistently approached the ideal value when the bridge is loaded from elastic to ultimate stages.

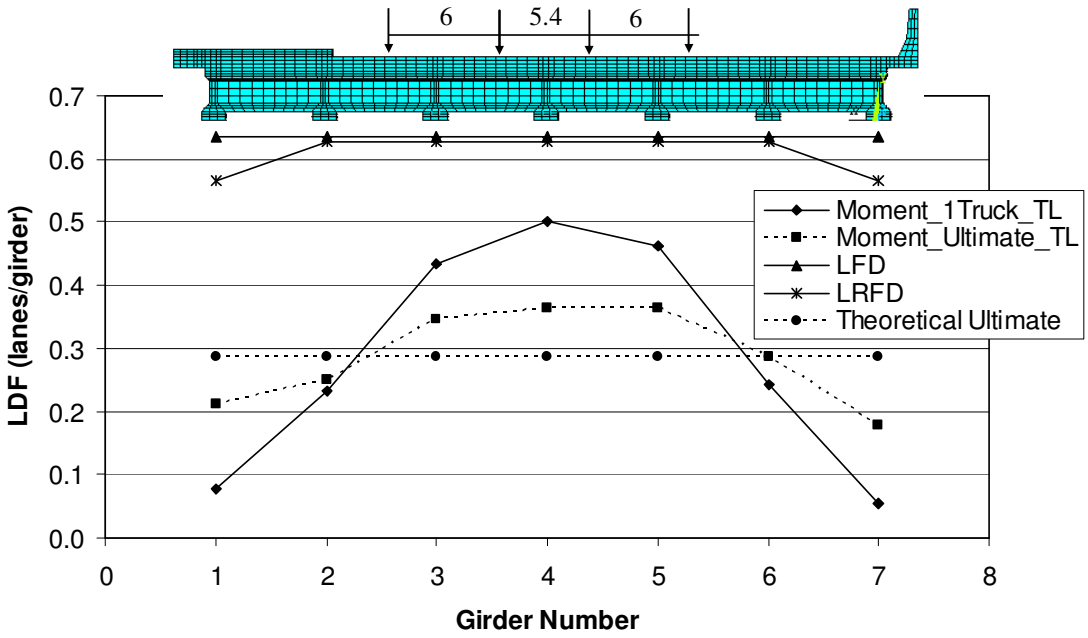

Figure 9.6
TL loading - without ID: comparison with AASHTO LRFD and AASHTO Standard

LDF calculations based on section moments produced the most realistic results, which were consistently acceptable in both linear ranges and ultimate stages. When a girder cracked, the load being carried was redistributed primarily to the adjacent ones. This phenomenon was clearly observed and illustrated with section moment based live load distribution progression curves

ranging from zero to ultimate load in figure 9.7. For example, when the bridge was loaded up to four trucks, girder 4 (G4) cracked and its load decreased while the load carried by girders 6 and 7 (G6 and G7) increased.

Load rating comparisons were performed as well. Load ratings are used to determine the safe live load carrying capacity of a highway structure. It is usually expressed as a Rating Factor (RF) or in terms of tonnage for a particular vehicle. There are two types of ratings: inventory and operational. Inventory rating determines if the structure considered is safe for legal loads, or indefinite crossings. Operational rating determines the maximum permissible load for the structure, suitable for one-time or limited crossings.

Load ratings of bridges are necessary to ensure the safety of general public because some bridges have aged and deteriorated over the course of their life. Also, different design vehicles have been used over the years for the design of bridges. To have a consistent method to determine the load carrying capacity, all bridges are rated using a standard loading vehicles, called legal loads.

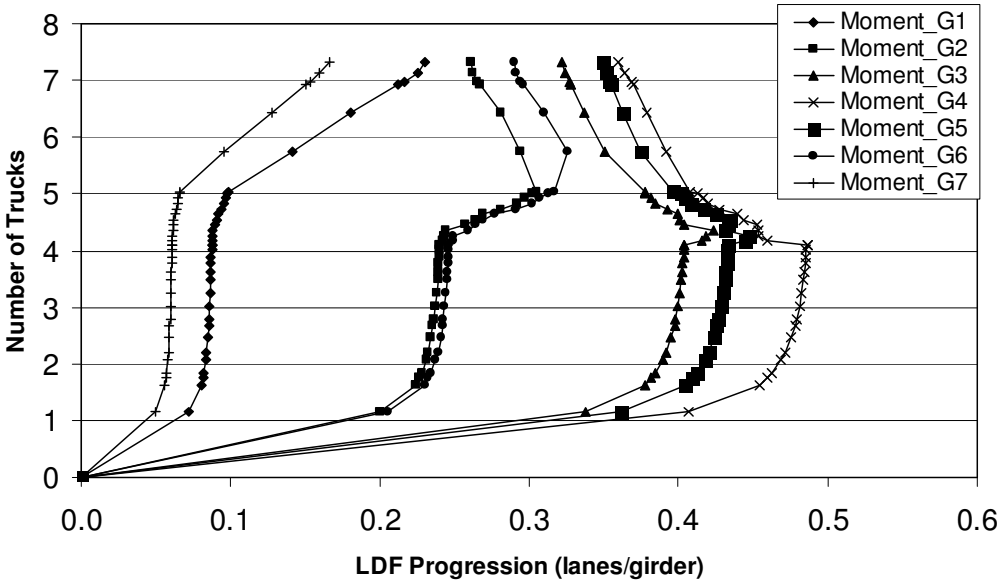

Figure 9.7
Load distribution progression curves - TL loading - without ID

9.5 Discussion of Results

9.5.1 Live Load Distribution

Load distribution factors were calculated using AASHTO LRFD (2004) and AASHTO Standard (2002) and finite element (FE) analysis. The calculation of LDFs from the FE results was obtained based on strains, deflections and section moments at the midspan with the respective equations presented above.

Figure 9.5 shows some of the calculated live load distribution curves for one of the three loading scenarios for Bridge 1 using the three calculation methods discussed earlier. In this figure, Moment_1Truck_SWDL represents service loading level. The nomenclature denotes that the load distribution was calculated using section moments and that both traffic lanes were loaded with one truck per lane. This description method applies to all legends. According to the results obtained, it was verified that the use of strains to calculate the LDF are acceptable in the elastic range (_1Truck cases), as expected. LDF values thus calculated resulted consistently in numbers of the same order as the ones obtained using deflections and moments. Using strains to calculate LDFs at ultimate stages (_Ultimate cases), however, led to unpredictability. This is explained by large strains which develop at crack locations at the bottom of the girders. Similarly, the use of deflections to calculate LDFs was consistently acceptable in the linear range only. Therefore, the use of strains and deflections to obtain LDFs should be limited to linear ranges in both experimental and computational analyses.

LDF calculations based on section moments produced the most realistic results, which were consistently accurate in both linear ranges and ultimate stages. When cracking occurs, the load being carried by a girder is redistributed primarily to the adjacent ones. This phenomenon was clearly observed and is illustrated with section moment LDF progression curves ranging from zero to ultimate load in figure 9.7.

9.5.2 Rating Factors (RFs)

RF for Bridge 1 would be 8.20 trucks considering ideal circumstances in which all loads are completely known, with uniform LDF and zero IM. This value is 7.81 trucks for Bridge 2. When these conditions were approached by the FE analysis, it produced an RF equal to 7.32 (TL without intermediate diaphragm) for Bridge 1 and 6.68 for Bridge 2. According to AASHTO LRFD, the RF for Bridge 1 without diaphragms of edge stiffeners are 1.38 and 2.30, inventory and operational respectively. The operational RF for Bridge 2 according to AASHTO LRFD (2004) equation is 2.12, which is 57.8% smaller than 6.68/1.33 (5.02 trucks) where the value 1.33 is the impact factor (IM).

The lowest RF produced by the FE analysis for Bridge 1 was 4.5 (RDL without diaphragms and without edge stiffeners). Dividing this value by 1.33 to account for the IM it becomes 3.38 or 32% larger than the code value. The lowest RF value produced for Bridge 1 with end diaphragm and edge stiffeners was 5.77 (RDL without intermediate diaphragm). Taking IM into consideration the RF becomes 4.34. For this bridge configuration, which is closer to reality, the RF produced is 89% larger than the one calculated by the code. This difference could potentially result in saving millions of dollars by avoiding unnecessary bridge postings, rehabilitation or decommissioning and replacement. The use of nonlinear finite element methods to load rate bridges would enable engineers to assess the true condition of existing bridge systems in a more realistic manner, as well as to predict long-term conditions of new bridges more accurately.

9.5.3 Effective Width

The effective width is an abstraction used in order to utilize line girder analysis and beam theory. Its concept introduction allows for design simplification by making use of rectangular beam design methodology. Values of maximum deflection and stresses are obtained from line-girder analysis by using an appropriate reduced flange width (Moffatt and Dowling 1978). An inelastic

effective flange width evaluation was carried out at different loading stages from service to ultimate for Bridge 2. Figure 9.8 depicts the bridge configuration and layering for effective flange width calculations.

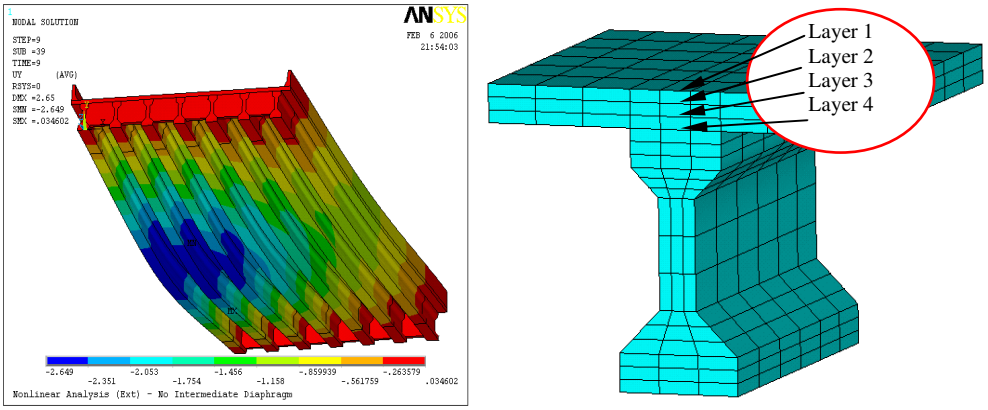

Figure 9.8
Bridge 2 configuration and deck layers for inelastic effective flange width

The effective width equation below was used to post-process the finite element results:

$$b_{eff} = \frac{\int_0^b \sigma_y dx}{\sigma_{y_{max}}} \qquad \text{Eq. 8.1}$$

where σ_y is the bending stress in the section, σ_{ymax} is the maximum bending stress in the section; and b is the girder spacing. Computations of moments, shears, torques, and deflections are directly affected by the effective flange width value.

The effective flange width for Bridge 2 is 72 inches according to AASHTO LRFD (2004), i.e., the girder spacing of this bridge. This is the maximum possible effective width a girder can achieve. For the loading considered in this study, the maximum effective width was 60.48 inches, obtained in Layer 2 of girder 2. There was some difference in effective width from linear to ultimate loading for all layers and girders. The most considerable change in effective flange width occurred on Layer 3 of girders 2, 3 and 4 which experienced decreases of 5.74, 8.36, and 6.72 inches, respectively. The decrease in effective width did not occur consistently from linear to ultimate, but

at different load steps because of continuous stress redistribution after cracking took place in girders. Figure 9.9 shows the deck stress distribution across the bridge and through the layers. Similar stress distribution trend was observed for service loading, but with lower values.

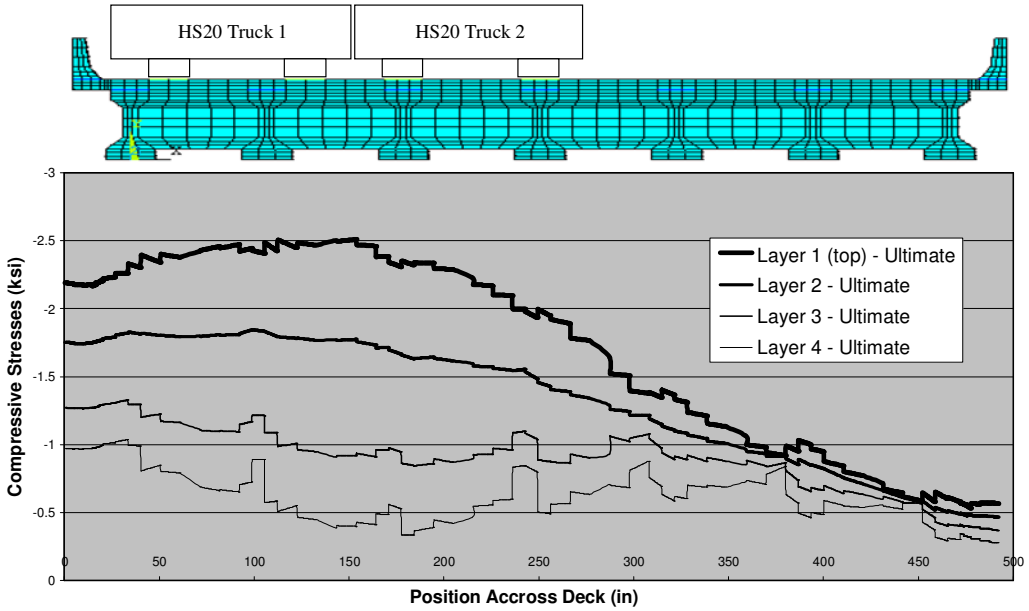

Figure 9.9
Stresses across the bridge deck

CHAPTER 10. CONCLUSIONS AND RECOMMENDATIONS

Nonlinear finite element analyses showed that the ultimate strength calculated according to AASHTO LRFD (2004) code specifications is conservative, underestimating the strength of the bridge. The actual strength is almost double that predicted by the code. Based on the linear and nonlinear simulations it is verified that section moments conveyed the best live load distribution results at ultimate loads. By applying this method, there was a convergence of LDF values toward the theoretical ultimate one, a case in which all girders are equally loaded before failure occurs. Also, it was observed that the inelastic finite element result for effective flange width for the loading case considered is smaller than the AASHTO LRFD (2004) and decreases as the truck loading redistributes among the girders due to cracking. The same trend was observed to all girders and concrete deck layers considered.

On bridge ratings, RFs calculated according to the current AASHTO LRFD code (2004) were conservative. This means that the strength of the bridge was underestimated. More accurate RFs can be achieved by applying section moment methods on results generated by nonlinear finite element models. Similar results were observed for Bridges 1 and 2. Accurate prediction of bridge capacities could potentially result in considerable savings by avoiding unnecessary weight-limiting postings, rehabilitation or decommissioning, and replacement.

Dynamic load tests simulating increasing pavement roughness were performed at 30 MPH, and 40 MPH on lane 1 and 38.5 MPH on lane 2. Wood boards with depths equal to 0.5", 1" and 1.5" were used to simulate the pavement unevenness, sometimes caused by defective approach slabs. The effect of pavement unevenness was quantified for load distribution and dynamic allowance (IM). The truck load was consistently more evenly distributed across the bridge with the increase in pavement unevenness. This trend was observed for load distribution based on strains and deflections results for all three speeds considered. In all cases the LDFs were well within the ones

calculated using AASHTO equations (LRFD, 2004 and Standard, 2002).

At 30 MPH the effect of pavement unevenness was not significant enough to create an IM greater the ones recommended by AASHTO (LRFD, 2004 and Standard, 2002). However, at 38.5 MPH, IM values were as high as 42% and 53% for girder G2, based on strains and deflections, respectively. This value exceeds the 33% recommended by AASHTO LRFD. These high IM values did not occur at the most loaded girder. Similarly, at 40 MPH, the highest IM value was almost twice as high as the value recommended by AASHTO LRFD and again did not occur at the most loaded girder. These values took place at girder G6 and were 56% and 65% based on strains and deflections, respectively.

It was observed that IDs decreased the LDF for interior girders and increased the LDF for exterior girders. Furthermore, IDs increased the deflection marginally for exterior girders and decreased the deflection for interior girders. Both with and without IDs, the deflections were observed to be within permissible limits, thereby indicating that deflection is not an important criterion influencing the decision to eliminate reinforced concrete (RC) IDs or to replace them with steel IDs.

Steel diaphragm configurations for different bridge configurations that could perform similarly to RC diaphragms were proposed. A study was done on the relative performance of RC IDs and steel IDs during bridge construction. The alternate steel diaphragms were proposed based on the minimum target stiffness as a proportion of the absolute diaphragm stiffness contributed by the existing RC IDs. These steel IDs were found to provide stability near that produced by RC IDs during the deck construction. Therefore, if the reinforced concrete diaphragms were provided only for the purpose of providing girder stability during construction, they could be replaced with steel diaphragms.

Reinforced concrete IDs and steel IDs under lateral impact loading were also investigated to

simulate collisions by over-height trucks. Results obtained from these impact tests indicated that RC IDs provided the greatest protection to exterior girders undergoing impact, when the impact occurred at the ID location. When the impact takes place at a location away from the ID, it was observed that the ID configuration did not significantly influence the bridge performance. It was concluded that the IDs could not be counted on for their ability to protect girders if the IDs are not right above the traffic lanes. In cases where there is no vehicle traffic under the bridge, steel IDs could be used as well, if their sole purpose is to provide stability.

A detailed description of the field testing was presented. Strains and deflections were acquired and used for comparison to finite element analysis. Finite element (FE) simulations showed that when 30% of the diaphragm design stiffness was considered, the results showed better conformity to experimental observations than when the full stiffness was used. Existing literature suggests that IDs contribute to about 30% of their stiffness. This conclusion was confirmed by the results of FE analysis conducted. Therefore, the maximum effect of IDs on load distribution is at a level of 5% for most beams.

Some recommendations are presented below in order to further investigate and apply the findings of this study.

1. If sufficient lateral bracings are provided during construction (either temporary or permanent) and over-height truck collision is not a concern (such as the cases where there is no traffic underneath the bridge), IDs can be eliminated. In terms of vertical live load distribution, IDs are beneficial to interior girders but harmful to exterior girders. The current AASHTO load distribution factor is conservative and provides adequate strength for the code specified live load, even though IDs are not used.

2. If IDs are to be provided to protect against lateral impact by over-height trucks, they should be placed as close as possible to the locations of possible collision. Concrete IDs are

recommended for this purpose since they provide better impact protection than the steel ones. If the impact is not near the ID location, IDs provide no direct protection. However, IDs located away from the impact point may help support the damaged girders.

3. For the purpose of construction stability, steel IDs can be used to replace concrete IDs. Therefore, where collision protection is not required, such as bridges over bayous, steel IDs can be used in place of the current concrete IDs.

4. If IDs are completely eliminated, there will be an increase of strain action for the interior girders. The live load design moment of interior girders can simply be increased by 5 percent to maintain the same safety level as that of bridges with IDs, as recommended by AASHTO LRFD (2004). After a higher level of confidence is achieved regarding the complete elimination of IDs, then the increase of live load might not be necessary anymore.

5. More dynamic tests are recommended in order to verify the need to increase IM values for future design, based on the pavement roughness condition of existing bridges. Correction factors could be proposed based on the likelihood of such roughness condition due to deterioration.

6. Nonlinear finite element load rating of bridges might not be a possibility yet due to the high computer "horse power" demand. However, when implemented, this method can predict the safe load carrying capacity of bridges more accurately, possibly avoiding unnecessary bridge postings and replacement.

REFERENCES

1. Abendroth, R. E. and Fanous, F., "Lateral impacts to PC girders in bridges with intermediate diaphragms." Proceedings of the 2003 Mid-Continent Transportation Research Symposium, Ames, Iowa, Iowa State University Press, 2003.

2. American Association of State Highway and Transportation Officials (AASHTO), "Standard specification for highway bridges," Washington, DC., 2002.

3. American Association of State Highway and Transportation Officials (AASHTO), "LRFD Bridge Design Specifications," Washington, DC, 2004.

4. Andrawes, B.O., "Lateral impact response for prestresssed concrete girder bridges with intermediate diaphragms" Thesis submitted to Iowa State University, 2001.

5. ASCE "Report Card for America's Infrastructure" 2003 Progress Report, An Update to the 2001 Report Card, 2005.

6. Barr P. J., Eberhard M. O., and Stanton J. F., "Live-Load distribution factors in prestressed concrete girder bridges" Journal of Bridge Engineering, pp. 298-306, September/October 2001.

7. Burdette, E.G. and Goodpasture, D. W., "Tests of four highway bridges to failure." J. of the Structural Division, Proceedings of the American Society of Civil Engineers, pp. 335-348, 1973.

8. Cai, C.S., Shahawy, A.M., and El-Saad, A., "Non-destructive test of field bridges in Florida." Proceeding, Structural Materials Technology, San Antonio, Texas, 1998.

9. Cai, C.S., Mohsen Shahawy and Robert, J. Peterman, "Effect of diaphragms on load distribution of prestressed concrete bridges." Transportation Research Record, J. of the Transportation Research Board, National Research Council, Washington D.C., No. 1814, pp. 47-54, 2002.

10. Cai, C.S., Shahawy, M., "Predicted and measured performance of prestressed concrete bridges." Journal of Bridge Engineering, ASCE, Vol. 9, No. 1, pp. 4-13, 2004.

11. Cai, C.S., Avent, R.R., Araujo, M.C., Chandolu, A., "Assessing the needs for intermediate diaphragms in prestressed concrete bridges." LTRC Project No. 03-3ST, State Project No. 736-99-1134, 2006.

12. Calcada, R., Cunha, A. and Delgado, R., "Analysis of traffic-induced vibrations in a cable-stayed bridge. Part II: Numeric Modeling and Stochastic Simulation." Journal of Bridge Engineering, 10(4), 482-489, 2005.

13. Chen, Y., "Refined and simplified lateral load distribution for bridges with unequally spaced girders: 1. Theory." Computers and structures, Vol. 55, No. 1, pp. 1-15, 1995.

14. Chen, Y., "Refined and simplified lateral load distribution for bridges with unequally spaced girders: 2. Applications." Computers and structures, Vol. 55, No. 1, pp. 17-32, 1995.

15. Chen, Y., "Prediction of lateral distribution of wheel loads on bridges with unequal girders." Computers and structures, Vol. 54, No. 4, pp. 609-620, 1995.

16. Chen, Y. and Aswad, A., "Stretching span capability of prestressed concrete bridges under AASHTO LRFD." Journal of Bridge Engineering, Vol. 1, No. 3, pp. 112-120, 1996.

17. Cheung, M. S., Jategaonkar, R., and Jaeger, L. G., "Effects of IDs in distributing live load in beam-and-slab bridges." Can. J. Civ. Engrg., Ottawa, Canada, Vol. 13, No. 3, pp. 278- 292, 1986.

18. Eamon, C. D. and Nowak, A. S., "Effects of edge-stiffening elements and diaphragms on bridge resistance and load distribution." Journal of Bridge Engineering, ASCE, Vol. 7, No. 5, pp. 258-266, 2002.

19. Eamon, C. D. and Nowak, A. S., "Effect of secondary elements on bridge structural system reliability considering moment capacity." Structural Safety, Vol. 26, pp. 29 – 47, 2004.

20. Ebeido, T. and Kennedy J.B., "Beam moments in continuous skew composite bridges." Journal of Bridge Engineering, ASCE, Vol. 1, No. 1, pp. 37-45, 1996.

21. Garcia, T. M., "IDs for precast prestressed concrete bridges." Western Bridge Engineer's Seminar, Seattle, Washington, Oct. 4, 1999.

22. Ghosn, M., Moses, F., and Gogieski, J., "Evaluation of steel bridges using in-service testing." Transp. Res. Rec. 1072, Transp. Res. Board, Nat. Res. Council, Washington, D.C., pp. 71-78, 1986.

23. Green, T. M., Yazdani, N., Spainhour, L., and Cai, C. S., "ID and temperature effects on concrete bridge performance" In Transportation Research Record, J. of the Transportation Research Board, National Research Council, Washington D.C., No. 1814, pp. 83-90, 2002.

24. Green, T. M., Yazdani, N., and Spainhour, L., "Contribution of intermediate diaphragms in enhancing precast bridge performance." Journal of performance of constructed facilities, ASCE, Vol. 18, No. 3, pp. 142-146, 2004.

25. Griffin, J.J., "Influence of Diaphragms on Load Distribution in P/C I-girder Bridges." PhD Dissertation, University of Kentucky, 1997.

26. Khaloo. R. and Mirzabozorg. H., "Load distribution factors in simply supported skew bridges." Journal of Bridge Engineering, ASCE 8 (4), 241-244, 2003.

27. Kostem, C.N., "Effects of diaphragms on lateral load distribution in beam-slab bridges." Transportation Research Record No. 645, Transportation Research Board, Washington D.C., 6-9, 1977.

28. LADOTD "Bridge Design Manual." Louisiana Department of Transportation and Development, Baton Rouge, LA, 2002.

29. Louisiana Regulations: trucks, vehicles and loads, LADOTD, 2000.

30. Lin, C. S. and VanHorn, D. A., "The effect of midspan diaphragms on load distribution in a prestressed concrete box-beams bridge." Fritz Engineering Laboratory Report No. 315.6, Lehigh University Institute of Research, 1968.

31. Moffatt, K. R., and Dowling, P. J., "British shear lag rules for composite girders." Technical Rep., Nebraska Department of Roads, Lincoln, Neb., 1978.

32. Nilson, A. H., "Nonlinear analysis of RC by the finite element method." ACI Journal, Vol. 65, No. 9, pp. 757-766, 1968.

33. Precast/Prestressed Concrete Institute (PCI), "PCI Design Handbook." 6th Edition, 2005.

34. Rashid, Y. R., "Ultimate strength analysis of prestressed concrete pressure vessels." Nuclear Engineering and Design, pp. 334-344, 1968.

35. Senders, W. W., "Distribution of wheel loads on highway bridges." National Cooperative Highway Research Program, Project 111, 1984.

36. Sengupta, S. and Breen, J. E., "The effects of diaphragms in prestressed concrete girder and slab bridges." Research Report 158-1F, Project 3-5-71-158, Center for Highway Research, University of Texas at Austin, Texas, 1973.

37. Sithichaikasem, S. and Gamble, W. L., "Effects of diaphragms in bridges with prestressed concrete I-section bridges." Structural Research Series No. 383, Illinois Cooperative Highway Research Series No. 128, University of Illinois at Urbana-Champaign, Urbana, Ill, 1972.

38. Stallings, J. M., Cousins, T. E., and Stafford, T.E., "Effects of removing Diaphragms from a steel girder bridge." Transportation Research Record No. 1541, Research Board, Washington D.C., pp. 183-188, 1996.

39. Stallings, J. M., and Yoo, C. H., "Tests and ratings of short-span steel bridges." J. of Struct. Eng., 119, pp. 2150-2168, 1993.

40. Suidan, M. and Schnobrich, W.C., "Finite element analysis of reinforced concrete." J. of the Structural Division, ASCE, pp. 2109-2121, 1973.

41. The Road Information Program (TRIP). "Showing their age: The nation's bridges at 40 - Strategies to improve the condition of our bridges and keep them in good shape." Washington, DC, 2002.

42. William, K. J., and Warnke, E. D., "Constitutive model for the triaxial behavior of concrete." Proceedings, International Association for Bridge and Structural Engineering,

Vol. 19, ISMES, Bergamo, Italy, p. 174, 1975.

43. Wong, A. Y. C. and Gamble, W. L., "Effects of diaphragms in continuous slab girder highway bridges." Structural Research Series No. 391, Illinois Cooperative Highway Research Series No. 138, University of Illinois at Urbana-Champaign, Urbana, Ill., 1973.

44. Zokaie, T., Osterkamp, T. A., and Imbsen, R. A., "Distribution of wheel loads on highway bridges." National Cooperative Highway Research Program, Project 12-26, Imbsen and Associates, Inc., 1991.

45. Zokaie,T., "AASHTO-LRFD live load distribution specifications." Journal of Bridge Engineering, ASCE, Vol. 6, No. 2, pp. 131-138, 2001.

APPENDIX A
SURVEY QUESTIONNAIRE

Assessing the Needs for Intermediate Diaphragms in Prestressed Concrete Bridges

STATE Project No. 736-99-1134
LTRC Project No. 03-3ST

QUESTIONNAIRE SURVEY

December 01, 2003
PROJECT TEAM

Dr. Steve Cai, P.E., Assistant Professor
Dr. Richard Avent, P. E., Professor
Marcio Araujo, Ph.D. Research Assistant

Civil and Environmental Engineering Department
Louisiana State University - 3510 CEBA
Baton Rouge, LA 70803
Phone: (225) 578-8898; Fax: (225) 578-8652
Email address: cscai@lsu.edu

PROJECT MANAGER

Mr. Walid Alaywan, P.E.
Louisiana Transportation Research Center (LTRC)
4101 Gourrier Avenue
Baton rouge, LA 70808
Phone: (225) 767-9106; Fax: (225) 767-9108
Email address: walaywan@dotd.state.la.us

Contact Information:

District/department name: _____
Respondent's name: _____
Position/Title: _____
Address: _____
Phone: _____ Fax: _____
Email address _____

---

1) Has your district/department ever built precast prestressed slab-on-girders concrete bridges that required the use of intermediate diaphragms (IDs)?

_____ Yes. How many in the last 10 years?_____

_____ No

2) Is your district/department satisfied with the use of reinforced concrete IDs in the construction, service, and maintenance stages?

_____ Yes _____ No

What are the major benefits? What are the major problems?

3) Does your district/department strictly follow the ID details specified in the LaDOTD design manual?

_____ Yes. If any exception, please explain and provide the details.

4) The LaDOTD manual specifies reinforced concrete IDs. Has your district/department ever used or considered to use steel IDs?

5) Would your district/department support the use of steel IDs for prestressed concrete bridges if justified by research? If not, what are your major concerns?

6) Would your district/department support the elimination of IDs for prestressed concrete bridges if justified by research? If not, what are your major concerns?

7) Has your district/department ever observed any damage or failure related to IDs? If yes, could you provide pictures and/or detailed information?

APPENDIX B
FIELD OBSERVATIONS ON DIAPHRAGMS

Diaphragm Types Encountered

Figure B1
ID Type I

Figure B2
ID Type II

Figure B3
ID Type III

Figure B4
ID Type IV

Figure B5
ID Type V

Figure B6
ID Type VI

Observed Diaphragm Damages

Figure B7
Deck cracks and large skew at LA 33 over I-20

Figure B8
Cracked ID at LA 21 over I-12

Figure B9
Cracked ID at LA 21 over I-12

Figure B10
Cracked ID at US 80 over I-220

Figure B11
Cracked cold joint at I-49 over LA 182

Figure B12
Damaged girder at I-10 over Highland Rd

Figure B13
Broken and exposed tendons at I-10 over LA 182

Figure B14
Damaged girder at I-20 over LA 17

Miscellaneous Observations

Figure B15
Tapered ID at LA 8 over I-49

Figure B16
Sharp edge ID at LA 1026 over I-12

Figure B17
Precast ID at I-49 over LA 3276

Figure B18
High skew bridge at US 90 over LA 83

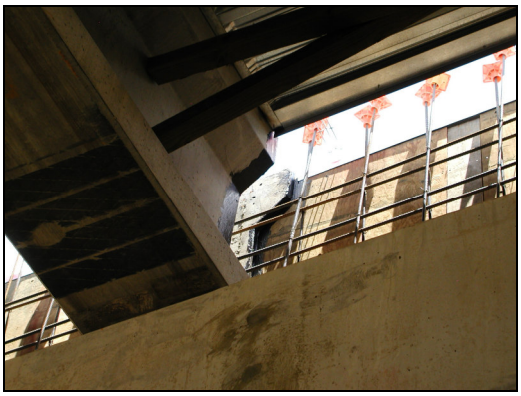

Figure B19
Diaphragm steel cage and formwork at I-10 over LA 27

Figure B20
Diaphragm steel cage at I-10 over LA 27

Figure B21
ID Curing

Figure B22

No EDs or IDs, of Texas bridge at Texas-Louisiana border

Figure B23

Edge stiffener detail of Texas bridge at Texas-Louisiana border

Figure B24

Edge stiffener detail at I-10 over Loyola Avenue in New Orleans

Figure B25
Exterior girder ID as built in 1937 (Perkins under I-10)

Figure B26
Overhang ID as built in 1937 (Perkins under I-10)

VITA

Mr. Araujo was born in the city of Parnaíba, in the Brazilian state of Piauí, in 1975. He received his bachelor's degree from Universidade Federal do Piauí in 1998. In 2002, Mr. Araujo received his master's in civil engineering at Louisiana State University and Agricultural and Mechanical College, under the direction of Boyd Professor Doctor George Voyiadjis. Mr. Araujo joined Doctor Steve Cai's Laboratory of Bridge Innovative Research and Dynamics of Structures (BIRDS) in August, 2003. Mr. Araujo worked full time as the operations manager for Fenner Consulting, a civil and structural design firm, from June 2006 to April 2008. He currently holds an engineering position with CDI Solutions working on industrial projects.

Mr. Araujo's experience with bridges is indicated by the following publications and projects:

Journal papers:

1. C. S. Cai, W. W. Wu, **M. Araujo** (2007), "Cable Vibration Control with a TMD-MR Damper System: Experimental Exploration", Journal of Structural Engineering, May 2007, pp. 629-637.

2. Cai, C. S., **Araujo, M.,** Chandolu, A., Avent, R. R., and Alaywan, W. (2007) "Diaphragm effects of prestressed concrete girder bridges - a review and discussion" Practice Periodical on Structural Design and Construction, ASCE, 12 (3), 161-167.

3. Cai, C. S., Shi, X. M., **Araujo, M.** and Chen, S. (2007) "Effect of Approach Span Condition on Vehicle-induced Dynamic Response of Slab-on-Girder Road Bridges." Engineering Structures, 29, 3210-3226.

4. Cai, C. S. Anand Chandolu and **Marcio Araujo**, "Quantification of Intermediate Diaphragm Effects of Prestressed Concrete Girder Bridges on Load Distributions" PCI Journal (Accepted).

Conference papers:

5. Cai, C. S., **Araujo, M.,** Nair, A. and Shi, X. M. (2007). "Static and dynamic performance evaluation of bridges through field testing and monitoring" The 2nd International Conference on Structural Condition Assessment, Monitoring and Improvement, Changsha, China, Nov. 19-21, 2007.

6. **Araujo, M.**, Cai, S. and Shi, X. (2007), "Analysis of Prestressed Concrete Bridges to Failure", 86th Transportation Research Board (TRB) Conference, January 21-25, 2007, Washington, DC

7. Cai, S., Shi, X., **Araujo, M.** and Suren Chen (2007), "Influence of Approach Span Conditions on Vehicle-Induced Dynamic Response of Slab-on-Girder Bridges: Field and Numerical Simulations", 86th Transportation Research Board (TRB) Conference, January 21-25, 2007, Washington, DC

8. **Araujo, M.** and Cai, C.S. (2006), "Performance of Prestressed Concrete Bridges – Evolution From Elastic to Failure Stages", 2006 Structures Congress, ASCE, May 18 – 21, St. Louis, Missouri, USA;

9. Cai, C. S., Anand Chandolu, **Marcio Araujo** (2005). "Quantification of Intermediate Diaphragm Effects of Prestressed Concrete Girder Bridges- Application to LRFD Design" Precast/Prestressed Concrete Institute, Annual Conference, Oct. Palm Springs, California.

10. **Araujo, M.**, Cai, C. S., Avent, R., Shi, X., Chandolu, A. and Alaywan, W. (2005), "Nonlinear Finite Element Analysis of a Prestressed Concrete Bridge", 2005 Joint ASME/ASCE/SES Conference on Mechanics and Materials, June 1-3, Baton Rouge, Louisiana, USA;

11. Cai. C. S., Wu, W. J., and **Araujo, M.** (2005). "Cable Vibration Control with TMD-MR Damper: Experimental Study." The joint /ASME/ASCE/SES Engineering Mechanics and Materials Conference, June 2005, Baton Rouge, Louisiana.

12. **Araujo, M.**, Cai, C. S., Teixeira, P.W. and Neiva, V. (2005), "Lateral Load Distribution in Prestressed Concrete Bridges – 3D Finite Element Evaluation of Intermediate Diaphragms Effects According to the Brazilian Code NBR 6118/203 and LA DOTD Manual", 1st National Conference for Research, Design and Production of Prestressed Concrete Structures, November 3-4, Sao Carlos, Sao Paulo, Brazil.

Research Reports:

13. Cai, S., Avent, R., **Araujo, M.** and Chandolu, A. (2006), "Assessing the Needs for Intermediate Diaphragms in Prestressed Concrete Bridge", LTRC Project No. 03-3ST, June 2006;

14. **Araujo, M.**, Cai, C. S., Liu, X.Z. (2006)"Overloading Strain Monitoring of Truss Bridge on US 190 Over Atchafalaya River" Conducted for Louisiana Department of Transportation and Development

15. **Araujo, M.**, Cai, C. S., Shi, X.M., Nair, A., Liu, X.Z., and Xia, M. (2006)"Intracoastal Waterway Bridge Behavior Under Over Loading Conditions" Conducted Free of Charge for Louisiana Department of Transportation and Development.

16. Cai, C. S., Wenjie Wu and **Marcio Araujo** (2004). "Structural Performance Evaluation of an Experimental Low Cost Building System, Phase II" A Final Report Submitted to David Baird Studio, 2241 Christian St., Baton Rouge, LA 70808.

Others

1. 86th TRB Conference (2007) presentation about ultimate analysis of prestressed concrete bridges.

2. Coordinated and supervised live load tests on:
    a. prestressed concrete bridge over Cypress Bayou on Hooper Road in Baton Rouge, LA (Feb. 20-22, 2006);
    b. steel girder bridge over the Intracoastal Waterway on LA 1 in Port Allen, LA (Jul. 10, 2006);
    c. truss bridge over Atchafalaya river on US 190 in Krotz Springs, LA (Oct. 9, 2006).

3. Performed field inspection in prestressed concrete bridges at more than 50 locations in all nine (9) LA DOTD districts for LTRC project (Aug 2003 – Dec 2004).

4. Reviewer for ASCE – Journal of Bridge Engineering.

5. Supervised the construction phase of the following bridge projects as an Engineer Intern at Rego Monteiro Construction Company (Dec 1997 – Nov 1998) in Piaui state, Brazil:
    a. replacement of four reinforced concrete bridges in the following cities: Campo Maior, Monsenhor Gil, Cocal de Telha, and Demerval Lobao;
    b. replacement of one steel girder bridge with reinforced concrete approaches in the city of Barreiras do Piaui.

The degree of Doctor of Philosophy is expected to be awarded to Mr. Araujo at the May 2009 commencement.